LAPPEENRANTA UNIVERSITY OF TECHNOLOGY
LUT School of Energy Systems
LUT Mechanical Engineering

Ville Kivelä

EXPERIMENTAL RESEARCH OF BUS BODY NOISE AND VIBRATION

In Espoo, May 21th, 2018

Examiners: Professor Jussi Sopanen
D.Sc. Janne Heikkinen

ABSTRACT

Lappeenranta University of Technology
LUT School of Energy Systems
LUT Mechanical Engineering

Ville Kivelä

EXPERIMENTAL RESEARCH OF BUS BODY NOISE AND VIBRATION

Master's thesis

2018

86 pages, 59 figures, 3 tables and 0 appendices

Examiners: Professor Jussi Sopanen
D.Sc. Janne Heikkinen

Keywords: NVH, ride comfort, operational modal analysis, experimental modal analysis, transfer path analysis

The noise and vibrations within vehicle interior have a major impact on the product quality image. For this reason, the research around passenger ride comfort in relation to noise and vibrations is an important part of the product development process within automotive industry.

This thesis discusses a case study of experimental noise and vibration investigations conducted for a city bus. The focus of the research is in the bus body interior noise and vibrations. The aim of the study was to reveal the most significant problems related to bus passenger ride comfort in an existing city bus to provide information for the future bus body development work. In addition, the thesis included an extensive literature review of the noise and vibration phenomena and research as theoretical background information.

The case study investigations included experimental noise and vibration investigations of the test vehicle operating in actual operating conditions. For example, order tracking analysis, operational and experimental modal analysis and transfer path analysis were utilized in the investigations to provide a comprehensive understanding of the noise and vibration properties of the bus body structure.

ACKNOWLEDGEMENTS

Most of all I would like to thank my family for the support, patience and understanding they have shown during this project. Without their input it would not had never been possible to carry through this project.

I am also most sincerely thankful for the expertise and support that all the project participants from SOE, VTT and Scania CV have provided along the way in addition to the time resources that Scania Suomi Oy organization has provided, enabling the fulfillment of one's personal ambitions.

Last, but not least, I want to thank Professor Jussi Sopanen and D.Sc. Janne Heikkinen for their supportive and positive attitude during this project.

Ville Kivelä
Espoo, May 21th, 2018

TABLE OF CONTENTS

LIST OF SYMBOLS AND ABBREVIATIONS

Latin symbols

a_0	Fourier constant term coefficient
a_n	Fourier cosine coefficient
a_v	Frequency-weighted total vibration value
a_w	Frequency-weighted r.m.s acceleration
$(a_w)_{equiv}$	Equivalent vibration magnitude
b_n	Fourier sine coefficient
c	Damping
$\mathbf{C}$	Damping matrix
$c_{rolling}$	Tyre nominal rolling circumference
$E[x(t)]$	Expected value
$F(\omega)$	Excitation spectrum
f_n	Natural frequency
f_s	Sampling frequency
$H(\omega)$	Frequency response function
j	Imaginary unit
k	Stiffness
$\mathbf{K}$	Stiffness matrix
k_i	Multiplying factor
L_p	Sound pressure level
m	Mass
$\mathbf{M}$	Mass matrix
N	Total number of samples
n_{drive_shaft}	Drive shaft rotational frequency
n_{engine}	Engine rotational frequency, Hz
$n_{engine,rpm}$	Engine rotational frequency, rpm
$n_{propshaft}$	Propeller shaft rotational frequency
p_{ref}	Reference sound pressure level
$q(t)$	Modal coordinate
$R_q(\tau)$	Autocorrelation function of the modal coordinate

$R_{xx}(\tau)$	Autocorrelation function
$R_{xy}(\tau)$	Cross-correlation function
$S_q(\omega)$	Auto spectral density of the modal coordinate
$S_{xx}(\omega)$	Auto spectral density function
$S_{xy}(\omega)$	Cross spectral density function
T, t	Period of time
t_k	Time record
$\boldsymbol{u}_i$	Mode shape vector for *i*th mode
v	Vehicle speed
VDV	Vibration dose value
VDV_{total}	Total vibration dose value
$X(\omega)$	Response spectrum
x_k	Digital form of analog signal $x(t)$
ΔL	Difference in total noise level
Δt	Sampling interval

Greek symbols

ζ	Modal damping ratio
θ	Generalized angle between two modal vectors
$\mu_{central\_gear}$	Gear ratio, central gear
$\mu_{transmission}$	Gear ratio, transmission
σ	Standard deviation
σ^2	Variance
τ	Time lag
$\boldsymbol{\Phi}$	Mode shape matrix
ω	Driving frequency
ω_T	Angular frequency within certain period of time
ω_i	Angular frequency (natural frequency) for *i*th mode

Abbreviations

CAN	Controller area network
DFT	Digital Fourier transform
EMA	Experimental modal analysis

FEM	Finite element method
FFT	Fast Fourier transform
FRF	Frequency response function
ISO	International Organization for Standardization
LE	Low-entry
MAC	Modal assurance criterion
MDOF	Multiple degree of freedom
MP	Measurement point
Mic	Microphone
NVH	Noise, vibration and harshness
ODS	Operational deflection shapes
OMA	Operational modal analysis
PDF	Probability density function
PSD	Power spectral density
r.m.s	Root-mean-square
SDOF	Single degree of freedom
SOE	Scania OmniExpress Bus Production
SPL	Sound pressure level
TPA	Transfer path analysis
VTT	The Technical Research Center of Finland

1 INTRODUCTION

The noise, vibration and harshness (NVH) performance has a major influence on the overall image of vehicle quality and this motivates the vehicle manufacturers to focus on the NVH properties as a part of their product development process. In addition, there are for example legislative requirements and customer demands that drive the manufacturers to refine their products in respect of passenger ride comfort.

Scania OmniExpress Bus Production Oy (SOE) is responsible for global bus body research and development within Scania Group, a major European commercial vehicle manufacturer. This thesis includes a literature review of the theoretical foundations of noise and vibration research and a case study, which discusses the experimental investigations of bus body interior noise and vibration conducted as a joint venture by SOE and VTT, the Technical Research Centre of Finland. The study is a part of the product development process for the next generation Scania bus body range.

1.1 Research background

This research is motivated by the need to understand the factors affecting the bus passenger ride comfort of the current bus range to support the ongoing product development process for the next generation bus body structures. Such extensive research of bus body noise and vibrations has not been conducted recently by the bus bodybuilder SOE.

As for the previous researches, for example Eriksson and Friberg (Eriksson & Friberg, 2000, p. 67 – 75) have conducted a partially corresponding investigation on bus body vibrations, but these previous researches are either outdated or otherwise unsuitable regarding the present research objectives. Also, separate noise and vibration investigations have been conducted by the bus chassis and powertrain development organizations within Scania, but no particular emphasis has been put on the bus body nor the bus passenger ride comfort.

1.2 Research problem and objectives

The aim of this research is to reveal the most significant ride comfort related problems in the present Scania bus body structure. This research problem is approached by conducting an

experimental investigation on a selected test vehicle, which represents a common bus body and chassis configuration. In addition, the research aims also to explain the root causes for the detected NVH problems to serve the future bus body development work.

1.3 Research methods

The thesis will first include a literature review on the theoretical background of vehicle NVH research and refinement. The review will be based on both printed and digital publications discussing e.g. the topic of noise and vibration measurement and analysis.

The literature review is followed by the case study, which discusses the experimental ride comfort investigations conducted with Scania Citywide LE city bus under actual operating conditions. The extensive case study investigations included noise and vibration measurements and e.g. operational modal analysis was conducted on the test vehicle. In addition, benchmarking measurements were conducted with a best-in-class competitor for reference.

1.4 Scope of the research

The literature review has been outlined so that it includes relevant theoretical background information related to the case study investigations as well as to vehicle NVH research in general. Thus, the literature review aims to provide sufficient understanding of the research topic without going in too deep in to the theoretical foundations of e.g. noise and vibration research.

As for the case study, the research focuses only on the vibroacoustic problems which have a significant effect on the bus passenger ride comfort. Thus, no emphasis has been put on e.g. drive-by-noise or other exterior noises. In addition, the purpose of the case study is to produce a comprehensive analysis of the bus body NVH problems but further research and development of the practical solutions is left outside of the scope of this thesis.

1.5 Contribution of the thesis

The literature review in the beginning of the thesis gives a summary of vehicle NVH related topics, such as human response to noise and vibration. In addition, e.g. the methods to measure and analyze the noise and vibrations in this context are explained.

The case study within this thesis produces an example of practical vehicle noise and vibration measurements and analysis. In addition, it provides a deterministic view of how the dynamic exciting forces from e.g. the powertrain and chassis cause noise and vibrations in the bus body interior.

2 VEHICLE BODY INTERIOR NOISE AND VIBRATION

This chapter first gives a quick overview to the topic of vehicle noise and vibration development. The chapter starts with a short review of vehicle NVH development scope and objectives together with NVH target setting and evaluation based on benchmarking and human response. In addition, the basic principle of vehicle body structure vibration and noise formation is introduced together with a review of the research conducted around the subject of bus body noise and vibration during the latest years. More detailed theoretical explanation of the vibration and noise phenomena is given for the relevant parts in the third chapter explaining e.g. the theory and application of experimental and operational modal analysis.

2.1 Vehicle NVH development scope and objectives

NVH development is an important part of the vehicle design process as the noise and vibration performance of the vehicle has a major impact on the overall image of the product quality. High levels of noise and vibration causes for example discomfort and a feeling of insecurity to the driver and the passengers inside the vehicle.

The motivation to develop the vehicle's NVH performance comes from e.g. legislation and increased competition. Simultaneously NVH refinement in a motor vehicle is a complex issue due to the interaction of several sources of noise and vibration, affecting the ride comfort. The airborne and structural borne noise and vibrations within the vehicle are mainly induced by the road surface, air flow (aerodynamic noise) and powertrain.

In addition, increasing demands concerning for example fuel efficiency, vehicle performance or functionality set a demand for vehicle design, which produces new challenges to noise and vibration development. An example comes from the study made by Eriksson and Friberg (Eriksson & Friberg, 2000, p. 67 – 75) where, for a city bus, the implementation of larger doors and low floor comes from the demands for high accessibility and a rapid passenger through-flow inside the bus. These properties are good for bus functionality but simultaneously the reduction of bending stiffness of the bus body structure deteriorates the ride comfort of the bus. (Wang, X. 2010, p. 3 – 4; Eriksson & Friberg, 2000, p. 67.)

2.2 NVH development target setting and evaluation

The targets for NVH development are derived from e.g. customer demands and regulatory requirements. For ride comfort, specific standards (e.g. ISO 2631:1997) are set as guidelines for evaluating the acceptable levels of human exposure to noise and vibration. Another example of a target setting method within vehicle development process is benchmarking, i.e. the vehicle performance is compared against best-in-class competitors to derive realistic design targets. The latter topic is discussed below shortly to give an understanding of the principle.

2.2.1 Benchmarking

According to Wang (2010) a benchmark study should be conducted for noise and vibration with similar vehicles, targeted to a similar market segment. The benchmark study should be objective but also subjective as then the results can be better related to customers' perception of the vehicle performance.

As stated earlier, the benchmark vehicles should be best-in-class competitors and tests should include e.g. engine noise, road noise and powertrain noise in both stationary as well as in dynamic operation. When tested in different operating conditions and taking in consideration different components and subsystems, it is possible to get a good reference point for noise and vibration development. (Wang, X. 2010, p. 20 – 21.)

2.2.2 Human response to noise and vibration

In this subchapter a short literature review is presented about the human response to both noise and vibration. Noise and vibration response are divided under separate headings for clarification.

Human response to vibration

According to the literature review, the most referred standard concerning mechanical vibrations' effect on human health is ISO standard 2631. Standard's first part (2631-1:1997) gives instructions for measurement and evaluation of whole-body vibration exposure based on frequency-weighted r.m.s (root-mean-square) acceleration values. According to ISO 2631-1 the amplitude of the exposure is defined by frequency-weighted r.m.s acceleration a_w:

$$a_w = \left[\frac{1}{T} \int_0^T a_w{}^2(t)dt \right]^{1/2} \quad (1)$$

For calculating a daily exposure which composes of several vibration exposures with duration of t_i and frequency-weighted accelerations $(a_w)_i$, the equivalent vibration magnitude can be calculated as follows:

$$(a_w)_{equiv} = \left[\frac{\sum_i (a_w)_i^2 t_i}{\sum_i t_i} \right]^{1/2} \quad (2)$$

In addition, if measurement data is available in different orthogonal directions *x*, *y* and *z*, the frequency-weighted total vibration value with predefined multiplying factors k_i is:

$$a_v = (k_x^2 a_{wx}^2 + k_y^2 a_{wy}^2 + k_z^2 a_{wz}^2)^{1/2} \quad (3)$$

A graphical presentation of the acceleration directions is shown below in Figure 1.

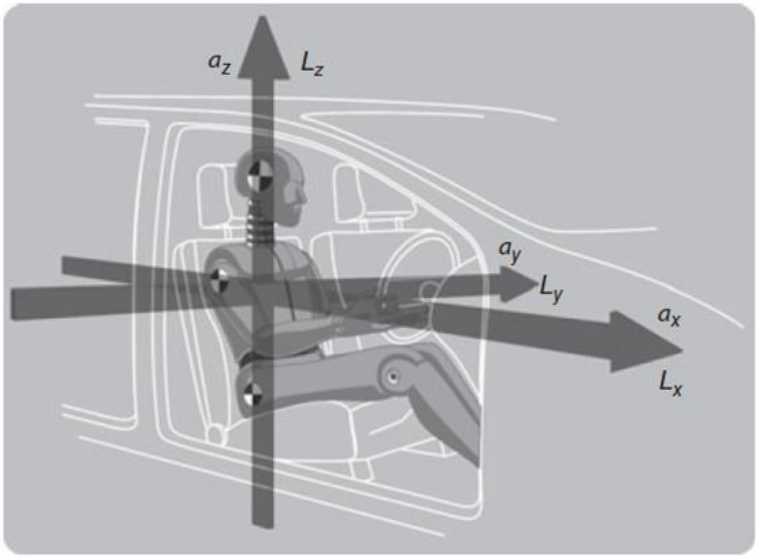

Figure 1. Directions of human body acceleration (Wang, X, 2010, p. 55).

Although the guidance in ISO 2631-1 does not use this value in human response evaluation, but also a vibration dose value *VDV* is defined as:

$$VDV = \left[\int_0^T \left[a_w(t) \right]^4 dt \right]^{1/4} \tag{4}$$

If the *VDV* occurs *i* times within a period, the total value is defined as:

$$VDV_{total} = \left[\sum_i VDV_i^4 \right]^{1/4} \tag{5}$$

ISO 2631-1 also gives an approximation of expected human reactions to different magnitudes of frequency-weighted rms acceleration as follows:

- < 0.315 m/s^2 not comfortable
- 0.315 – 0.63 m/s^2 a little uncomfortable
- 0.5 – 1.0 m/s^2 fairly uncomfortable
- 0.8 – 1.6 m/s^2 uncomfortable
- 1.25 – 2.5 m/s^2 very uncomfortable
- > 2.0 m/s^2 extremely uncomfortable

In addition to the magnitudes of vibration, also to be considered regarding the human response is the frequency range in which the vibrations occur. In Figure 2 is depicted the human responses to vibration and noise in relation to different frequencies. (ISO 2631-1, 1997; p. 1 – 25; Wang, X. 2010, p. 53 – 56; Piersol & Paez. 2010. p. 1152 - 1158):

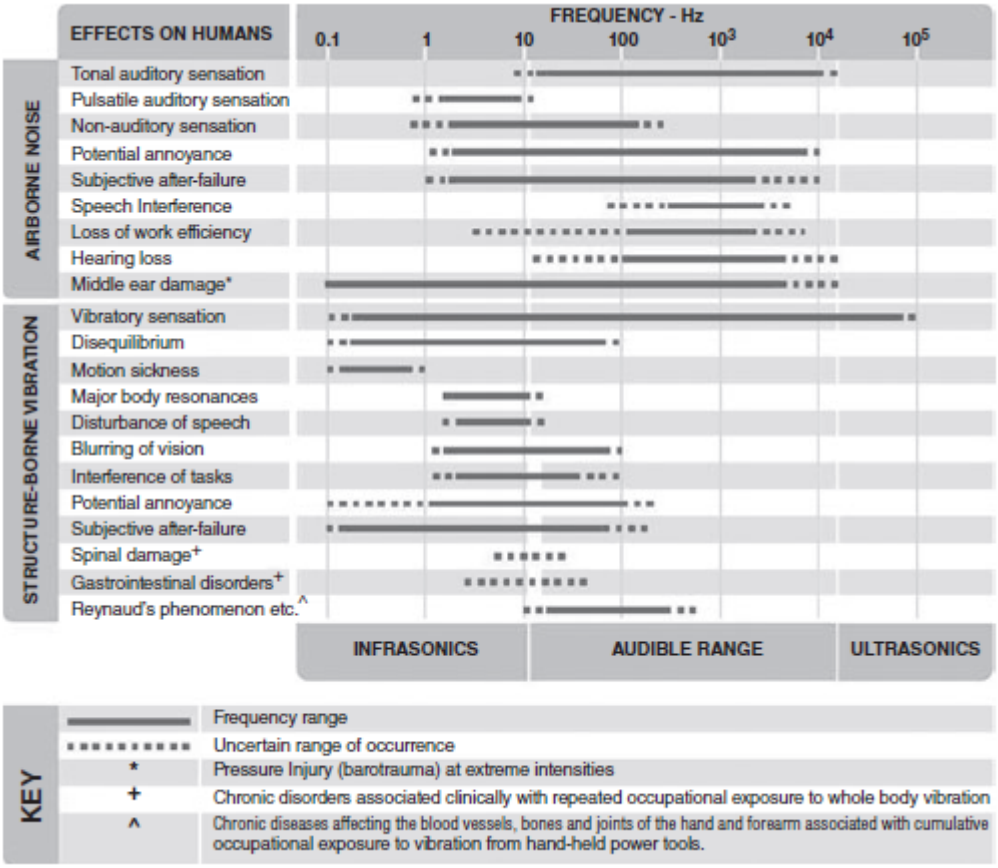

Figure 2. Human response to vibrations and noise in different frequency ranges (Wang, X, 2010, p. 55).

Human response to noise

Audible sound and noise is the human perception of air vibrating in different frequency and amplitude. Human hearing response to sound is frequency-dependent. The human hearing responses with varying sensitivity to sounds between the frequency range of about 20 Hz up to about 20 kHz.

An A-weighting adjusts the measuring of sound level to approximate the human hearing response. In practice also B, C and D weightings exist, but the A-weighting correlates best with subjective evaluation and is most commonly used. The A-weighting curve is presented in Figure 3.

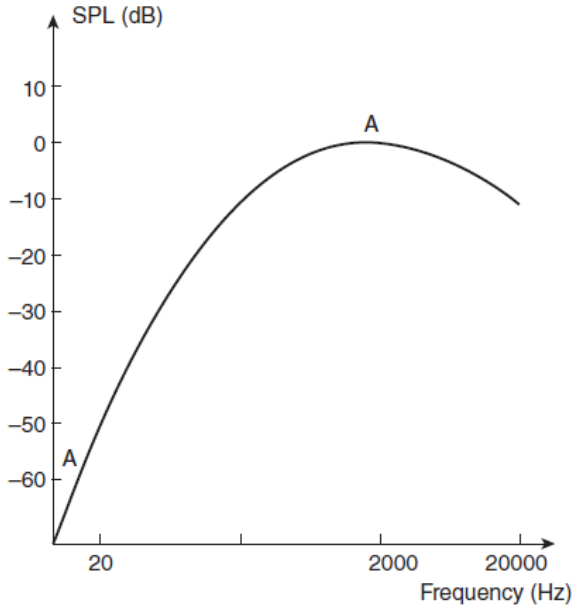

Figure 3. Human hearing response to frequency (Wang, X, 2010, p. 72).

The threshold sound pressure amplitude level value for human hearing is 20 x 10^{-6} Pa. The sound pressure level is usually presented in a logarithmic scale to base 10. I.e. the logarithmic scale for sound level ranges from 0 dB (hearing threshold) to 140 dB (threshold of pain). The sound pressure level L_p can be calculated in decibels as follows with p_{ref} being the human threshold for hearing 20 x 10^{-6} Pa.

$$L_p = 20\log_{10}\left[\frac{p}{p_{ref}}\right] \tag{6}$$

The sensitivity of human hearing to different sound pressure levels in relation to frequency is depicted in Figure 4. In the figure, the curves of perceived equal loudness (phon) present the perceived loudness of a sound when compared to a 1 kHz reference. Therefore, it can be concluded from the figure for example, that a sound in 50 Hz frequency with a sound pressure level of 80 dB is perceived with equal loudness as a 1 kHz tone with 60 dB sound pressure level. (Wang, X, 2010, p. 72 – 78; Möser, M. 2009, p. 9 – 13.)

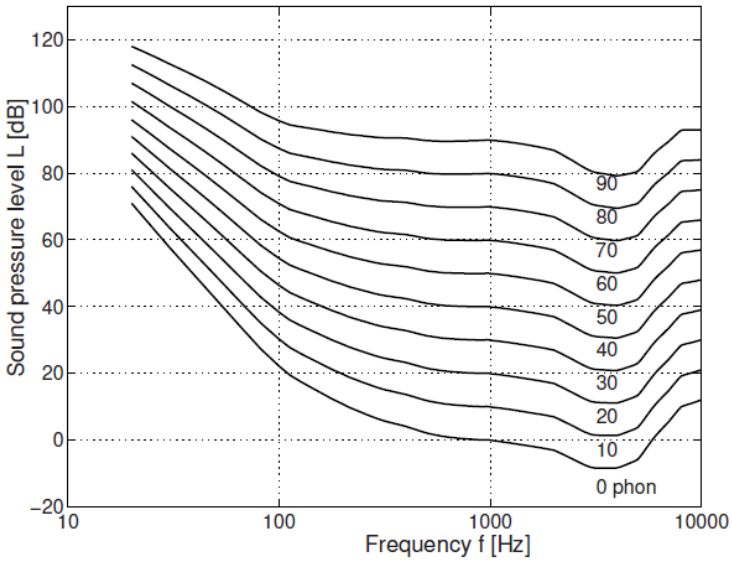

Figure 4. Human hearing perceived loudness (Möser, M. 2009, p. 9).

To determine the addition of sound pressure level from different noise sources, the simplified method is to utilize the graph in Figure 5. For example, in the figure two different noise sources have a 3dB difference *(L2 – L1)* in noise levels and this sums to a 1.7 dB difference in the total noise level ΔL. In the case where two equal magnitude sources of noise (*L2 – L1* = 0) are combined, the increase in total noise level is 3dB. In general, a sound level difference less than 3 dB will not be noticed by human perception and a difference of 10 dB can be perceived as twice as loud or quiet when compared to starting point. (Wang, X, 2010, p. 76 – 78.)

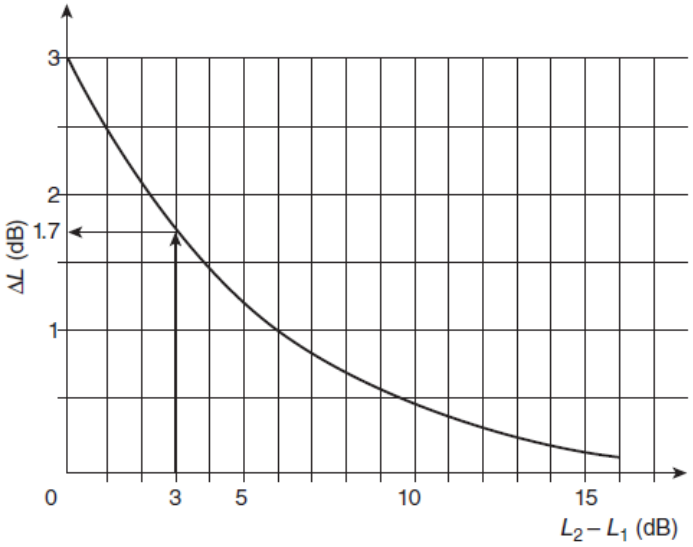

Figure 5. Addition of noise levels (Wang, X, 2010, p. 77).

2.3 Vehicle body structure noise and vibration

Vibration energy is conducted through the vehicle body structure both as airborne noise as well as structure-born noise. Thus, the vehicle body, consisting of the global body structure, body attachments and body panels, has an important role in determining the vibroacoustic atmosphere inside the vehicle. Minimizing the problem can be done e.g. by blocking the vibration energy (i.e. increasing the incoming energy impedance) or by altering the resonance frequencies of the body so that they are separated from the excitation frequencies.

However, when a motor vehicle has multiple paths through which the noise and vibration can be conducted to the body from a single source of vibration, it is generally more efficient to fix the problem at the source of the vibration than at the receiver end. In Figure 6 is presented an example of the source-path-receiver model for a vehicle. (Wang, X. 2010, p. 351 – 357.)

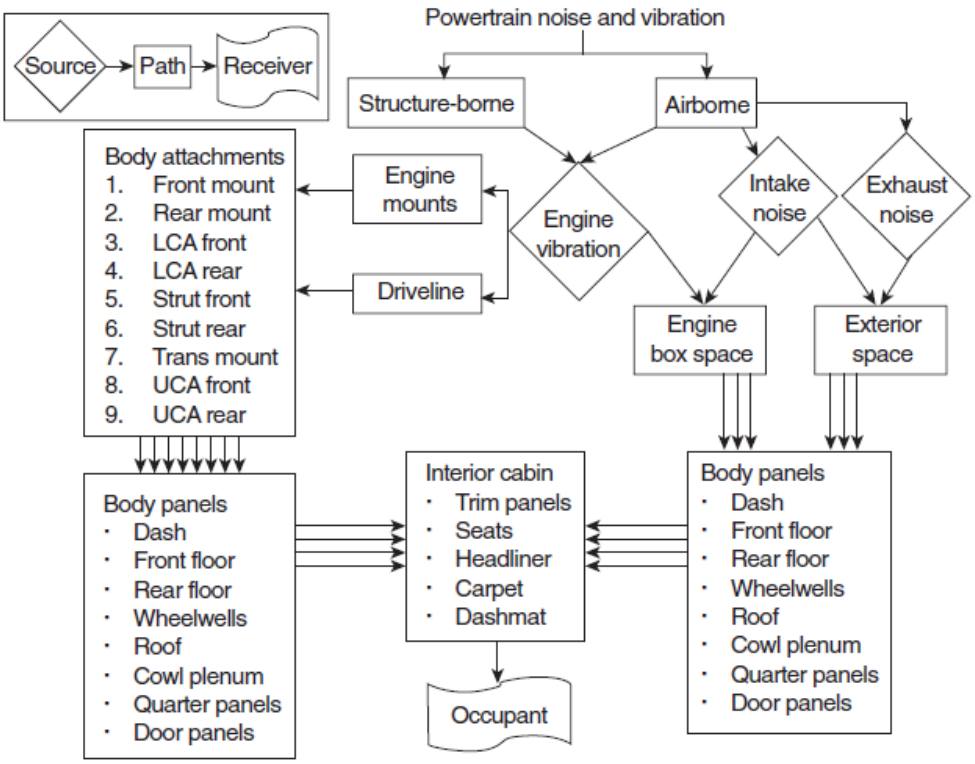

Figure 6. Example of a source-path-receiver model (Wang, X. 2010, p. 353).

2.4 Literature findings around the bus body interior vibrations

The vibro-acoustics of bus passenger compartments has been studied with experimental and modelling methods. As a general finding it has been noticed that most studies are referring to ISO standards 2631-1:1997, 2631-5:2004 and European Council directive 2002/44/EC, which are all discussing the requirements and limitations concerning mechanical vibrations' and whole-body vibrations' effect on human health. These standards are guidelines for evaluating the health effects and ride comfort of a bus passenger or driver as explained previously in this thesis.

The literature findings are divided into two categories: the studies with experimental approach and the studies with a mathematical modelling approach. This division is implemented although there are also studies employing both approaches in which case the modelling approach is the defining one.

2.4.1 The experimental approach

The experimental studies have been done to identify the areas of development regarding the vibro-acoustic properties in a bus passenger compartment. The conducted researches have been studying the noise and vibration levels with regards to e.g. bus body type (Thamsuwan, O. et al, 2013), seat stiffness and damping parameters (Jonsson, P. et al, 2015) and seat locations (Damijan, Z., 2010; Aydin, K. et al, 2016). The measured variables have been for example bus floor and seat vibrations and noise levels in various positions around the passenger and driver compartment. The data acquisition has been accomplished with e.g. acceleration measuring equipment and sound level meters. Furthermore, the analysis of the data and evaluation of the results has been done in accordance with e.g. standard ISO 2631-1.

2.4.2 The modelling approach

In the modelling approach computer simulations have been run based on numerical models. The simulations have been done alone or in parallel with experimental methods for e.g. model validation purposes. Similar with the experimental approach, the results of the simulations are evaluated with the standards as reference. The software, used in the studies, are MATLAB (Sekulic, D. et al. 2013), ADAMS multibody system dynamics package (Sekulic, D. et al. 2016) and, for the finite element method (FEM) models, ABAQUS

(Eriksson & Friberg, 2000) and ANSYS (Yansong, W. et al, 2010). In addition to the different modelling methods, the differences between the discussed studies are for example the design variables in focus (e.g. power unit insulation vs. seat suspension) and the fact that other studies were investigating only the vibrations and other studies have made a coupled analysis of both noise and vibration across the vehicle.

3 VEHICLE NOISE AND VIBRATION TESTING AND ANALYSIS

This chapter will introduce the theory and implementation for testing of vehicle noise and vibration. The chapter will present the theoretical background as well as the practical execution principles of vibration and noise testing in general and a more detailed look will be taken on the modal testing methods: experimental modal analysis (EMA) and operational modal analysis (OMA). The chapter includes also information of both measurement equipment and random signal processing and analysis. Also, a short review of operational deflection shapes (ODS) and transfer path analysis (TPA) will be given in this chapter.

3.1 Measuring equipment used in noise and vibration measurements

In this subchapter a short introduction is given to most common equipment used in noise and vibration measurements. The topics are divided between measuring of vibrations and measuring of noise.

3.1.1 Vibration measurements

The equipment used in vibration testing depends on the method used in the vibration investigations. In EMA the investigated structure is excited with a controlled source of excitation i.e. with an exciter. However, in OMA, only the response is measured under actual operating conditions, thus no exciter is needed. In both cases, the responses are measured with transducers. In addition to exciters and transducers the vibration testing system includes e.g. a signal conditioner, an analog to digital converter to digitize the measured analog signals and an analysis system to review and analyze the measured data. (Inman, D., 2007, p. 534 – 538; Siemens AG, 2014a, p. 1 – 3.)

The exciters, which are used in relation to EMA, are most commonly shakers or impact hammers. Both exciter types are used together with a force transducer, which measures the input force. A shaker provides a force to the structure relative to e.g. a sinusoidal signal in a variable frequency range or a random signal. An impact hammer is used to hit the structure thus exciting a wide range of excitation frequencies. (Inman, D., 2007, p. 534 – 538.)

The most commonly used transducer type in vibration measurements is a piezoelectric accelerometer. The operation of these accelerometers is based on the phenomenon that piezoelectric materials generate an electrical charge output proportional to force when strained. In practice the transducer consists of two masses which are separated by piezoelectric material. The other mass is fixed to the transducer case and the other is stationary. Hence, vibration of the case, fixed to the measured structure, causes varying force to be applied to the piezoelectric material and thus an analog output signal is generated. (Wang, X., 2010, p. 36 – 39.)

3.1.2 Noise measurements

Measuring microphones are specific type of microphones used for sound measurement purposes. In principle all microphones convert pressure fluctuations in air into an electrical signal. The type of microphone typically used for vehicle noise measurements is a condenser microphone due to its broad frequency response range. In a condenser microphone a tensioned metal diaphragm and a metal backplate form a simple air-capacitor. When the diaphragm vibrates due to air pressure fluctuations in a sound field, the capacitance of the air-capacitor varies and generates an output voltage which follows the air pressure fluctuations. (Wang, X. 2010, p. 80 – 83; Brüel & Kjær, 1994, p. 3 – 6.)

3.2 Signal processing and analysis

The excitations in a vehicle may occur in various forms. Random excitations from the road surface, harmonic excitations from rotating unbalances, such as unbalanced wheels, and non-harmonic periodic excitations from e.g. engine piston movements are examples of the types of excitations that may be encountered in vehicle vibration measurements. In this subchapter the topic of signal processing and analysis is covered for those parts within the scope of this thesis. For example, the digital Fourier transform (DFT) process is described, as most of the analysis within vibration research is done in the frequency domain. In addition, the analysis of random signals is discussed for relevant parts.

3.2.1 Digital Fourier transform

The method used for converting measured analog time-domain vibration data in to digital frequency-domain information is called digital Fourier transform. The method is based on the Fourier transform or Fourier series. As for any periodic signal $F(t)$ with period T,

Fourier's theory states that it may be represented by an infinite series of harmonic components in the following form:

$$F(t) = \frac{a_0}{2} + \sum_{n=1}^{\infty} \left(a_n \cos n\omega_T t + b_n \sin n\omega_T t \right) \tag{7}$$

where:

$$\omega_T = \frac{2\pi}{T} \tag{8}$$

$$a_0 = \frac{2\pi}{T} \int_0^T F(t)\, dt \tag{9}$$

$$a_n = \frac{2\pi}{T} \int_0^T F(t) \cos n\omega_T t dt \quad n = 1, 2\ldots \tag{10}$$

$$b_n = \frac{2\pi}{T} \int_0^T F(t) \sin n\omega_T t dt \quad n = 1, 2\ldots \tag{11}$$

Thus, it is the Fourier coefficients or spectral coefficients a_n and b_n defined in equations (10) and (11) which represent the frequency-domain information of a time-domain signal. In Figure 7 is presented the principle of Fourier transform in practice, i.e. an arbitrary periodic signal is decomposed in to two harmonic signals with different frequencies.

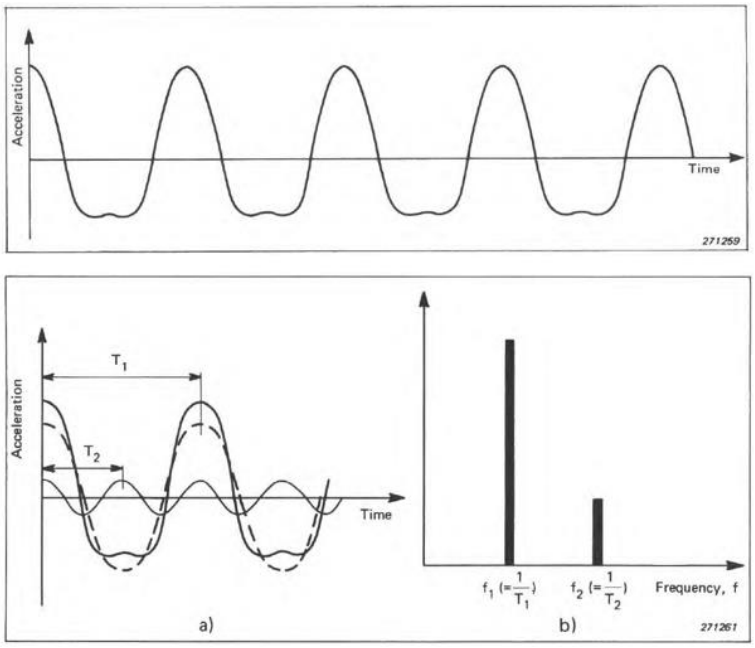

Figure 7. Fourier transform of a periodic signal (modified from Broch, J. T., 1984, p. 23 – 24).

As for DFT, the analog signal *x(t)* must first be converted into digital form x_k. Signal x_k is constructed by dividing the signal *x(t)* in to equally spaced time records t_k, with $k = 1, 2, \ldots, N$, where N is the total number of samples and Δt is the sampling interval. Thus, the Fourier transform equations 7 to 10 are converted into form:

$$x_k = a_0 + \sum_{i=1}^{N/2}\left(a_i \cos\frac{2\pi t_k}{T} + b_i \sin\frac{2\pi t_k}{T}\right) \qquad k = 1, 2, \ldots N \tag{12}$$

where,

$$a_0 = \frac{1}{N}\sum_{k=1}^{N} x_k \tag{13}$$

$$a_i = \frac{1}{N}\sum_{k=1}^{N} x_k \cos\frac{2\pi ik}{N} \tag{14}$$

$$b_i = \frac{1}{N}\sum_{k=1}^{N} x_k \sin\frac{2\pi ik}{N} \tag{15}$$

The number of samples N in DFT is for computational reasons usually a power of two (e.g. 1024, 2048, 4096…). In addition, there are a few significant things that must be taken in consideration in relation to DFT. These topics are discussed shortly below. (Inman, D., 2007, p. 538 – 543.)

Aliasing

If the DFT sampling rate is too low it may cause a phenomenon called aliasing. Aliasing means in practice that not all details of the measured analog signal are noticed due to too low sampling rate. To avoid aliasing the sampling rate or sampling frequency $f_s = 1/T$ (samples per second) should be at least twice the bandwidth of the measured signal. Modern digital signal analysis systems include also an anti-aliasing filter i.e. a low-pass filter, which cuts off all frequencies above Nyquist frequency ($f_s/2$). (Inman, D., 2007, p. 540 – 541.)

Leakage

In DFT, the periodic signals are sampled with finite sample intervals. This may cause a problem called spectral leakage if a sample cuts the signal midperiod. Leakage causes erroneous frequencies to occur in the spectrum as well as distortion in the amplitude information. This problem is solved by using a window function, e.g. a Hanning window. In a window function the original analog signal is multiplied by a weighting function, which forces the signal amplitude reduce to zero in the beginning and in the end of the sampling period. The principle of leakage is presented in Figure 8a and window function is presented in Figure 8b. (Inman, D., 2007, p. 542 – 543.)

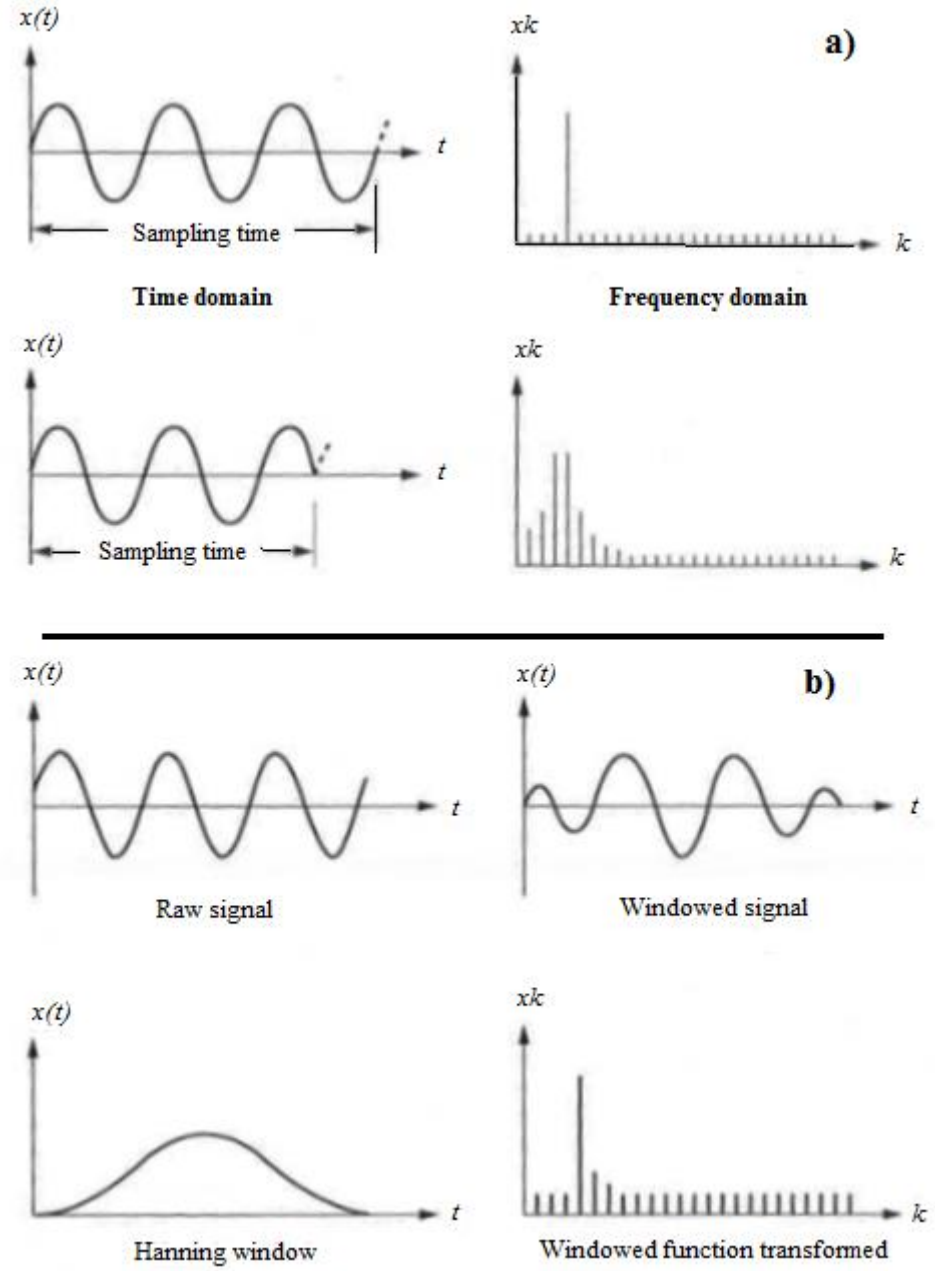

Figure 8. Principle of leakage (a) and window function (b) (modified from Inman, D., 2007, p. 543).

3.2.2 Random signal analysis

Random signals are defined so that they have no obvious pattern and no mathematical equation can describe their properties. Thus, for example for random function *x(t)*, depicted in figure 9b, the value of *X* in any given value of *t* is known only statistically and it can be described only by probability density function (PDF) as depicted in Figure 9a. In other words, the PDF describes the probability for *X* being in any particular interval of *x* + *dx*.

(Inman, D., 2007, p. 218 – 219; Brincker & Ventura, 2015, p. 17 – 19; Wang, X., 2010, p. 93 – 95.)

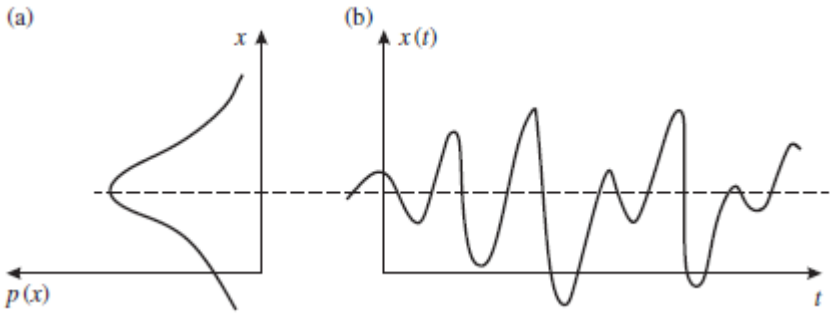

Figure 9. Random signal (b) and corresponding PDF (a) (Brincker & Ventura, 2015, p. 18).

Time-domain measures

The average $\bar{x}$ or expected value *E[x(t)]* for a random signal, which is presented by the dashed line in Figure 9 above, is defined by:

$$E\left[x(t)\right] = \bar{x} = \lim_{T\to\infty} \frac{1}{T} \int_0^T x(t)dt \tag{16}$$

In a stationary random signal, the average value of the signal stays constant during the period of observation. The mean-square value taken about the mean equals to variance σ^2, which defines the magnitude of the fluctuations in the random signal. The square root of the variance is the standard deviation σ. The variance can be defined as following:

$$E\left[\left(x(t)-\bar{x}\right)^2\right] = \sigma^2 = \lim_{T\to\infty} \frac{1}{T} \int_0^T \left(x(t)-\bar{x}\right)^2 dt \tag{17}$$

Autocorrelation function can describe both how fast the value of a variable changes as well as how big is the correlation of the variable at two different points *x(t)* and *x(t + τ).* As for the situation when $\tau = 0$, the autocorrelation function equals variance σ^2. The mathematical definition of autocorrelation $R_{xx}(\tau)$ is presented in Equation 18 and in Figure 10 is shown an example of the autocorrelation graph for a wide frequency band signal which shows how the correlation decreases as the time lag τ increases.

$$R_{xx}(\tau) = \frac{1}{T}\int_0^T x(t)x(t+\tau)dt \tag{18}$$

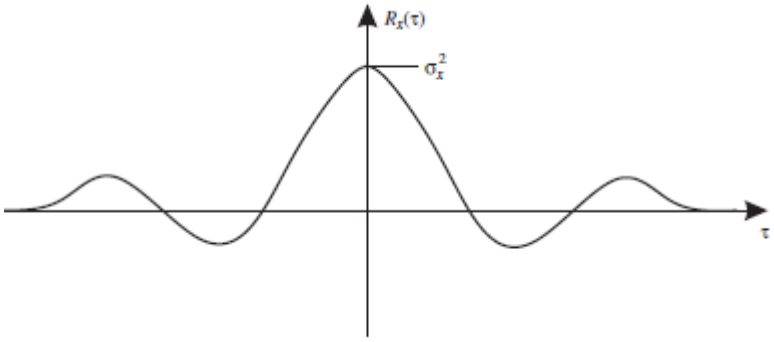

Figure 10. Autocorrelation graph for a wide frequency band signal (Brincker & Ventura, 2015, p. 25).

When discussing about the correlation between two different signals *x(t)* and *y(t)*, it defined by cross-correlation functions $R_{xy}(\tau)$ and $R_{yx}(\tau)$, which are defined by:

$$R_{xy}(\tau) = \frac{1}{T}\int_0^T x(t)y(t+\tau)dt \tag{19}$$

$$R_{yx}(\tau) = \frac{1}{T}\int_0^T y(t)x(t+\tau)dt \tag{20}$$

(Inman, D., 2007, p. 220, 224; Wang, X., 2010, p. 95 – 96, 100 – 102; Brincker & Ventura, 2015, p. 19 – 21, 24 – 27.)

Frequency-domain measures

The frequency-domain measures in random signal analysis are defined as the Fourier transforms of their time-domain equivalents. First is handled the auto spectral density $S_{xx}(\omega)$, which is the Fourier transform of the autocorrelation function $R_{xx}(\tau)$. The auto spectral density describes how energy is distributed as a function of frequency and thus it is also called the power spectral density (PSD). The auto spectral density is defined by:

$$S_{xx}(\omega) = \frac{1}{2\pi} \int_{-\infty}^{\infty} R_{xx}(\tau) e^{-j\omega\tau} d\tau \quad (21)$$

When discussing of a white noise random signal *x(t)*, it is defined that there is no correlation with *x(t + τ)* excluding $\tau = 0$. And, as for the spectral density, the value of PSD is constant for a white noise signal.

Following the logic of autocorrelation to PSD conversion, also the cross spectral density function $S_{xy}(\omega)$ is a Fourier transform of the time-domain equivalent, cross-correlation function $R_{xy}(\tau)$, and thus defined by:

$$S_{xy}(\omega) = \frac{1}{2\pi} \int_{-\infty}^{\infty} R_{xy}(\tau) e^{-j\omega\tau} d\tau \quad (22)$$

(Inman, D., 2007, p. 220; Wang, X., 2010, p. 106 – 109; Brincker & Ventura, 2015, p. 125 – 126, 130.)

3.3 Experimental modal analysis

Modal parameters, i.e. natural frequencies, mode shapes and modal damping ratio are properties for a mechanical structure which determine its response under dynamic excitation. Modal testing methods experimental modal analysis and operational modal analysis are experimental methods to produce these information for e.g. NVH development purposes. (Siemens AG, 2014a, p. 1.)

When looking at the excitation forces and structural responses in frequency domain, the variation of the amplitudes might seem uncorrelated, as can be seen in Figure 11. This is due to the response will either amplify or attenuate as the driving frequency passes by the resonant frequencies i.e. natural frequencies of the system. Amplification will occur close to the resonances and attenuation occurs at frequencies away from the resonances.

Modal analysis is a method to determine the dynamical behavior of a structure. The response, i.e. vibrations, can be measured with accelerometers and the modal parameters for each mode of vibration can be obtained by modal analysis. The modal parameters are:

- *natural frequency*: frequency in which the structure's oscillation amplifies during excitation.
- *modal damping ratio*: the amount of damping as a fraction to critical damping i.e. how fast the vibrational energy dissipates in the structure
- *mode shape*: way the structure moves in a particular mode of vibration

In experimental modal analysis, the input forces and output accelerations are measured in time domain. For example, a structure is excited with an impact hammer and the response is measured in various position of the structure with accelerometers. This measurement data is then transferred to frequency domain by fast Fourier transform (FFT) resulting in excitation spectrum *F(f)* and response spectrum *X(f)*. To be able to determine how the structure responds to dynamical input forces the output response spectrum needs to be divided with the input excitation spectrum to derive the frequency response function (FRF). The relation between FRF and input force and output response is depicted below in Figure 11. The modal parameters, as mentioned above, can be derived from the FRF as described further on in this thesis. (Structural Vibration Solutions; Wang, X., 2010, p. 117 – 118; Siemens AG, 2014a, p. 2.)

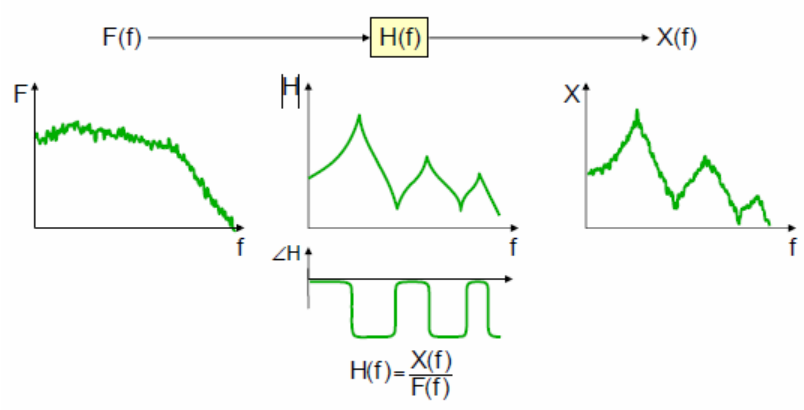

Figure 11. The FRF's relation to input force and output response spectrum (Brüel & Kjaer, 2003, p. 11).

3.3.1 Theoretical background of experimental modal analysis

Even though the real-life structures usually are multiple-degree-of-freedom (MDOF) systems, in modal analysis the system is decomposed in to several single-degree-of-freedom (SDOF) systems for computational purposes. Below, in Figure 12, is presented an example

of a simple, damped SDOF system and further on is explained how a frequency response function is calculated for such system under forced harmonic excitation.

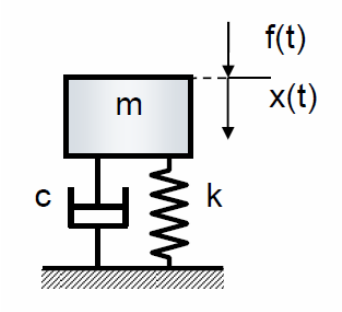

Figure 12. Damped single-degree-of-freedom system (Brüel & Kjær, 2003, p. 6).

The equation of motion for the system in figure 12 can be written as follows:

$$m\ddot{x}(t) + c\dot{x}(t) + kx(t) = f(t) \tag{23}$$

where *m*, *c* and *k* are the mass, damping and stiffness respectively. The acceleration and velocity vectors are defined respectively as the second and first-time derivatives of displacement vector *x(t)* and the applied force vector is denoted *f(t)*.

Both *x(t)* and *f(t)* can also be written in complex exponential form, i.e. $x(t) = xe^{j\omega t}$ and $f(t) = fe^{j\omega t}$, where $j = \sqrt{-1}$, and thus equation 23 can be written in the form:

$$(-m\omega^2 + j\omega c + k)xe^{j\omega t} = fe^{j\omega t} \tag{24}$$

Rearranging the equation gives the frequency response function equation:

$$H(\omega) = \frac{X(\omega)}{F(\omega)} = \frac{1}{(-m\omega^2 + j\omega c + k)} \tag{25}$$

When discussing about random signals and thus more practical situations, a significant connection is described in equation 26 between the PSD of the input force $S_{ff}(\omega)$, PSD of the

response $S_{xx}(\omega)$ and the FRF $H(\omega)$, i.e. the equation describes the equivalent for equation 25 when dealing with random excitation.

$$S_{xx}(\omega) = |H(\omega)|^2 S_{ff}(\omega) \tag{26}$$

(Inman, D., 2007, p. 126 – 129, 222 – 223; Wang, X., 2010, p. 123 – 125; Brüel & Kjaer, 2003, p. 6 – 7; Piersol & Paez, 2010, p. 571 – 573.)

3.3.2 Estimation of modal parameters from the FRF

The extraction of modal parameters (natural frequency, modal damping ratio and mode shapes) from the FRF is usually done by a process called curve fitting, which in practice is conducted by analysis software for more complex cases. There are various of curve fitting methods available for the purpose, but these are not discussed further in the scope of this research. Instead principles of modal data estimation are described through simple examples. (Wang, X., 2010, p. 133; Avitable, P., 2001, p. 8.)

Natural frequencies

Figure 13 shows the magnitude plot $|H(\omega)|$ as well as the phase plot $\angle H(\omega)$ of the FRF for a MDOF system. In simple cases measured frequency response function magnitude plot can be used to derive the modal parameters of the system. For example, in the peak picking method, picking the peaks from FRF magnitude plot can be used to determine the resonance frequencies but this simple method is only applicable if there doesn't exist closely spaced resonances and if damping is light. In other words, the peaks can be clearly separated in the plot. In addition, the phase plot of the FRF can be used to confirm the resonance peaks derived from the magnitude plot as the phase of the FRF should be +90˚ or -90˚ relating to the resonance. (Inman, D., 2007, p. 546 – 550; Wang, X., 2010, p. 133 – 136.)

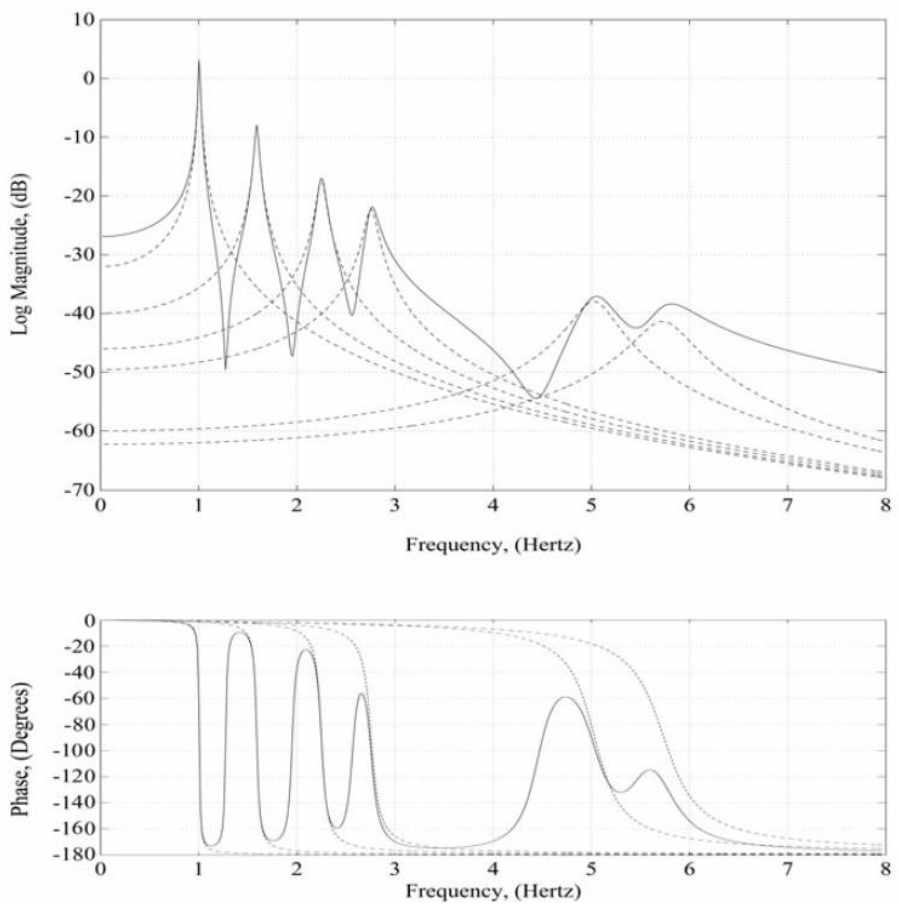

Figure 13. FRF amplitude and phase plot (Piersol & Paez, 2010, p. 584).

Modal damping

The FRF magnitude plot can be used also for the determination of modal damping ratios ζ. Figure 14 shows how modal damping ratio can be concluded from the FRF magnitude plots as they are on the 3 dB down points of the natural frequencies' amplitude peak value for a particular mode (ω_i) and can be calculated as stated in equations 27 and 28 for lightly damped systems. (Inman, D., 2007, p. 547 – 548; Wang, X., 2010, p. 133 – 136.)

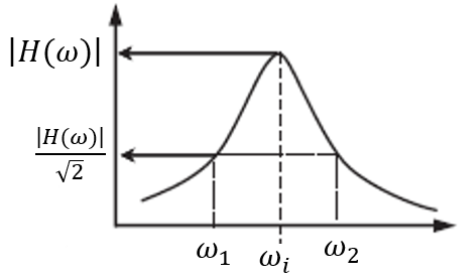

Figure 14. Determination of modal damping ratio from FRF plot (modified from Wang, X., 2010, p. 135).

$$\left|H\left(\omega_1\right)\right| = \left|H\left(\omega_2\right)\right| = \frac{\left|H\left(\omega_i\right)\right|}{\sqrt{2}} \tag{27}$$

And, as $\omega_2 - \omega_1 = 2\zeta\omega_i$, then

$$\zeta = \frac{\omega_2 - \omega_1}{2\omega_i} \tag{28}$$

Mode shapes

There are various methods available to calculate the estimation of mode shapes in a MDOF system. In the example below, the transfer function matrix or receptance matrix can be utilized to calculate the mode shape vectors as described by Inman (Inman, D., 2007, p. 554 – 560). Referring to the equation of motion (24) and denoting $xe^{j\omega t} = \boldsymbol{u}e^{j\omega t}$, where $\boldsymbol{u}$ is the response vector, the equation can be written in the form:

$$\mathbf{u} = (\mathbf{K} - \omega^2\mathbf{M} + j\omega\mathbf{C})^{-1} f = \boldsymbol{\alpha}(\boldsymbol{\omega}) f \tag{29}$$

Where **K**, **M** and **C** are stiffness, mass and damping matrices respectively. Equation 29 includes the receptance matrix **α(ω)**, defined as:

$$\boldsymbol{\alpha}(\boldsymbol{\omega}) = (\mathbf{K} - \omega^2\mathbf{M} + j\omega\mathbf{C})^{-1} \tag{30}$$

By utilizing the transformation used to derive modal coordinates in modal analysis theory, the equation can be formulated to following form:

$$\boldsymbol{\alpha}(\boldsymbol{\omega}) = \sum_{i=1}^{n}\left[\frac{\mathbf{u}_i\mathbf{u}_i^T}{(\omega_i^2 - \omega^2) + (2\zeta_i\omega_i\omega)\,j}\right] \tag{31}$$

The equation 31 presents a form of the system's transfer function which gives a connection between the receptance matrix and the mode shapes of the system. $\boldsymbol{u}_i$ is the *i*th mode shape

vector of the system, ω_i is the ith measured natural frequency, ω the driving frequency and ζ_i the ith measured damping ratio. Below in Figure 15 is presented an example of a mode shape matrix $\mathbf{\Phi}$ for a 4 DOF system containing the mode shape vectors $\boldsymbol{u_i}$ in each column.

$$\mathbf{\Phi} = \begin{pmatrix} \mathbf{u}_1 & \mathbf{u}_2 & \mathbf{u}_3 & \mathbf{u}_4 \\ -0.0207 & 0.0467 & 0.0347 & -0.0099 \\ -0.0207 & 0.0132 & -0.0154 & 0.0529 \\ -0.0207 & 0.0032 & -0.0211 & -0.0151 \\ -0.0207 & -0.0205 & 0.0161 & 0.0016 \end{pmatrix}$$

Figure 15. Mode shape matrix for a 4 DOF system with the mode shape vectors highlighted in each column.

In addition, Figure 16 presents a plot of the 4 DOF system mode shapes, occurring separately at the four natural frequencies of the system, based on the mode shape matrix presented in Figure 15. From the plot can be concluded that the first mode of the system is a rigid body mode with no relative displacement between the nodes and the other three modes are elastic modes with varying relative displacements between the nodes. (Inman, D., 2007, p. 554 – 560.)

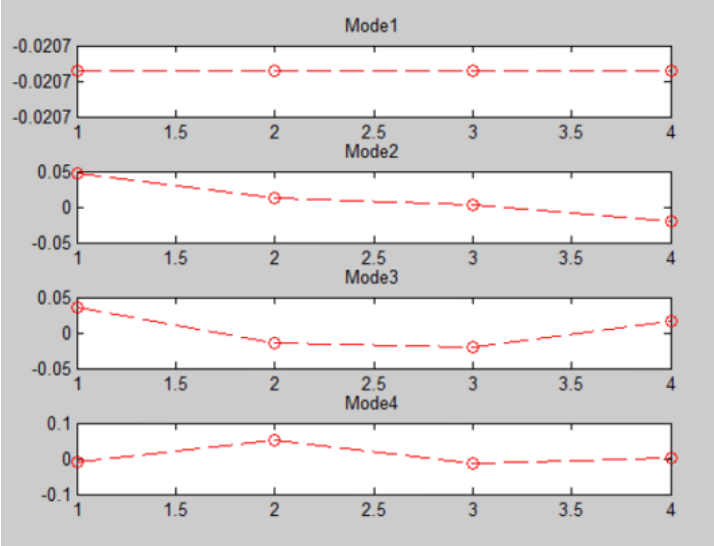

Figure 16. Plots of the mode shapes of a 4 DOF system.

3.3.3 Modal assurance criterion

The modal assurance criterion (MAC) can be used to analyze the correlation between two mode shape vectors acquired by e.g. EMA or OMA. If the mode shape vectors are like each other the MAC will have a value of one or 100 % and if the mode shape vectors are different, the MAC value will be close to zero. I.e. a mode shape compared to itself will have a MAC value of one or 100 %. In an ideal case the mode shapes should be unique and thus have a different shape compared to the other modes.

The MAC analysis can be used to two different purposes in validation of EMA or OMA results: First, MAC can be used to verify the uniformity of results from two mode sets. Secondly, MAC can be utilized to compare a mode set to itself in order to verify that each of the mode shapes are unique.

The MAC values can be visualized by a MAC matrix as shown in Figure 17. A MAC matrix is a matrix of bar graphs containing the MAC values. And, as described above, the diagonal elements of the MAC matrix should be close to 100 %

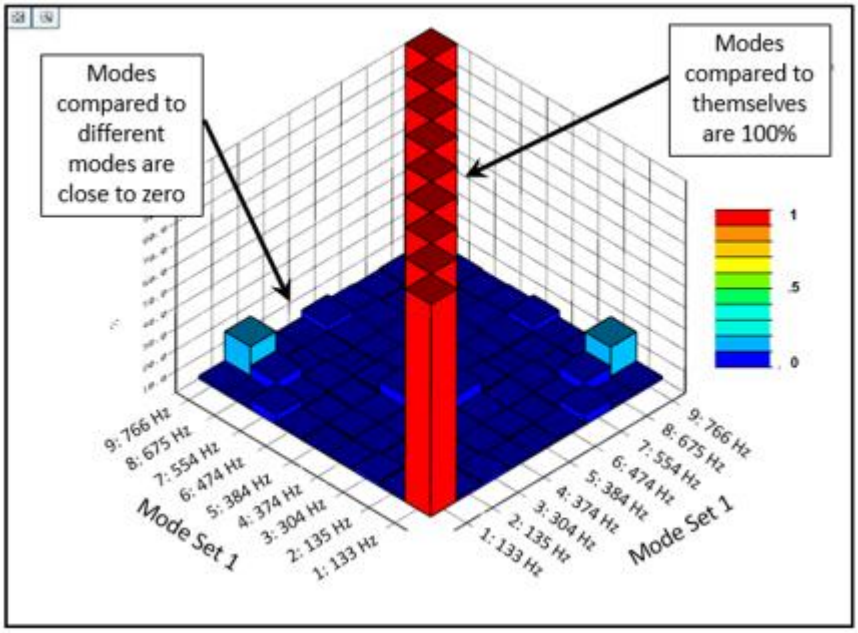

Figure 17. MAC matrix (Siemens AG, 2016).

As mentioned before, MAC shows the correlation between the two modal vectors. The mathematical definition of MAC is given below in equation 32. When taking in

consideration that: $a^H a = |a|^2$, $b^H b = |b|^2$ and $a^H b = |a||b|\cos(\theta)$, the reformation of the equation shows that MAC value is equal to the $cos^2(\theta)$, where θ is the generalized angle between two modal vectors *a* and *b*. (Siemens AG, 2016; Brincker & Ventura, 2015, p. 296, 35 – 36.)

$$MAC(a,b) = \frac{|a^H b|^2}{(a^H a)(b^H b)} = \frac{\left[|a||b|\cos(\theta)\right]^2}{(|a||b|)^2} = \cos(\theta)^2 \quad (32)$$

3.4 Operational modal analysis

For example, in vehicle noise and vibration research it is not possible to implement experimental modal analysis in actual operating conditions. This is one of the reasons for utilizing operational modal analysis as a research method instead. In OMA, the structure is tested under normal operating conditions and only the response is measured. In other words, the excitation forces are not known and the dynamic properties i.e. the modes of the structure are estimated from the response through certain assumptions made on the input forces.

In OMA, part of the input is assumed to be a Gaussian white noise stochastic process, which means that the assumed exciting random signal has equal energy level in all frequencies (constant value of PSD), the probability distribution of the signal is Gaussian and the correlation of the signal is zero. In other words, the input excites all the modes equally. Other part of the excitation comes from an imaginary loading filter, which shapes the white noise signal to have similar energy distribution as the unknown input forces through the frequency range of interest, i.e. the response of the system is assumed to consist of the dynamic properties of the system when excited by white noise filtered by a loading filter as depicted in Figure 18. (Ranieri, C & Fabbrocino, G. 2014, p. 1 - 3; Brincker, R. & Ventura, C. 2015, p. 1 – 3.)

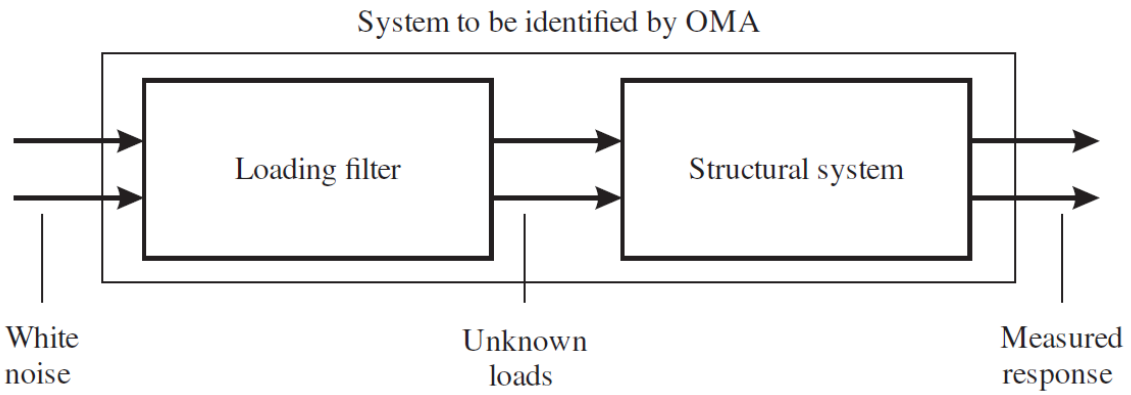

Figure 18. OMA process description (Brincker & Ventura, 2015, p. 2).

3.4.1 Practical execution of OMA measurements

In practice, the requirement of OMA is that the system must be excited sufficiently by multiple inputs in a broad banded frequency range to satisfy the above-mentioned assumption that all modes are excited equally. In vehicle testing this part is taken care of e.g. by the random input from the road surface added with powertrain related excitations when vehicle is in movement. The responses are measured usually with accelerometers positioned in various points of the tested structure, forming a test setup. The measurements might be done with just single test setup or various test setups i.e. the transducers are moved from one point to another between repeated measurements. The information derived from each test setup is called a data set.

In case of multiple test setups, few of the transducers are kept in their positions during all the test setups. Purpose of the reference transducers is to provide reference point for e.g. scaling purposes between the test setups and the mode shapes measured in each setup. Thus, it is good to have the reference transducers positioned in such positions, where at least one mode of interest produces good amplitude response through all test setups. In practice this is secured by using more than one reference transducer in measurements. (Rainieri & Fabbrocino. 2014, p. 8 - 10; Brincker & Ventura. 2015, p. 11 – 13.)

3.4.2 Estimation of modal parameters in OMA

For the estimation of modal parameters, same frequency-domain method can be used which was described previously in subchapter 3.3.2, i.e. the peak-picking method. The assumption is that the structure will have amplified responses near the modes of vibrations, i.e. natural

frequencies. These “peaks” can be identified from the PSD plots computed from the measured time-domain measurement data. In this context Brincker & Ventura (2015) gives an example in connection of OMA for calculating the mode shapes based on autocorrelation function. The response ***x(t)*** in frequency-domain dominated by a single mode is:

$$\mathbf{x}(t) = \mathbf{u}_i q(t) \tag{33}$$

where $\boldsymbol{u}_i$ is the mode shape of the particular mode and *q(t)* is the modal coordinate for the mode. Following this, the autocorrelation function of the modal coordinate is defined by:

$$R_x(\tau) = E\left[\mathbf{x}(t)\mathbf{x}(t+\tau)^T\right] = \mathbf{u}_i E\left[q(t)q(t+\tau)\right]\mathbf{u}_i^T = R_q(\tau)\mathbf{u}_i\mathbf{u}_i^T \tag{34}$$

where $R_q(\tau)$ is the autocorrelation function of the modal coordinate. Hence the spectral density matrix of the response is:

$$\mathbf{S}_{xx}(\omega) = \mathbf{S}_q(\omega)\mathbf{u}_i\mathbf{u}_i^T \tag{35}$$

From where the mode shapes $\boldsymbol{u}_i$ can be estimated from the columns in $\mathbf{S}_{xx}(\omega)$. (Ranieri & Fabbrocino. 2014, p. 127 – 130; Brincker & Ventura. 2015, p. 265 – 266.)

3.5 Operational deflection shapes

As stated by Brincker & Ventura (2015) Operational deflection shapes (ODS) can be defined as deflection of two or more points on a structure produced by an excitation in a particular frequency. In distinction to EMA or OMA, ODS contains both forced and resonant responses of the structure whereas EMA and OMA characterize only the resonances. I.e. the ODS are defined for a particular frequency instead of OMA and EMA, where modes are related to natural frequencies only. (Brincker & Ventura. 2015, p. 10 – 11.)

3.6 Transfer path analysis

Transfer path analysis (TPA) is utilized to assess the paths of structure- and airborne vibration and noise from the source to receiver. Through TPA it is possible to evaluate the contribution of different sources and paths of noise and vibration to a particular receiver

location as described in principle in Figure 19. TPA can be used to supplement ODS and experimental modal analysis methods EMA and OMA in NVH investigations. (Siemens AG, 2014b, p. 1 – 6.)

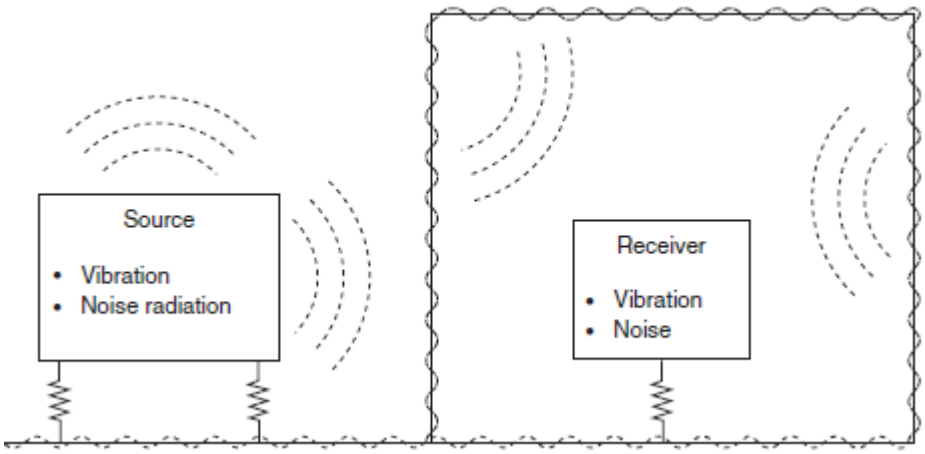

Figure 19. Noise and vibration paths from source to receiver (Wang, X. 2010, p. 190).

4 CITY BUS INTERIOR NOISE AND VIBRATION MEASUREMENTS

In this chapter is described the execution and results of noise and vibration investigations for Scania Citywide LE city bus. Also benchmarking measurements were conducted for a Mercedes-Benz Citaro city bus for reference. The investigations are also discussed in the reports by VTT (Nieminen, V. 2018; Lamula, L. et al. 2017)

The measurements included two phases: First phase noise and vibration measurements were conducted to establish basis for further investigations. In this phase also benchmarking measurements were conducted with a best-in-class competitor for target setting purposes. Second phase extended investigations were conducted only with Scania Citywide LE and the measurements were planned based on the first phase measurement results. The extended investigations included e.g. operational modal analysis measurements, with the purpose of finding out the sources and paths of noise and vibration in the bus passenger compartment and to understand how the vehicle behaves dynamically when operated in normal operating conditions.

A technical introduction of both vehicles is given in the beginning of this chapter and next the research methods are described for both the first and second phase measurements. In addition, the results and analysis of the measurements are presented together with the method description so that the reader can get a complete perception of the investigation process and produced outcome. A summary of the results and analysis is also given further on in the Discussion-chapter.

4.1 Vehicles under investigation

In this subchapter is given the technical description for primary test vehicle Scania Citywide LE city bus and the benchmarking vehicle Mercedes-Benz Citaro. The properties of the bus body as well as the chassis and powertrain are described for those parts that are seen relevant for the scope of this thesis.

4.1.1 Scania Citywide LE

The test vehicle, Scania Citywide LE, chassis type K 280 UB4x2LB, depicted in Figure 20, is a bus designed for city transportation. The assembly and design of the bus body structure is executed by Scania OmniExpress Bus Production (SOE). The chassis and powertrain is assembled and designed by Scania CV in Södertälje, Sweden. The vehicle has been manufactured in 2016 and has been mainly used for prototyping purposes at SOE.

Figure 20. Scania Citywide LE

The body has a low entry structure, which means that both doorways of the bus are on low level for easier accessibility and, from the rear doors to the aft of the bus, the floor level rises to accommodate the rear axle and other powertrain and chassis components. The design is depicted below in Figure 21.

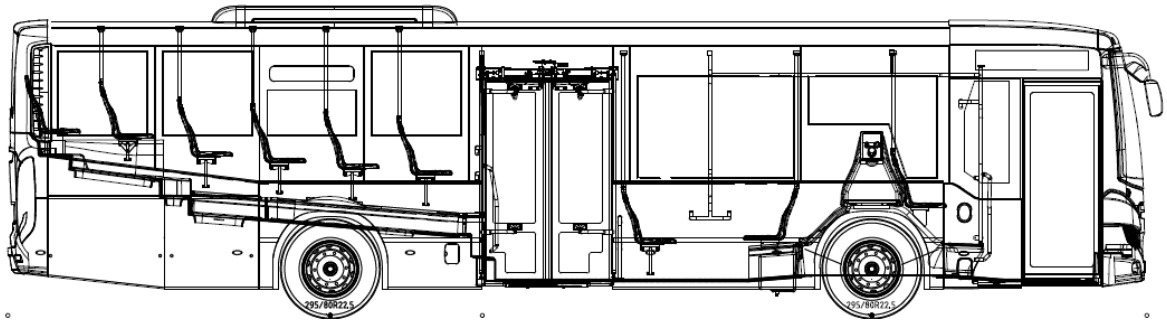

Figure 21. Overview of the low-entry bus body structure.

Body structure

The 12 meters long bus body structure, depicted in Figure 22, has been manufactured of a stainless-steel tube frame. The body structure is attached with fixed welded joints to the chassis front and rear chassis modules. The outer skin of the bus body is assembled mainly of steel sheets fixed with adhesives to the body structure. The interior of the bus body is constructed of polymers or polymer-based composites. For example, the floor structure, visible also in Figure 22 is manufactured of several composite modules, fixed to the body frame with adhesives. The primary noise and vibration attenuation in the body structure is executed with a combined layer of damping and absorption material fixed to the composite floor structure.

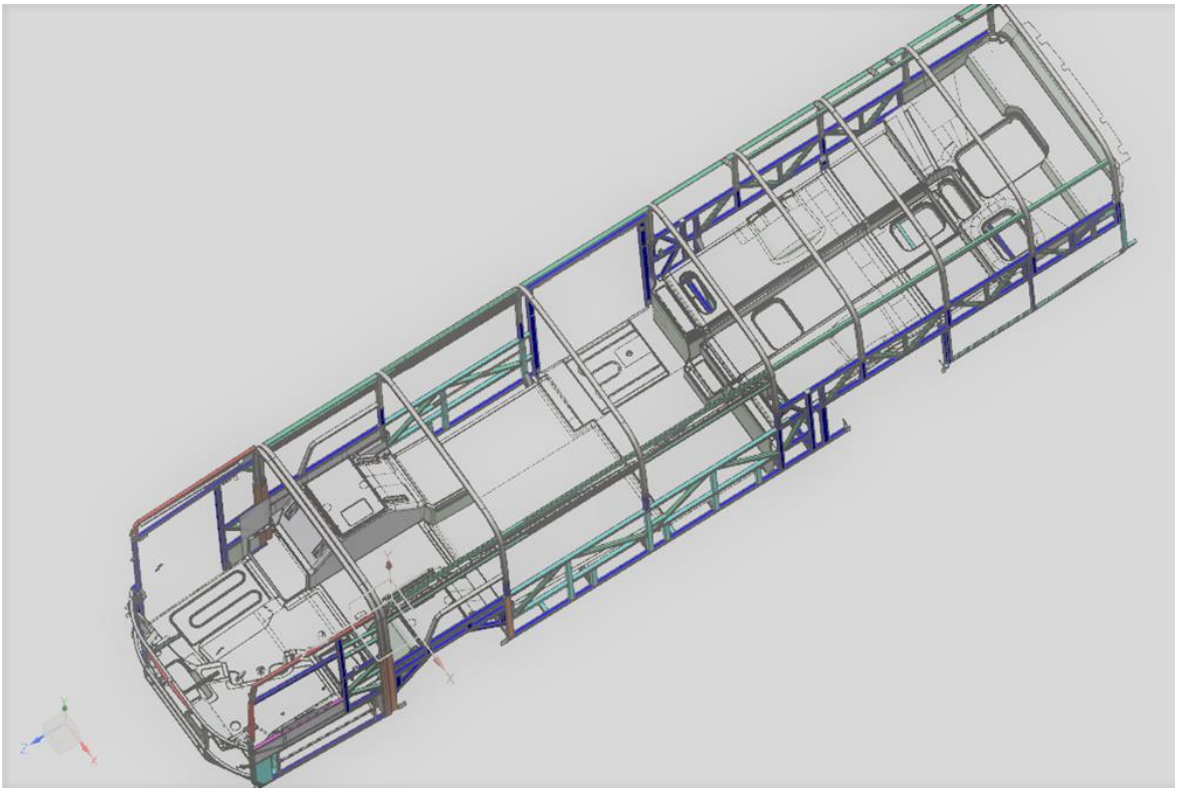

Figure 22. Scania Citywide LE body structure.

Chassis components

The chassis structure of the bus is constructed of front and rear chassis modules which include the chassis frame structure and all chassis and powertrain components. An overview of the rear and front chassis modules (excluding most powertrain components) is presented in Figure 23.

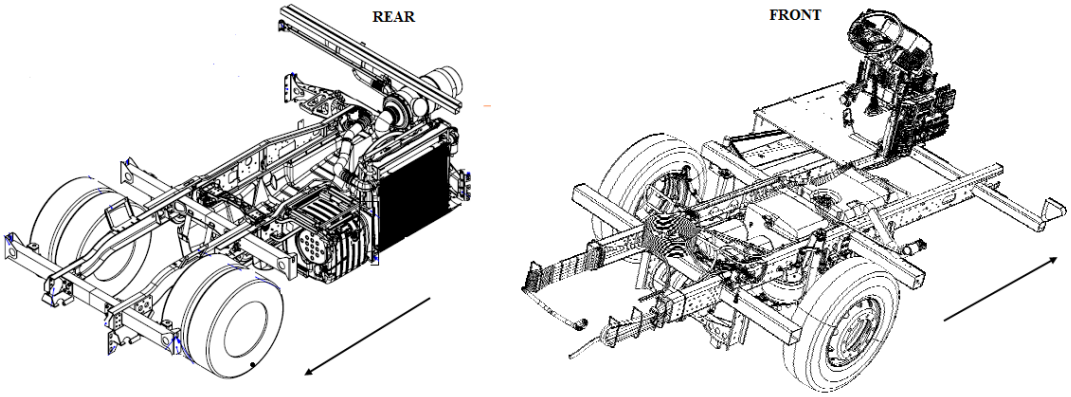

Figure 23. Front and rear chassis modules.

The vehicle has two axles, both air-sprung and equipped with shock absorbers. The rigid front axle is sprung with two air bellows and the conventional type driving axle is sprung with four air bellows. Components are attached to the chassis frame with rubber bearings working as shock and vibration isolators. An overview of the front and rear axle suspension assembly is depicted in Figure 24.

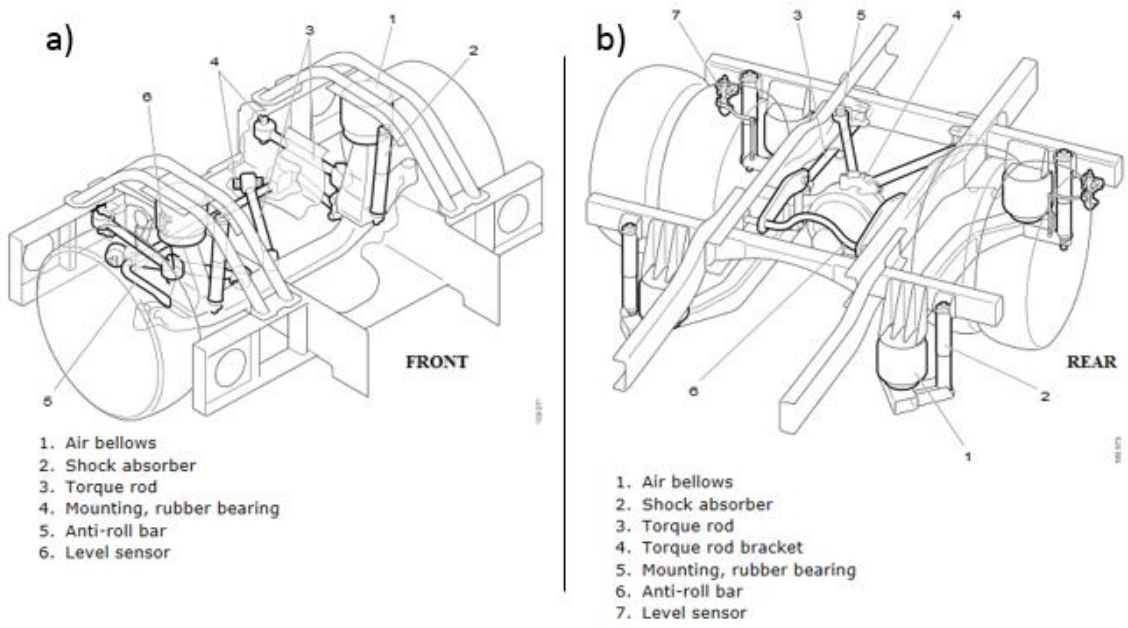

Figure 24. Front (a) and rear (b) axle suspension.

Powertrain components

The 280hp, 7-liter, 6-cylinder, Euro 6, inline diesel engine is fixed to the chassis frame from two points with vibration insulators, as depicted in Figure 25. The purpose of the insulators

is to block the engine vibrations to be transmitted to the chassis frame and thus to other parts of the vehicle.

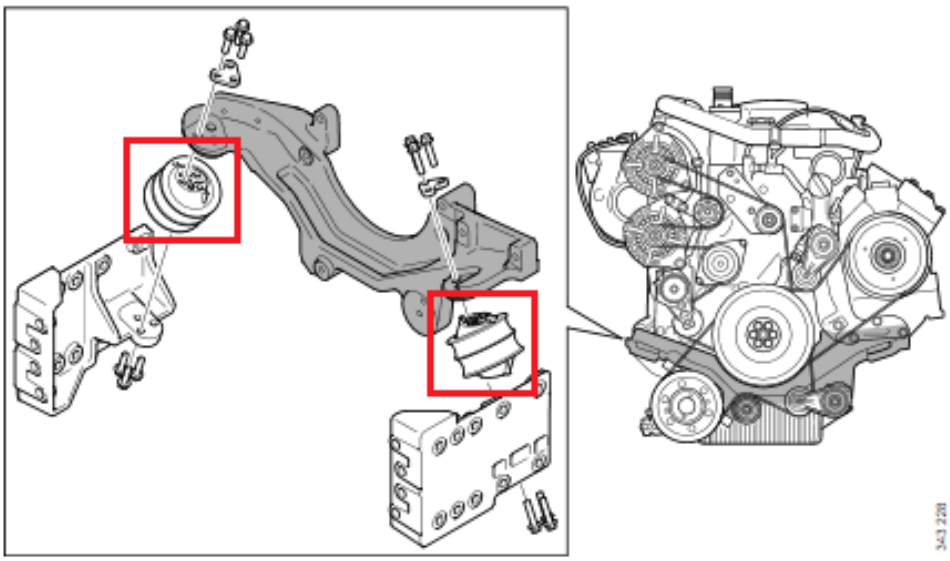

Figure 25. Engine vibration insulators.

The vehicle has a 6-gear ZF Ecolife automatic transmission transmitting the engine torque further on to the powertrain. The gear ratios of the transmission are presented below in Table 1 excluding reverse gear.

Table 1. Gear ratios of the ZF Ecolife automatic transmission.

Gear:	*1st*	*2nd*	*3rd*	*4th*	*5th*	*6th*
Gear ratio:	3.36	1.91	1.42	1.00	0.72	0.62

As was described previously for the engine, also the transmission is attached from two points to the chassis frame with vibration insulators. These are depicted below in Figure 26.

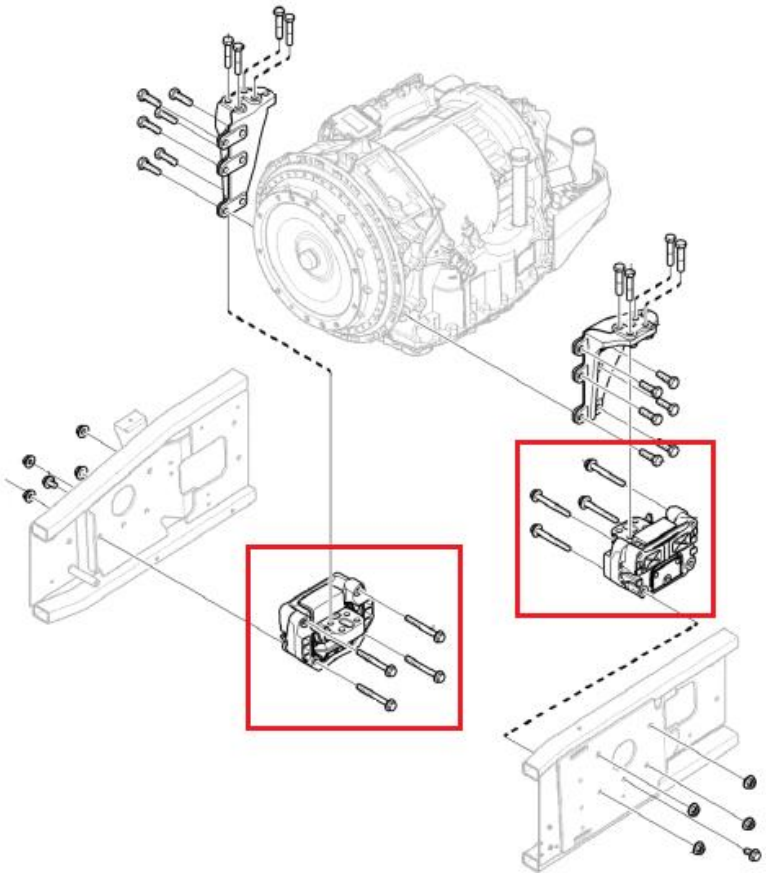

Figure 26. Transmission vibration insulators.

In the test vehicle, the gear ratio of the rear axle central gear was 5.57. The pinion (7 teeth) and the crown wheel (39 teeth) determine the driving axle gear ratio and produce the gear reduction between the transmission output and the wheels. An overview of the driving axle gear is presented below in Figure 27, where is also highlighted the main central gear components crown wheel (1), pinion (2) and axle differential (3).

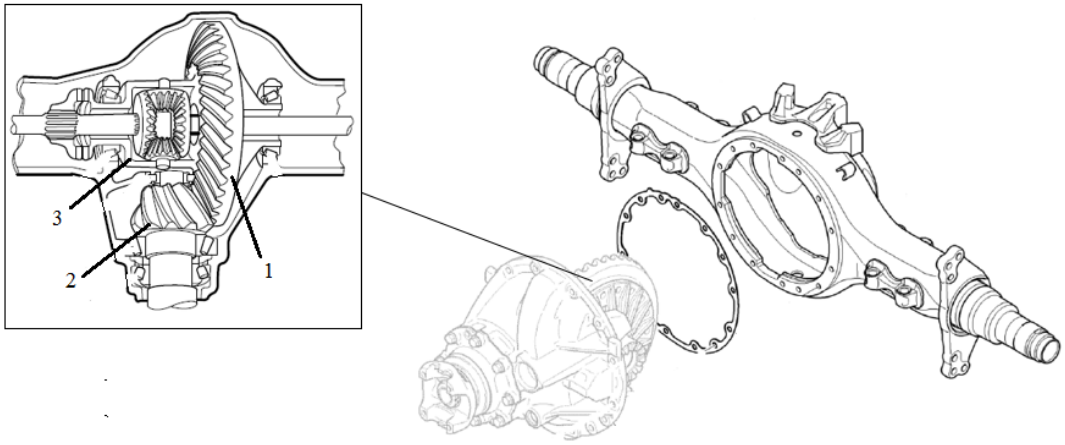

Figure 27. Rear axle gear, with main components: crown wheel (1), pinion (2) and axle differential (3).

Tyre dimensions in the bus were 295 / 80 R22.5 for both the driving axle and the front axle. Scania technical specification states that nominal rolling circumference for these type of tyres is 3.184 m. This value is used in the calculations of wheel speed related frequencies.

As a summary, the powertrain configuration is presented in Figure 28 with gear ratios μ positioned in the graph following equations for calculating the rotational frequencies n. Also, the vibration insulators for both transmission and engine are depicted with approximated positions.

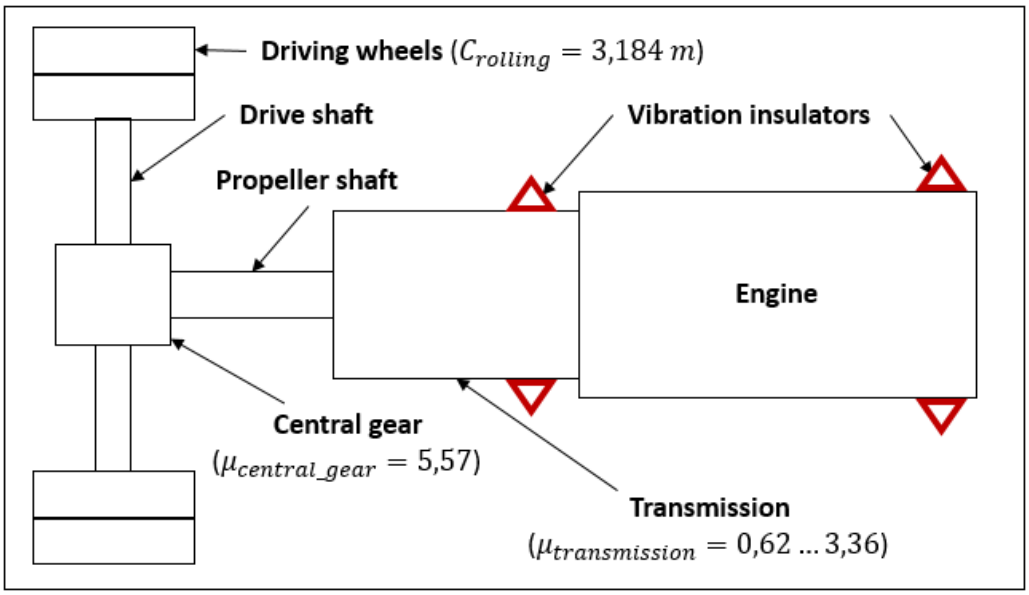

Figure 28. Powertrain configuration of Scania Citywide LE.

The engine rotational frequency in rpm can be converted into engine rotational frequency (Hz) as stated below:

$$n_{engine} = \frac{n_{engine,rpm}}{60} \tag{36}$$

The propeller shaft transmits the engine torque to driving axle central gear from transmission output. The gear ratio of the selected gear in transmission $\mu_{transmission}$ determines the propeller shaft rotational frequency (Hz) as defined below:

$$n_{propshaft} = \frac{n_{engine}}{\mu_{transmission}} \tag{37}$$

The drive shaft rotational frequency and thus also wheel rotational frequency (Hz) is determined by the driving axle central gear ratio $\mu_{central\_gear}$. The drive shaft rotational frequency can be calculated by equation:

$$n_{drive\_shaft} = \frac{n_{propshaft}}{\mu_{central\_gear}} \tag{38}$$

Finally, the radial velocity of the wheels and thus the vehicle speed in km/h can be calculated with the aid of tyre nominal rolling circumference value $c_{rolling}$ as stated below:

$$v = n_{drive\_shaft} \cdot c_{rolling} \cdot 3.6 \tag{39}$$

4.1.2 Benchmarking vehicle

The benchmarking vehicle used in this study was a Mercedes-Benz Citaro, year model 2014. The vehicle has been used in city transportation operations by a local bus transportation company in Lahti, Finland. The vehicle, corresponding the one depicted in Figure 29, has similar type of configuration of the body structure and chassis as the test vehicle by Scania. The 12 meters long two-axial vehicle has a 6-cylinder, 7.7 liters, 295hp Euro 6 inline diesel

engine and an automatic transmission. The chassis is air sprung with the difference that the front wheels are independently suspended without a rigid front axle.

Figure 29. Mercedes-Benz Citaro city bus (Wikimedia Commons).

4.2 First phase noise and vibration measurements

The first phase noise and vibration measurements were conducted for the primary test vehicle Scania Citywide LE as well as the benchmarking vehicle from Mercedes-Benz. The purpose of the measurements was to measure the noise and vibration levels in different positions within the bus interior as well as conduct an analysis of the noise and vibration in frequency domain. The frequency domain data of the measured vibration and noise data was also compared to engine and wheel rotational frequency orders to estimate the sources for measured amplitude peaks.

4.2.1 Test procedure and instrumentation

The measurements were made with vehicles stationary (engine running) and vehicles in acceleration and constant speed motion to collect data in different operating conditions. The driving sequences included both slow and fast accelerations and decelerations with constant driving speeds being approximately 50 and 80 km/h.

Tests were conducted in Lahti-Vesivehmaa airfield taxiway with approximately 1-kilometer length of the test track. The test track is depicted in Figure 30.

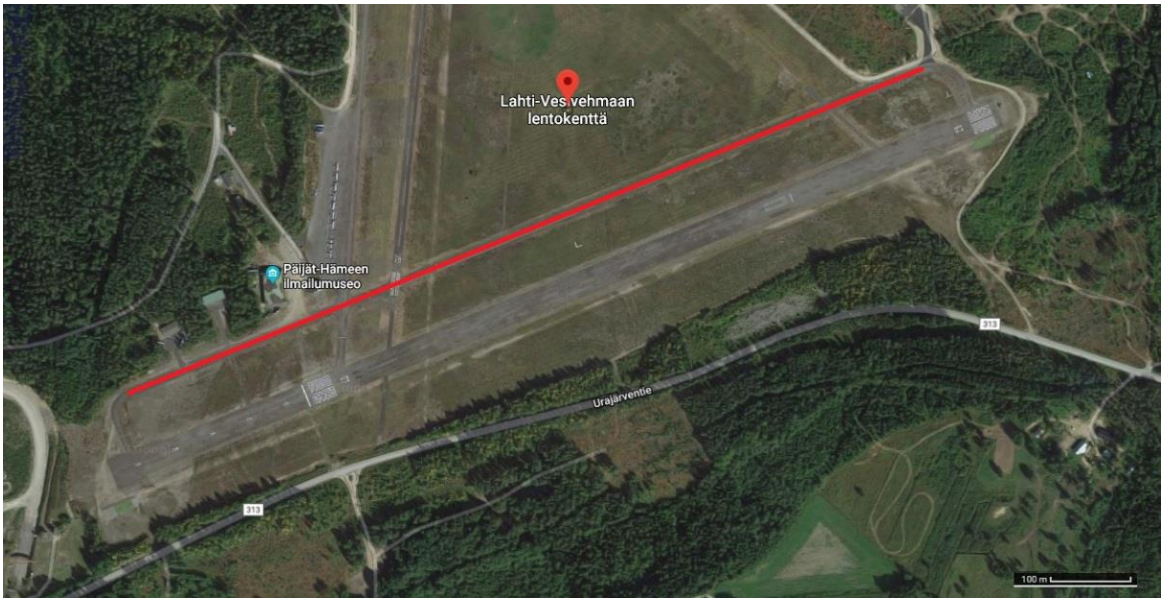

Figure 30. Test track for the first phase measurements at Lahti-Vesivehmaa airfield (modified from maps.google.com).

The measurements with the Scania were conducted with seven condenser microphones (Brüel&Kjaer 4189) and five tri-axial piezoelectric accelerometers (Kistler 8766A50M5) positioned in various positions inside the bus interior as depicted in Figure 31, one accelerometer positioned in the chassis frame cross beam and one accelerometer positioned in the engine compartment close to the engine vibration insulator in the right-side chassis frame beam. The main data acquisition system used in the measurements was a Siemens LMS Scadas SC310-UTP and the data was analyzed with Siemens LMS Test.Lab software. In addition, parallel measurements were conducted with three one-axial accelerometers (MEAS 4604) mounted tri-axially in a mounting block and connected to a Dewesoft DEWE 43 A data acquisition system and data was analyzed by the Dewesoft X software. This system was also connected to the vehicle CAN bus to collect e.g. engine rpm and wheel speed data needed in the order tracking analysis. Synchronization of the measurements between the two different systems was done by giving an impact to the driver seat platform before each test sequence. The positions of the accelerometers are depicted in the Figure 31 and the positions of the microphones in Figure 32.

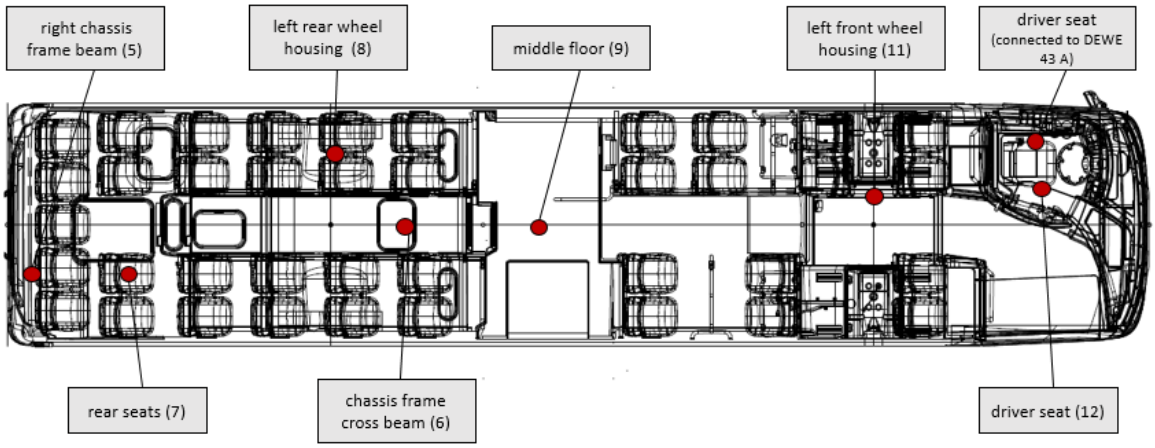

Figure 31. Accelerometer positions for first phase measurements.

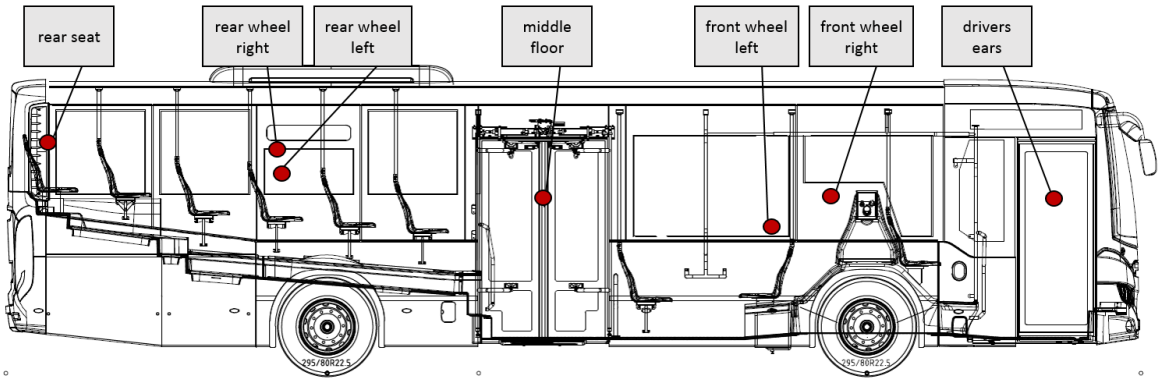

Figure 32. Microphone positions for first phase measurements.

The measurements with the benchmarking vehicle were made with 7 microphones and only one tri-axial accelerometer. The positions of the microphones were identical to the setup with the Scania measurements shown in figure 32. The accelerometer was positioned in the engine compartment, close to the engine vibration insulator during the stationary measurements and when the vehicle was tested in motion, the accelerometer was attached to the driver seat platform. No parallel measurements were made with Dewesoft hardware and thus no CAN data was neither collected. The data acquisition system used in the benchmarking measurements was a portable Siemens Scadas SC-XS12-A.

4.2.2 Results

The results of the first phase measurements are divided in benchmarking noise and vibration level results between Scania and the Mercedes-Benz and this is followed by a more deeper review on the noise and vibrations in frequency domain for the Scania bus. Due to being

able to get e.g. engine rpm, wheel speed and selected gear information by logging the Scania's CAN bus, it was possible to compare this information with the measured noise and vibration data. This enabled order tracking i.e. estimating whether some order of certain operating frequencies (e.g. engine combustion frequency) in the vehicle are equal to the resonance frequencies in the bus body structure.

To be noted regarding most presented spectrums and spectral maps within this research is, that an autopower linear function is implemented when presenting averaged amplitude data in frequency domain. The autopower linear function first squares the measured amplitudes and then takes a square root of the squared values. This is done to take away the phase information away from the amplitude spectrum thus providing more meaningful amplitude information.

Benchmarking results

When comparing the interior averaged A-weighted noise levels between the Scania and Mercedes-Benz in e.g. constant driving speed of 50 km/h, Scania produced higher sound pressure levels in all measurements positions. In Figures 33 and 34 are presented the A-weighted, averaged autopower sound pressure spectrum plots together with averaged sound pressure values measured from the rear left wheel and middle floor measurement points respectively. In the frequency range from 0 to 1000 Hz Scania produced in average 3dB higher level of noise in averaged sound pressure levels in both, the middle floor region as well as the rear wheel region.

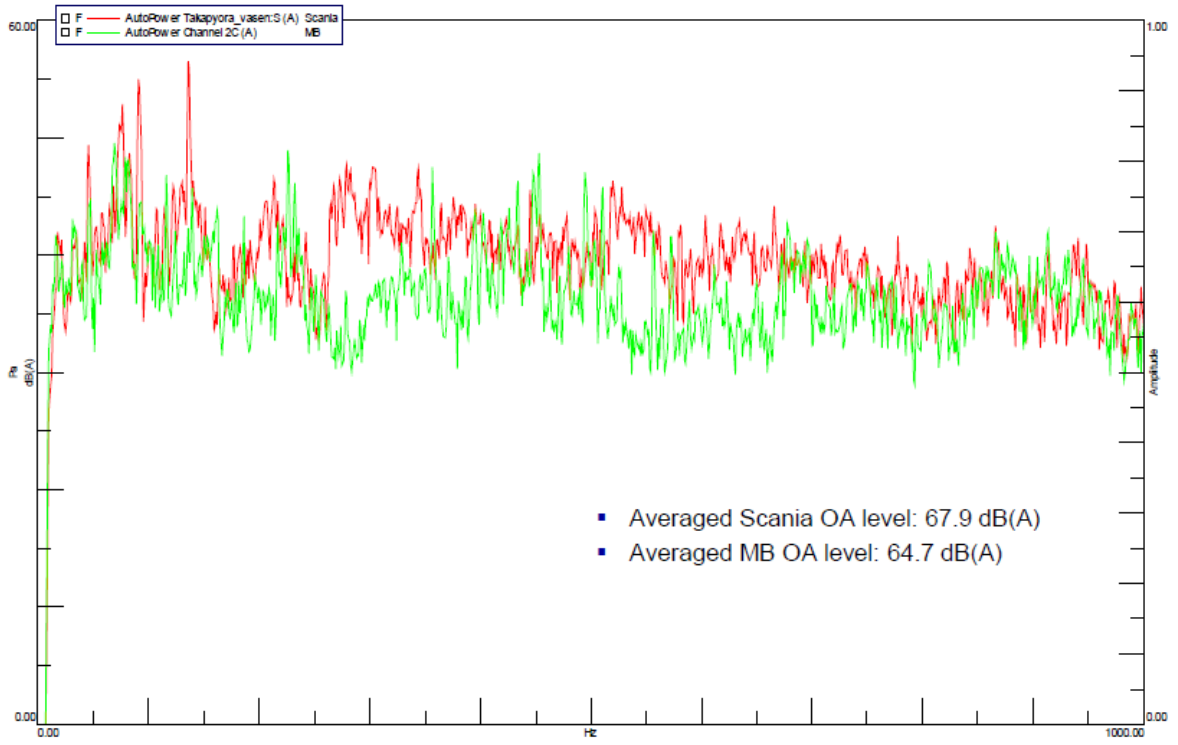

Figure 33. Rear left wheel noise. Green lines represent the measured values for Scania and the red lines represent values measured for Mercedes-Benz.

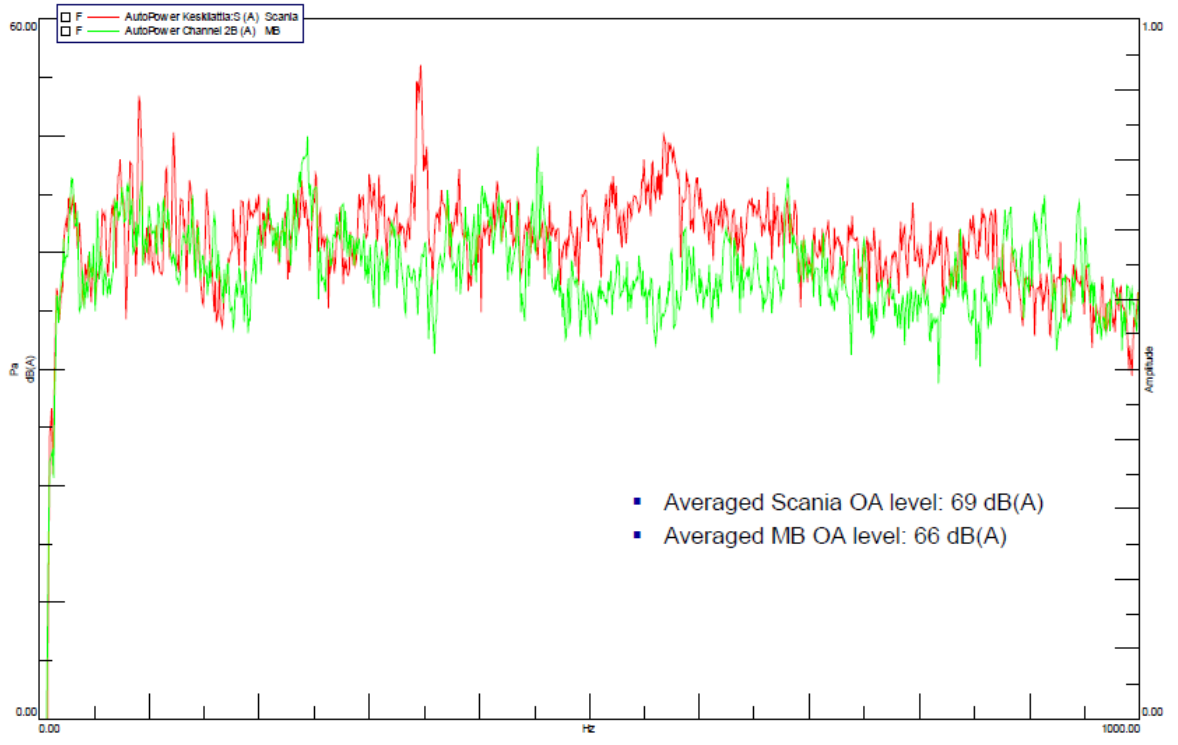

Figure 34. Middle floor noise. Green lines represent the measured values for Scania and the red lines represent values measured for Mercedes-Benz.

As for the idling situation, with vehicles stationary, the vehicles did not seem to produce so significant difference in the sound pressure levels. Both vehicles however showed almost 10 dB difference in sound pressure levels when appliances, i.e. air compressor for the pneumatic system and air conditioning system where turned on. Figure 35 shows the A-weighted sound pressure measurement result from middle floor measuring point with vehicles idling with appliances turned off in the upper plot and appliances turned on in the lower plot.

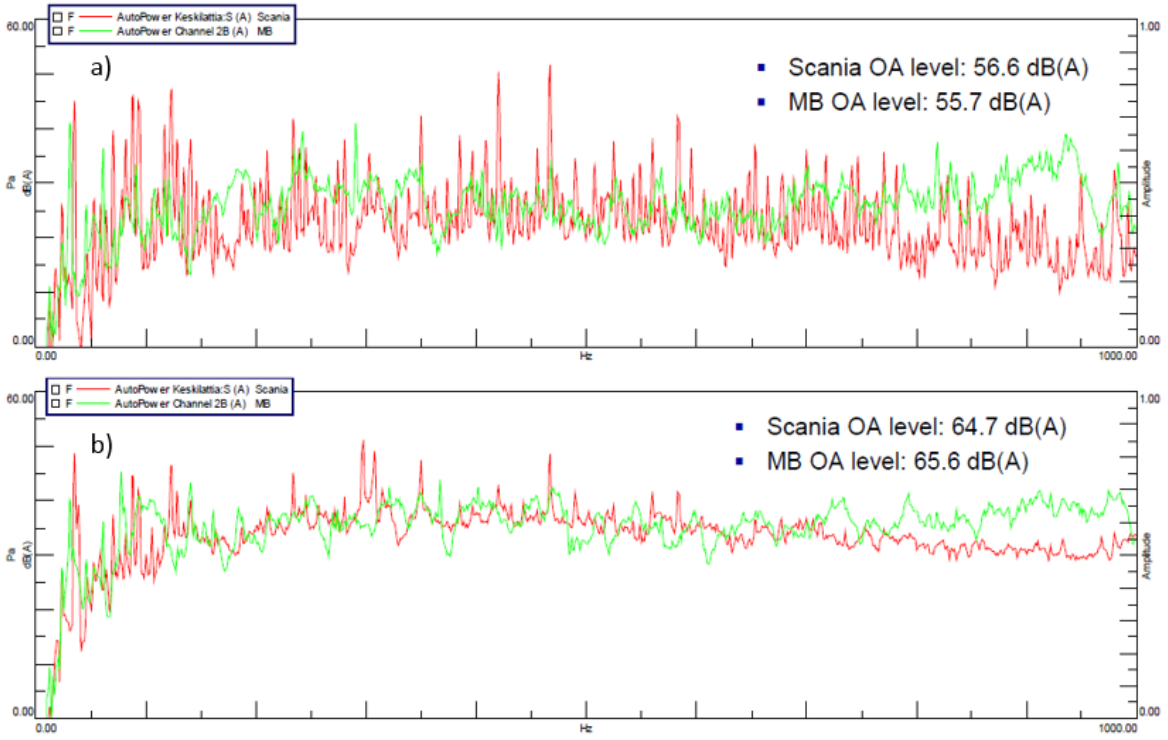

Figure 35. Stationary vehicle noise level measurements from middle floor region with appliances off (a) and appliances on (b).

The subjective view from the benchmarking measurements, conducted on two successive days for the vehicles, was discussed on-site between the investigators. As a result, it was unanimously agreed that the ride comfort of the Scania Citywide LE was perceived poorer when compared to the benchmarking vehicle Mercedes-Benz Citaro. This subjective perception comprised both the situations when the vehicles were tested while stationary as well as while in motion. Especially the higher level of perceived vibrations and lesser capability to attenuate shocks from the road surface were seen disturbing with Scania Citywide LE. The conclusion was similar throughout the bus body interior as the participants switched positions inside the bus in between separate test phases.

Order tracking analysis of Scania

The problem frequencies estimated from the spectral analysis of the measurements variated between different measurement points and operating conditions (e.g. vehicle idling vs. vehicle driven in varying velocities). Based on the first phase measurements, the estimations for possible resonance frequencies of the bus body structure were approximately 11, 14, 35, 80, 130 and 350 Hz. The sources for the noise and vibration in these frequency ranges were estimated by order tracking analysis. This analysis showed that the resonances at 11 and 14 Hz was excited by the wheel orders, 350 Hz resonance was concluded to be coming from the rear axle central gear mesh (crown wheel teeth) and the frequencies 35, 80 and 130 where excited by the engine orders.

For the resonances at 11 and 14 Hz frequency range, Figure 36 shows the averaged autopower spectrum of 50 km/h constant speed measurement, where the amplitude peak at approximately 11 and 14 Hz frequencies are visible at rear and front wheel, middle floor and driver's seat locations (measurement points 8, 9, 11 and 12). Based on calculation with equation 39, the wheel rotational frequency at 50 km/h is approximately 4.36 Hz. The third order of this frequency is close to these suspected resonance frequencies and is thus suspected to be the source of excitation.

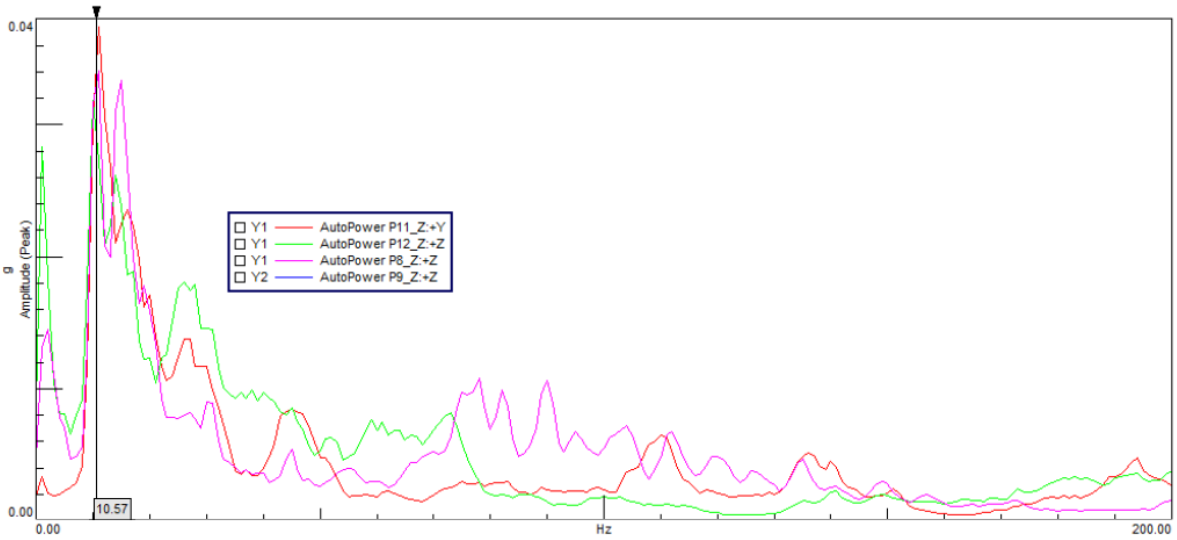

Figure 36. Averaged autopower amplitude spectrum of accelerations at rear and front wheel, middle floor and driver's seat locations.

For the confirmation of the source of excitation, spectral map of front wheel measurement point (11) acceleration in relation to vehicle speed gives an indication that the excitation at 50 km/h, i.e. approximately 260 rpm wheel rotational speed, would come from the third order of wheel rotational frequency. The spectral map plot from acceleration from 0 to 80 km/h is shown in figure 37 below.

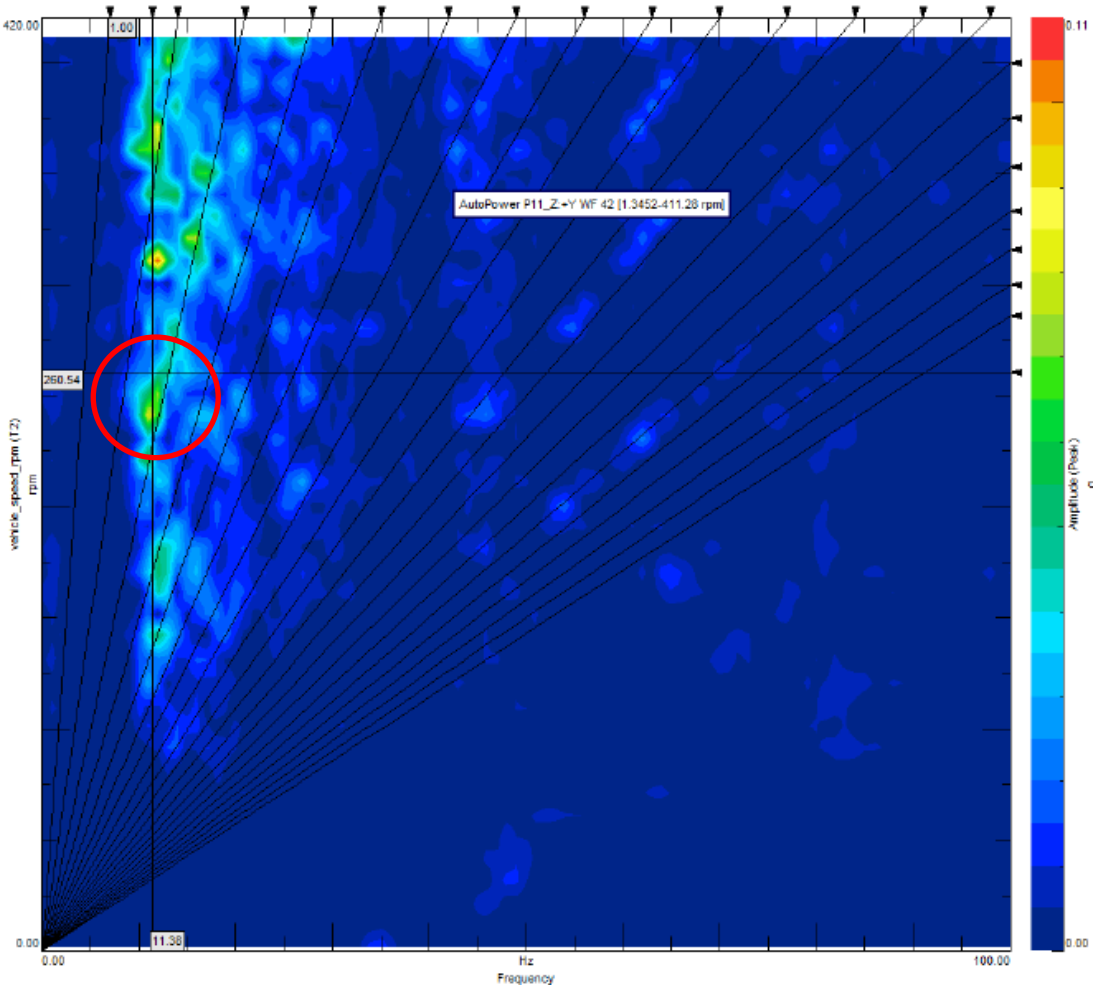

Figure 37. Spectral map of averaged acceleration from bus body interior measuring point (11) close to left front wheel versus vehicle speed information collected from CAN bus at 0 – 80 km/h acceleration. The 11 Hz vibration, occurring at approximately 50 km/h speed (260 rpm) and excited by the third wheel order is highlighted in the figure.

The 35 Hz resonance was noticed only when vehicle was stationary and the engine was idling at 700 rpm without any appliances activated. As can be calculated with equation 36, 35 Hz is the third order of the engine rotational frequency at 700 rpm, which in a 6-cylinder engine is the firing frequency. This resonance can be seen below in Figure 38, in the plot of

the averaged FFT of acceleration amplitude from the engine idling measurement. The measurement is done with the accelerometer positioned at the driver seat platform (12).

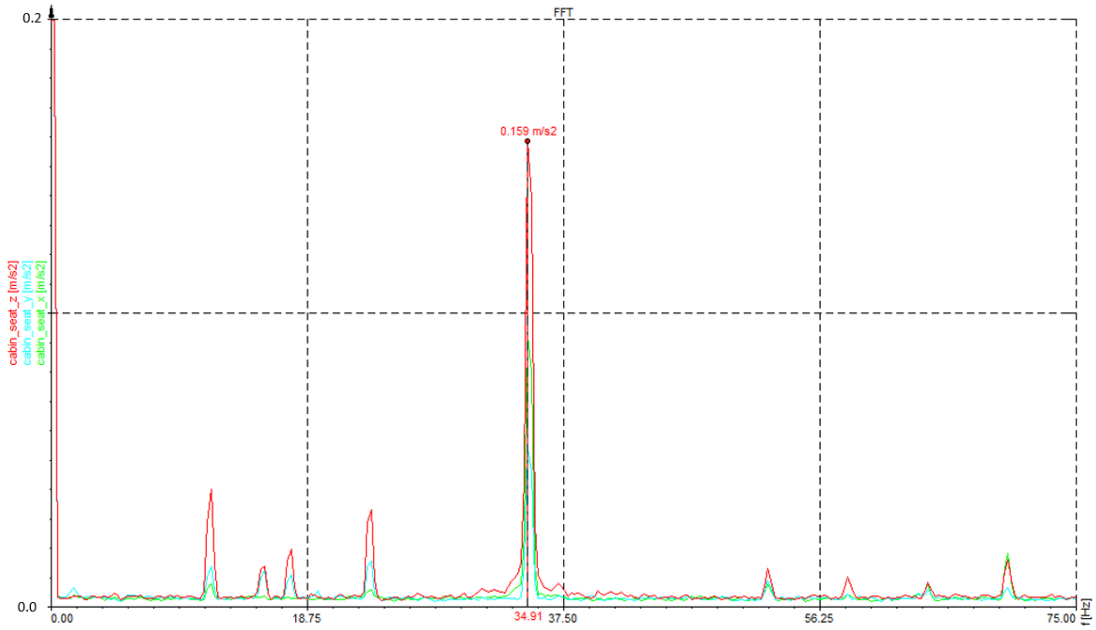

Figure 38. 35 Hz vibration measured from driver's seat platform at engine idling with 700 rpm rotational speed.

For the noise and vibration at 80 and 130 frequency range, Figure 39 shows the sound pressure peaks from averaged, A-weighted noise level measurements with the left rear wheel microphone at 50 km/h constant speed driving.

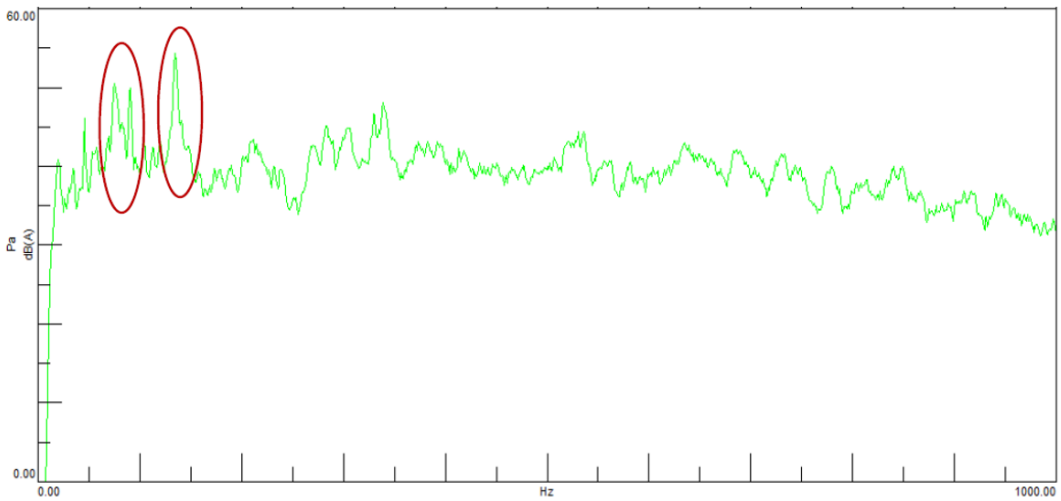

Figure 39. Averaged noise level from left rear wheel microphone at 50 km/h constant speed.

Based on calculations with equations 36 to 39, the vibration and noise at 80 Hz range could be excited by the fifth and sixth engine orders and noise at 130 Hz range could be excited by 8th and 9th engine orders at constant speed of 50 km/h. At this speed, while vehicle running on sixth gear, the engine speed is around 900 rpm. In Figure 40 is shown the spectral map of the left rear wheel microphone from 0 to 80 km/h acceleration, which shows the measured noise spectral density in relation to engine rotational speed. Referring to Figure 39, the plot gives an indication that the noise at 80 and 130 Hz range would be excited by engine orders 5, 6, 8 and 9 at around 900 rpm, which would suit also the estimation produced by calculations.

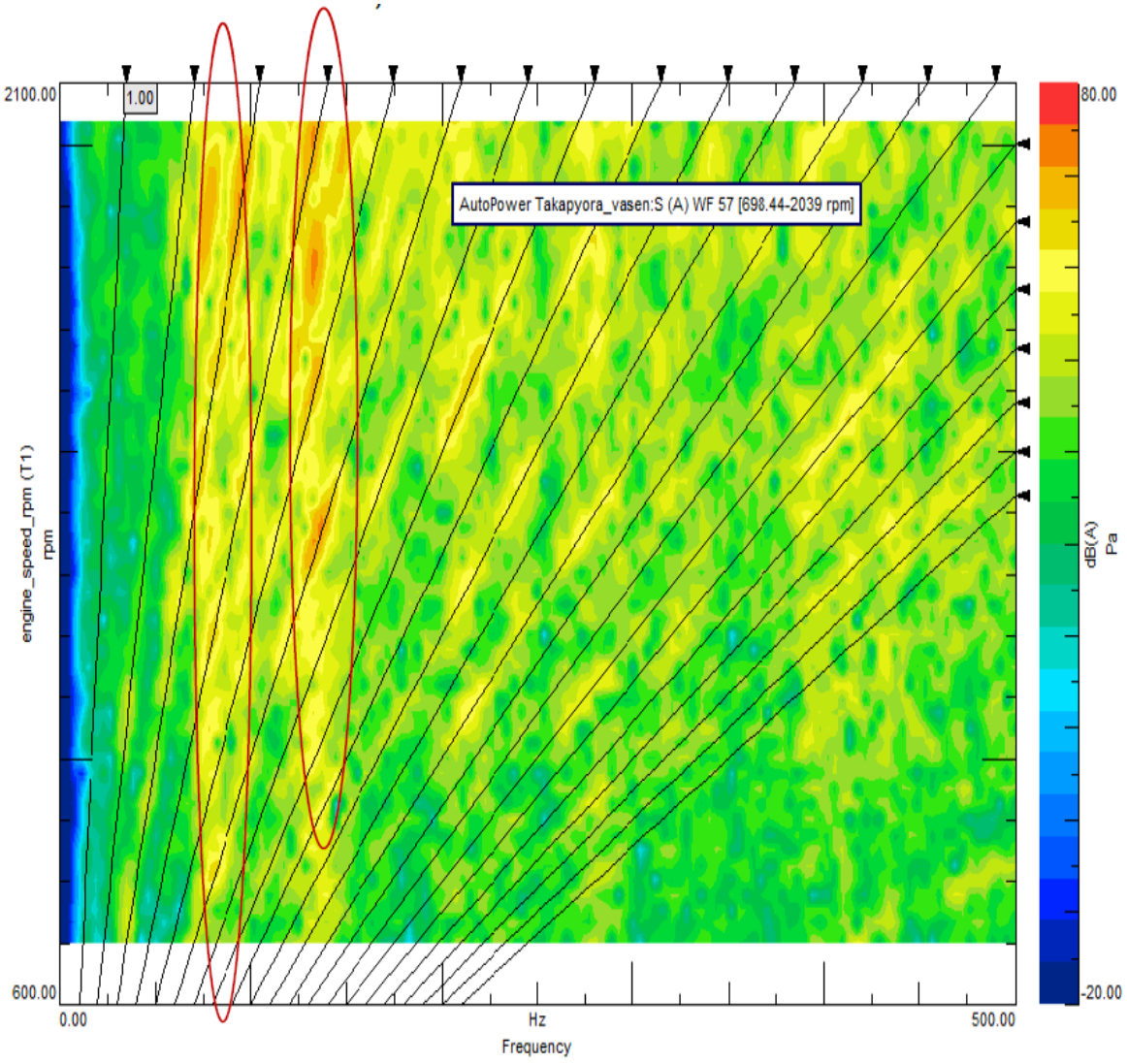

Figure 40. Spectral map of bus body interior noise near rear left wheel during 0 – 80 km/h acceleration.

The highest noticed possible resonance in the measurements was found at approximately 350Hz. Calculated drive shaft rotational frequency 4.36 Hz at 50 km/h multiplied by the number of teeth (39) in the rear axle central gear crown wheel gives around 170 Hz frequency for first order of the rear axle gear. The second order of this frequency, 340 Hz, corresponds to the measured resonance and is thus believed to be exciting noise and vibration at this frequency range.

4.3 Extended noise and vibration measurements

The extended noise and vibration measurements were conducted for more deeper investigation of the test vehicle dynamic properties in actual operating conditions. Objective of the investigation was to identify the sources and paths for the most significant vibration and noise responses in the bus body interior. The measurements included both operational and experimental modal testing as well as operational deflection shape and transfer path analysis.

4.3.1 Test procedure and instrumentation

The measurements were conducted on public roads at Lahti region in Finland. The measurements included four similar test runs during which four test setups were executed with accelerometers and measuring microphones positioned throughout the test vehicle. Each, approximately 27 kilometers long test run included 50 and 80 km/h constant speed measurements, 0 to 80 km/h acceleration and deceleration measurements and vehicle stationary measurements, which included both engine idling and engine speed run up measurements from 700 to 2000 rpm. The test route is depicted in figure 41 below.

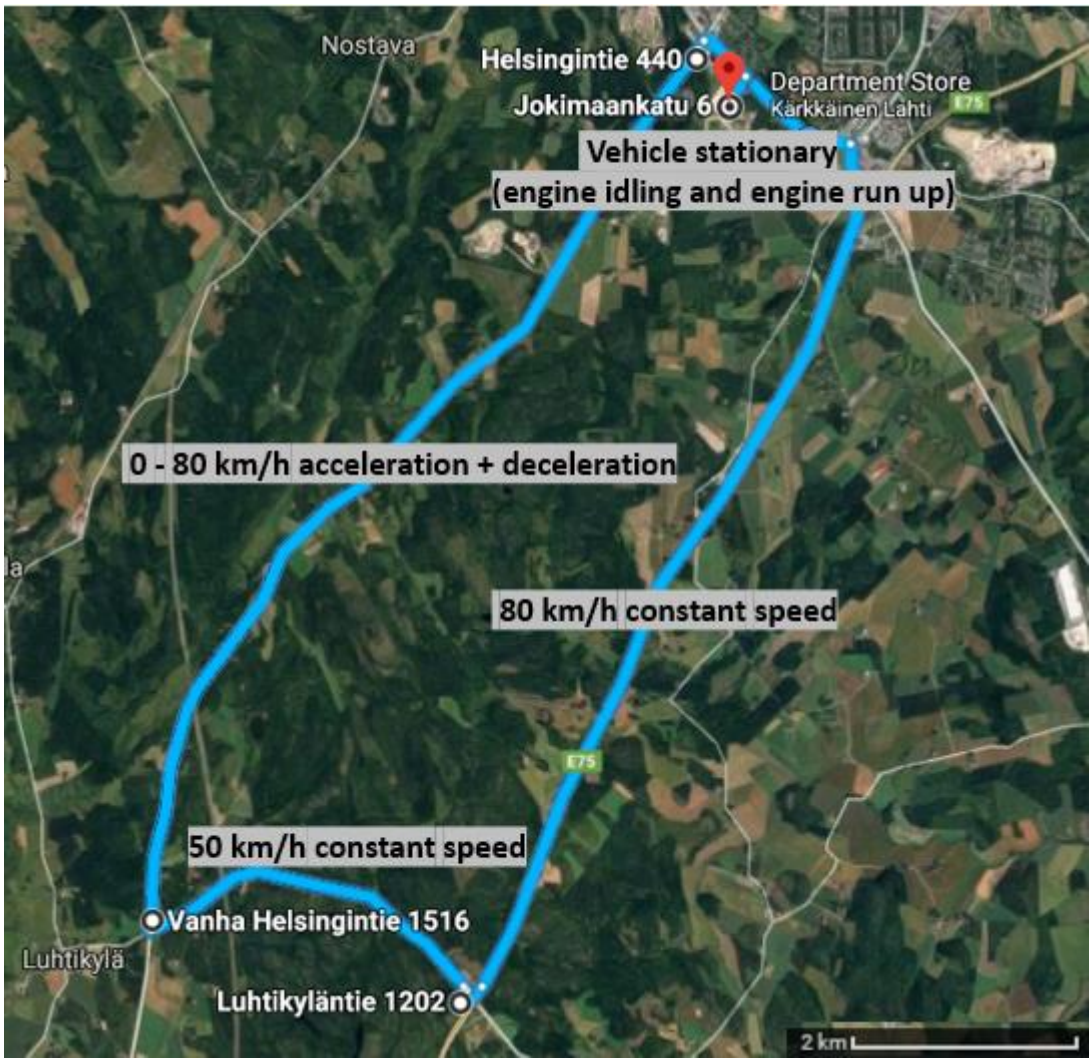

Figure 41. Test route for extended investigations, with the measurement phases included (modified from maps.google.com).

The vibration measurements were conducted with totally 54 tri-axial accelerometers: 36 of the accelerometers were positioned in the bus body, four attached to the rear chassis module frame, five attached to the transmission and engine covers and nine attached to the axles. Two of the acceleration measurement points (3 and 4), were defined as reference points and these accelerometers were kept in same positions during all four data sets. In addition, four measuring microphones were positioned at driver's position (Mic 1), middle floor area (Mic 2), rear seat (Mic 3) and engine compartment (Mic 4). The types of the used accelerometers were Endevco 65-100, Kistler 8766A50M5 and PCBHT356B11 and the model of the used microphones was Bruel & Kjaer 4189. In the extended measurements data acquisition system Siemens LMS SCADAS Mobile SCM209 enabled the logging of vehicle operational data from the vehicle CAN bus. Hence no additional data acquisition system was

needed for this purpose. The accelerometer positions in the body are depicted in Figure 42 and the accelerometer positions in the chassis and axle suspension are presented in the Figures 43 and 44 respectively.

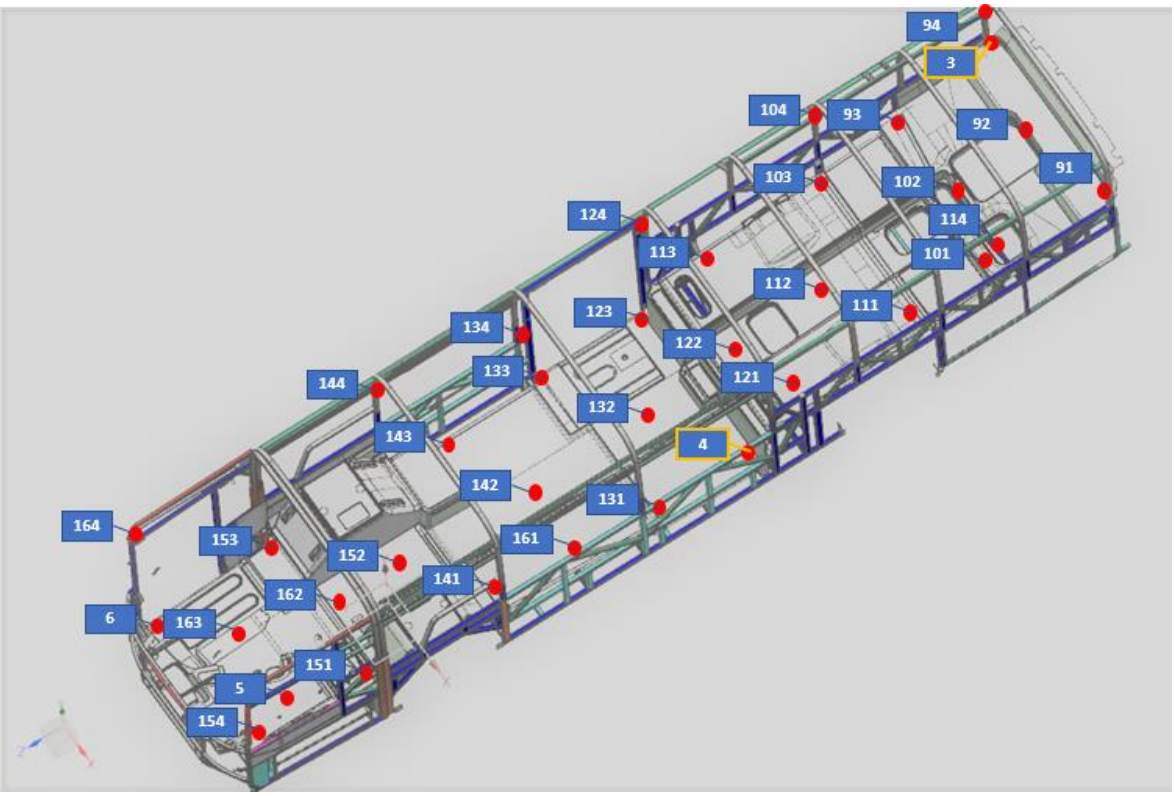

Figure 42. Accelerometer locations in the bus body.

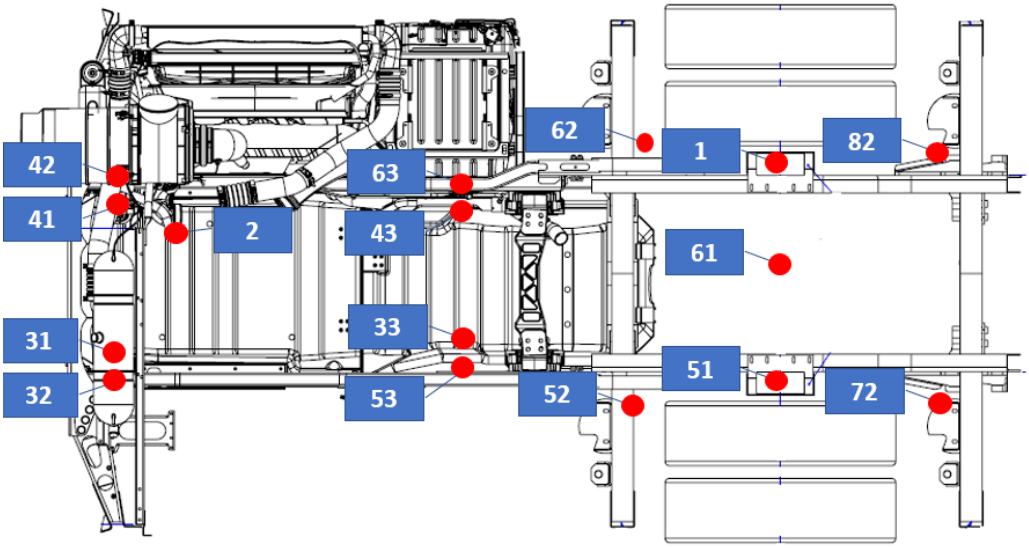

Figure 43. Accelerometer locations in the bus chassis rear module.

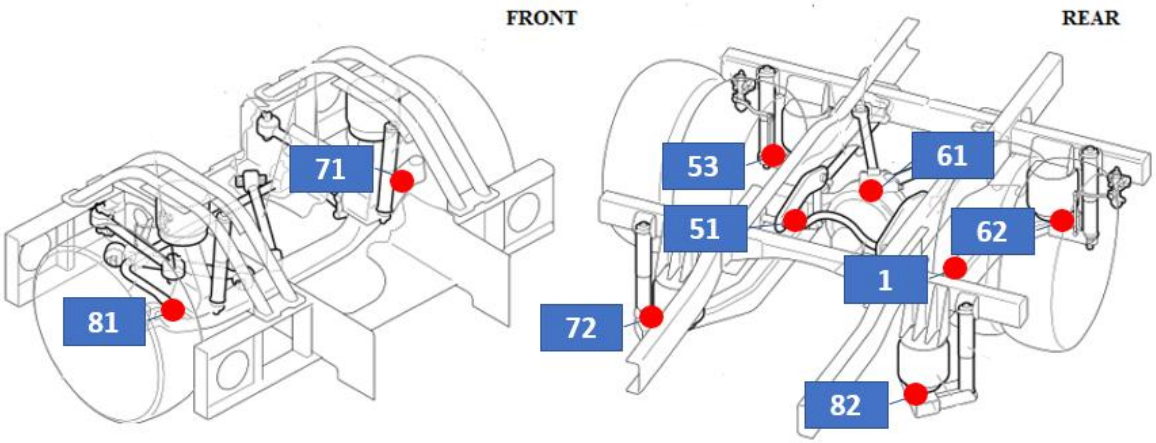

Figure 44. Accelerometer locations at rear and front axle suspension.

4.3.2 Results

The results of the measurements are divided in low frequency range vibrations and high frequency range vibrations and noise. In addition, the vibrations which occurred while the vehicle was stationary and engine idling is reviewed separately as it was considered as a significant single problem related to passenger ride comfort.

Low frequency range vibrations

Operational modal analysis of vehicle acceleration from approximately 50 to 80 km/h with fixed sixth gear indicated nine different natural modes for the low frequency range. In Table 2 is presented the natural frequencies f_n, modal damping ratios ζ and descriptions of the mode shapes associated with these modes.

Table 2. Modes of vibration at low frequency range.

Mode	f_n **(Hz)**	ζ **(%)**	**Mode shape description**
1	1.12	11.8	rigid body pitching
2	1.69	21.7	rigid body vertical movement
3	8.27	0.8	lateral bending of body with engine and transmission in phase
4	10.49	2.7	lateral torsion of body with front axle in phase
5	11.19	7.3	rear axle bouncing and engine and transmission assembly pitching in opposite phase
6	12.24	1.1	lateral bending and torsion of body with powertrain components in opposite phase
7	15.04	1.4	engine and transmission assembly pitching and rolling together with body lateral torsion
8	17.69	1.6	body lateral bending with the engine and transmission in phase
9	19.39	3.0	rear axle yawing together with engine yawing and rolling in opposite phase

Siemens LMS Test.Lab analysis software enabled animated, three-dimensional visualization of each mode shape. This simplified the interpretation of each mode shape. In Figure 45 below is shown a still frame of the mode shape animation for the fourth natural mode with lateral torsion of the bus body together with front axle rocking and bouncing in phase at 10.49 Hz.

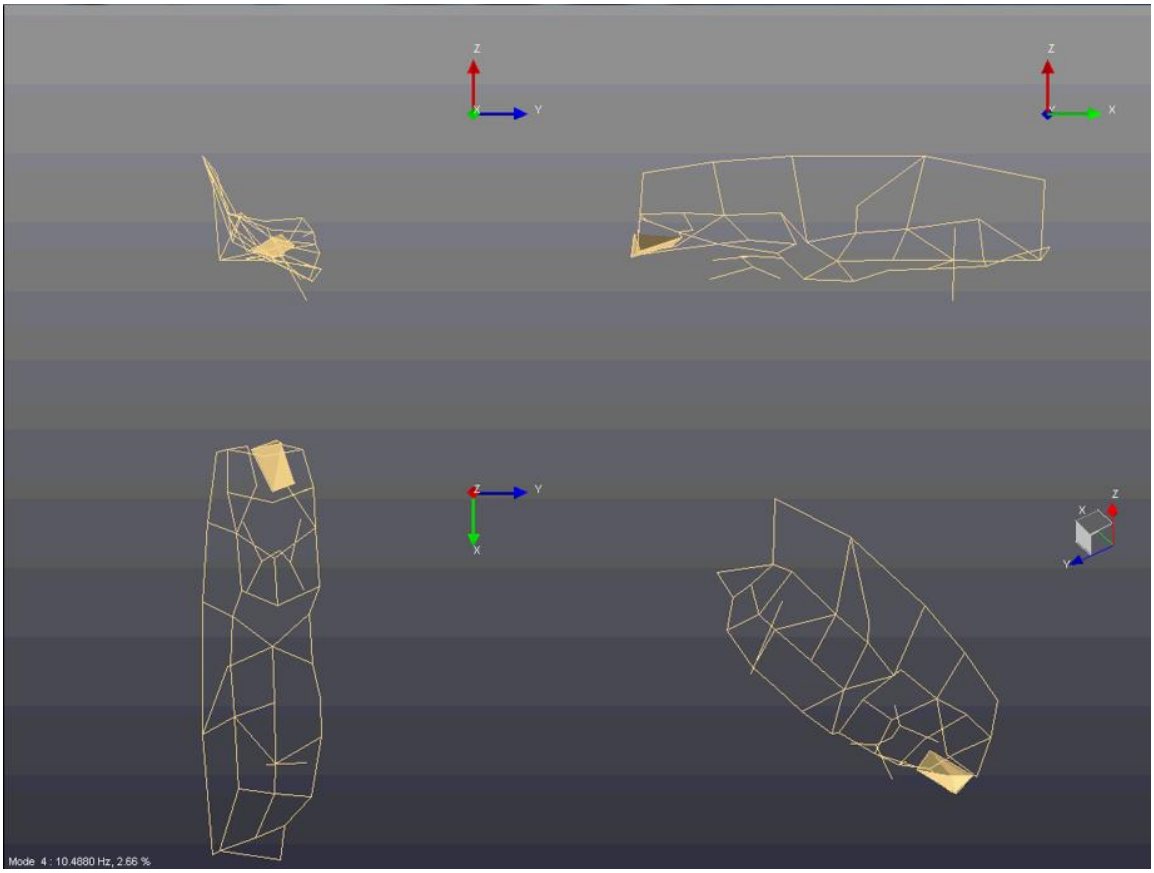

Figure 45. Siemens LMS Test.Lab analysis software three-dimensional visualization of the mode shape for 4th mode at 10.49 Hz.

Figure 46 shows the averaged autopower acceleration spectrum for 0 – 80 km/h acceleration with all gears included. In the figure can be seen the acceleration amplitudes in lateral and vertical directions for various acceleration measurement points around the bus body interior. The natural modes are marked with cursors in the figure and it can be seen, that the highest response levels in the low frequency range, rigid body modes excluded, occur in the range of 10 – 12 Hz.

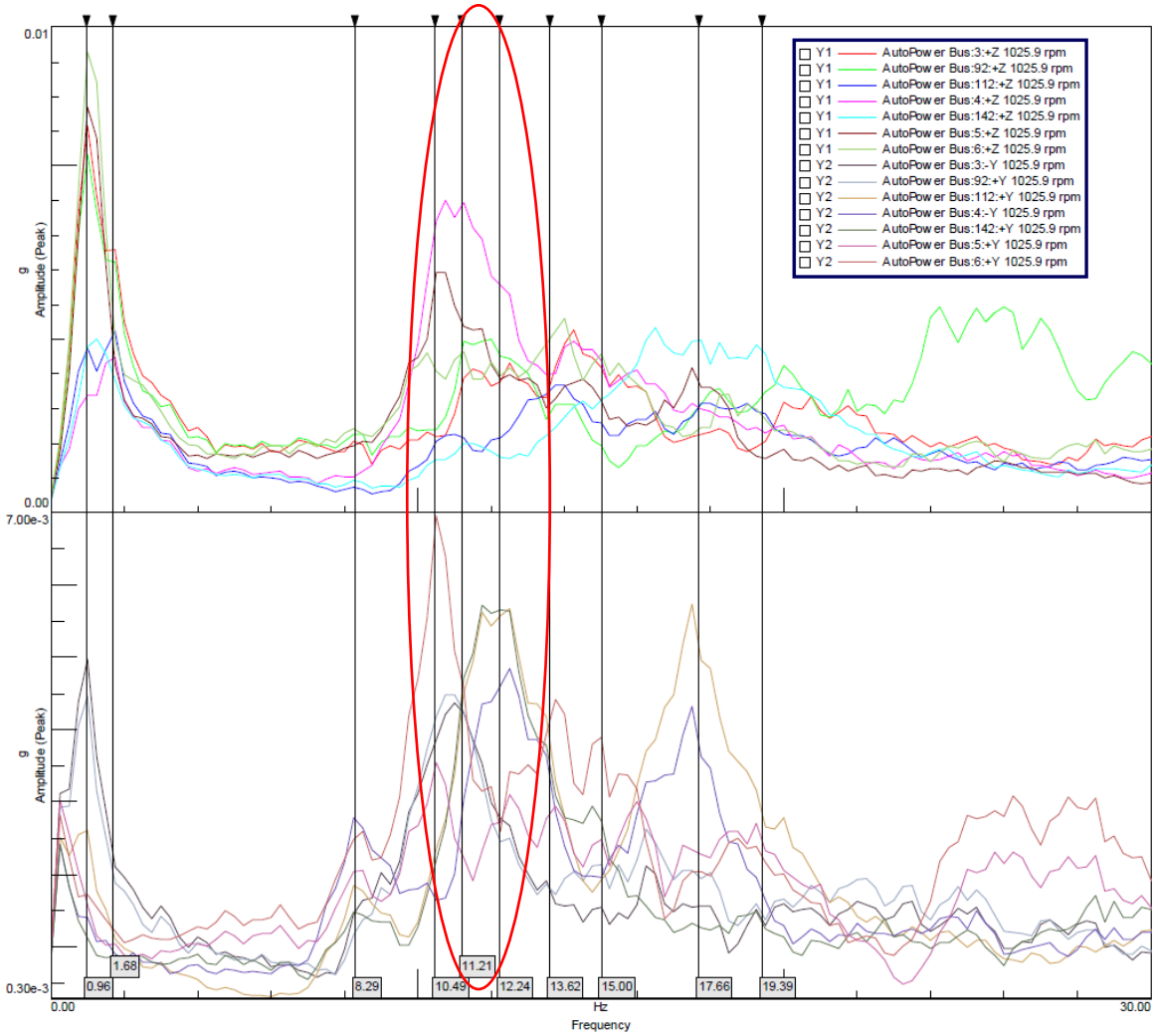

Figure 46. Averaged acceleration spectrum from several measuring points for 0 – 80 km/h acceleration with all gears included.

In Figure 47 is shown the spectral map of bus rear corner (MP 3) vibration in lateral direction versus engine rotational frequency. The measurement has been done during 50 – 80 km/h acceleration with fixed sixth gear. As the plot has been made against engine rotational frequency, the wheel orders must be transformed in to engine orders by taking in consideration the gear ratios of the transmission and rear axle gear. The lateral vibration of the bus body rear corner seems to be excited mostly by the second wheel order which equals to 0.58^{th} engine order in Figure 47.

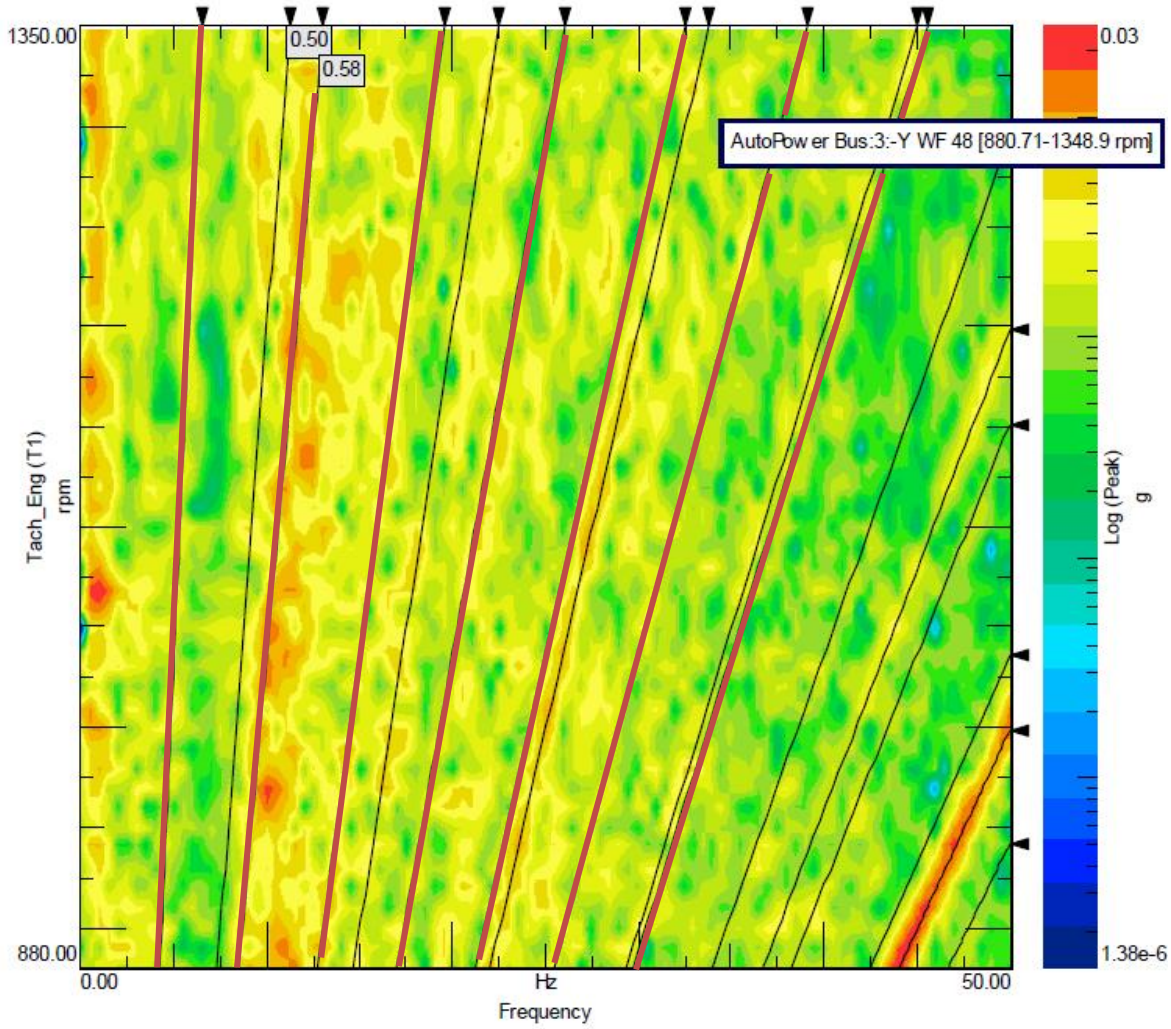

Figure 47. Spectral map of the lateral vibration of the bus body rear corner versus engine rotational frequency. Engine orders (0.29, 0.58, 0.87 …), corresponding wheel orders (1, 2, 3 …) marked with bolded red lines in the figure.

The Figure 48 shows the relatively broadband wheel excitation in vertical direction from rear axle measuring point (MP 1). This broadband excitation from the rear axle would explain the excitation of modes in broad frequency range. This broad distribution of vibration energy is supposed to be due to high level of damping in the wheel suspension system which is also indicated in Table 2 as high modal damping ratio (7.3 %) for the fifth natural mode with approximately 11.2 Hz natural frequency.

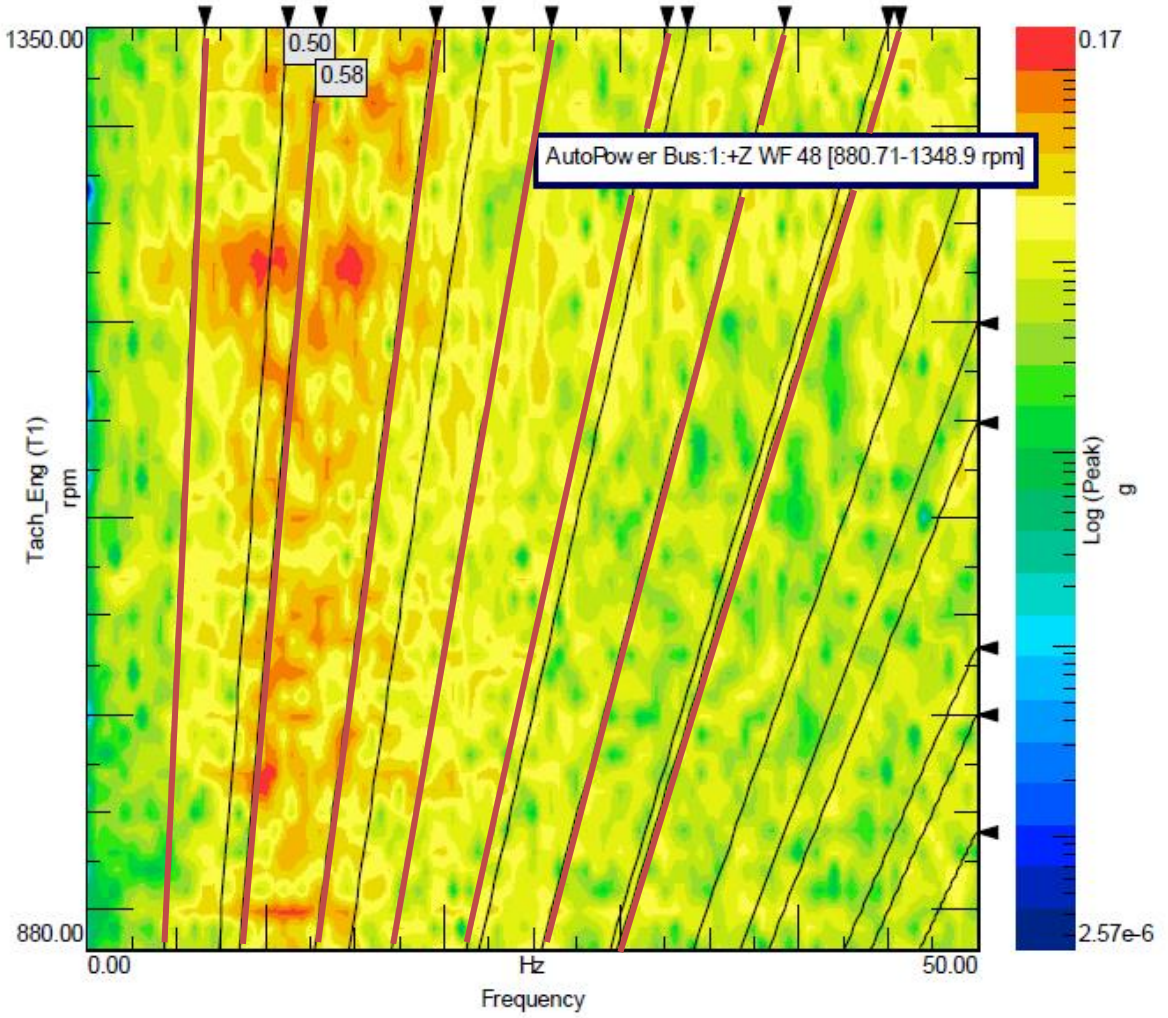

Figure 48. Spectral map of the vertical vibration of the rear axle (MP 1) versus engine rotational frequency. Engine orders (0.29, 0.58, 0.87 …), which correspond wheel orders (1, 2, 3 …) marked with bolded red lines in the figure.

In Figure 49 is shown another example of the low frequency range vibrations. The plot presents the spectral map of bus middle floor vibrations (MP 4) in vertical direction versus wheel rotational frequency during neutral gear deceleration from 80 to 0 km/h. As the vehicle was on neutral gear during the deceleration, the powertrain was disengaged without any torque transmitted from engine to wheels. Also, the engine was idling, which is indicated as a steady 35 Hz excitation in the figure corresponding to engine firing frequency during idling. The figure shows how also the middle floor vibrations at around 10 – 12 Hz are excited by the second and third wheel orders independent of the torque in the powertrain.

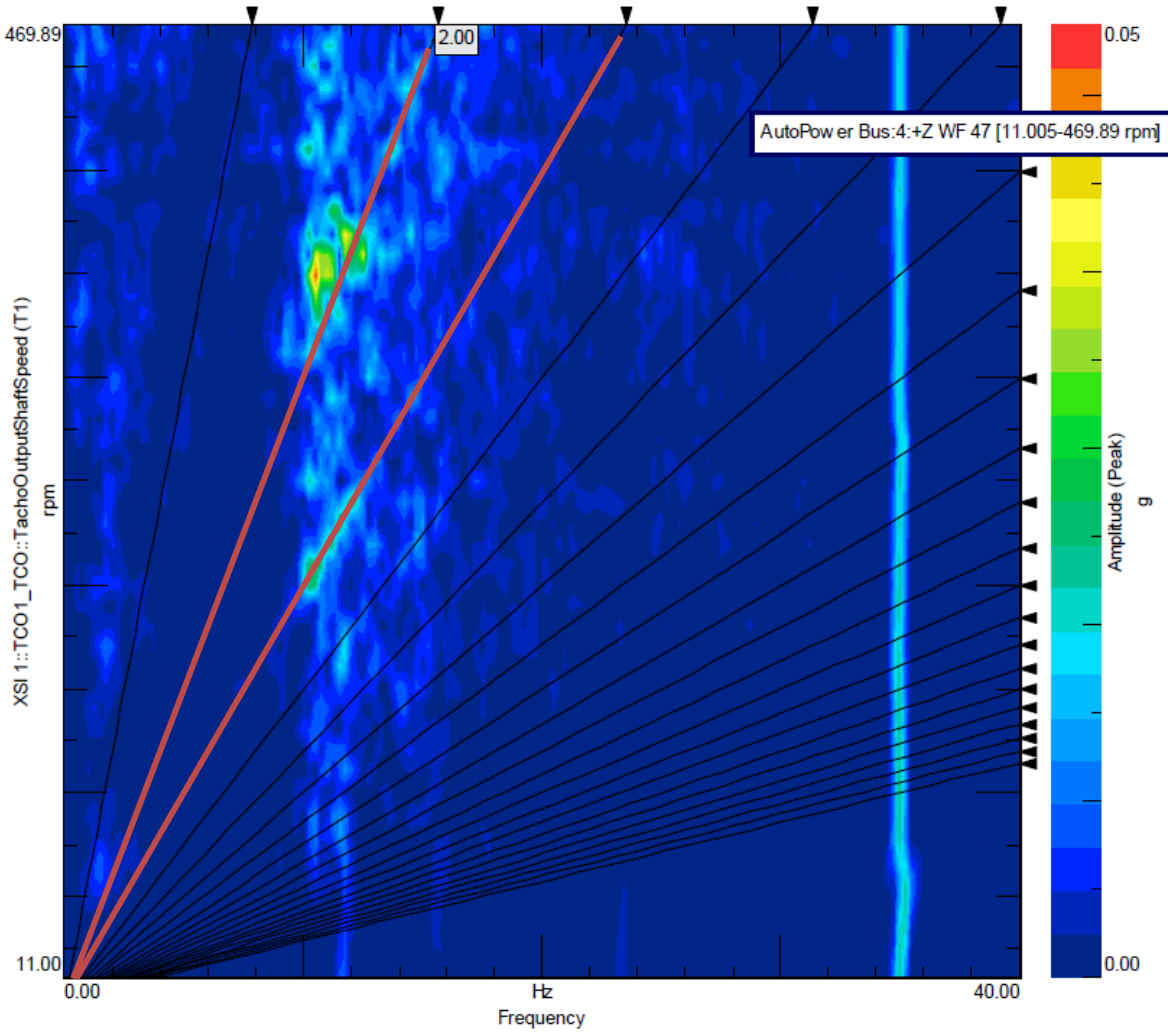

Figure 49. Spectral map of bus middle floor vibrations (MP 4) in vertical direction versus wheel rotational frequency during neutral gear deceleration from 80 to 0 km/h. Second and third wheel orders marked in the figure with bolded red lines.

Idling problem

As was stated already previously in the first phase measurements, a resonance at around 35 Hz was noticed while the engine was idling. The engine firing order (3) causes the resonance when engine rotational frequency is under 40 Hz (800 rpm). This is shown in spectral map in Figure 50 below. The spectral map presents accelerations of the bus body rear right corner (MP 3) in lateral direction versus engine rotational speed.

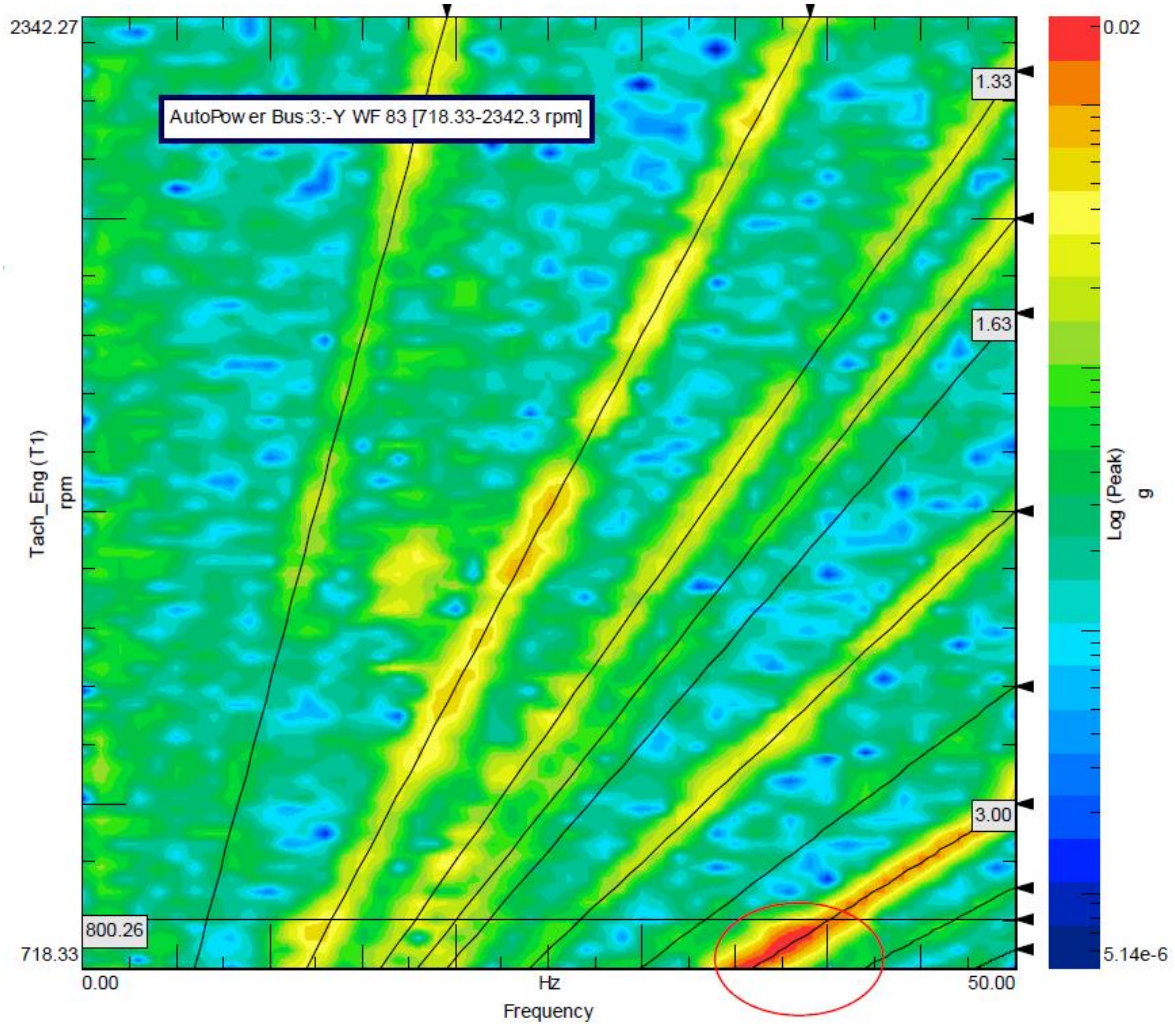

Figure 50. Spectral map of the engine orders versus engine rotating frequency with idling vibration at 35 Hz highlighted in the figure.

According to conducted operational deflection shape analysis for 35 Hz, the engine is rolling and yawing and the rear chassis frame is in lateral and vertical movement. In consequence the rear floor vibrates vertically causing whole bus body resonance. This vibration throughout the whole bus body was also clearly visible also in the first phase measurements, when measuring the vibrations during idling from the driver seat platform. Operational deflection shape analysis gives an indication that the problem only occurs during engine idling when the powertrain is disengaged as similar response does not occur during measurements where vehicle is in motion i.e. torque is transmitted from the engine to the driving wheels.

In addition to ODS, also EMA measurements were conducted for stationary vehicle to investigate the idling problem. The EMA tests were conducted with 20 accelerometers positioned in the rear end of the bus body and chassis as described in Figure 51. The force input was given with an impact hammer (IMI 086C42) to positions at the right chassis frame beam (42) and rear right corner of the body frame (3).

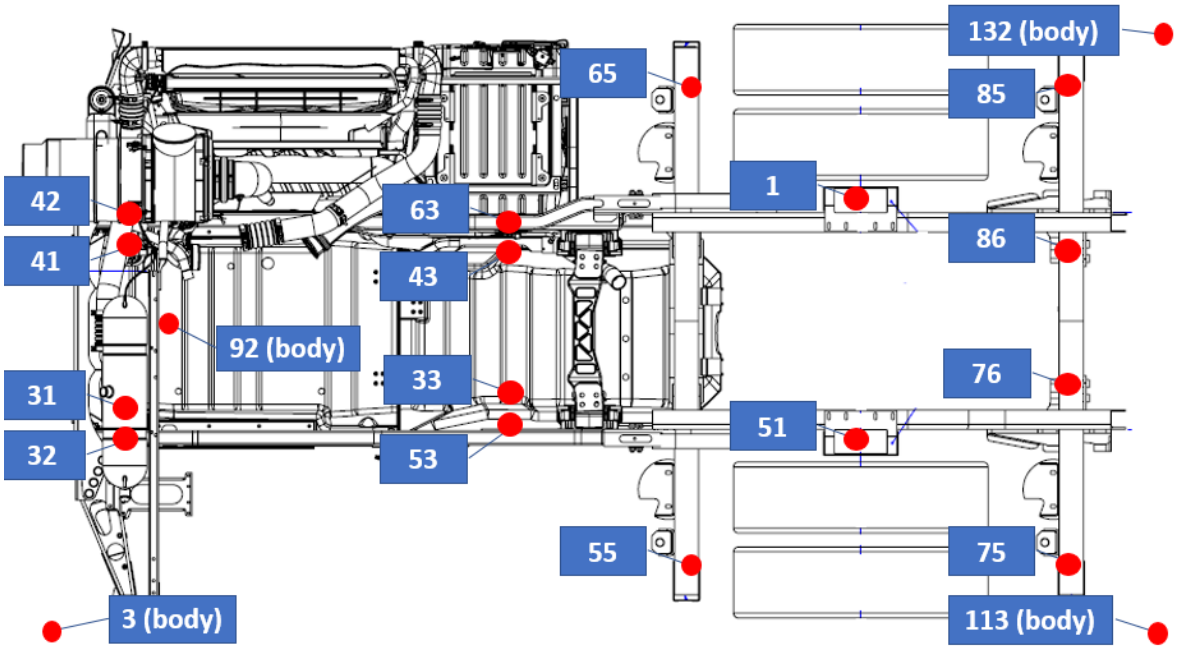

Figure 51. EMA vibration measuring points in the bus rear end.

In these tests several rear chassis frame natural modes where found in the range of 30 to 35 Hz and the main conclusion from the measurement was that the rear chassis frame is flexible in lateral direction. Thus, excitation from the engine at idling causes a clearly noticeable response in the chassis frame structure and consequently in whole bus body structure. The natural modes at 35 Hz range concluded from the EMA measurements are presented below in Table 3

Table 3. Natural modes at 30 – 35 Hz range derived from EMA investigations.

Mode	f_n **(Hz)**	ζ **(%)**	**Mode shape description**
1	30.3	1.2	rear chassis frame lateral movement
2	33.5	2.8	rear chassis frame lateral movement + rear floor vertical movement
3	35.6	2.7	rear chassis frame lateral and vertical movement + rear floor vertical movement
4	36.5	2.3	rear chassis frame lateral movement in opposite phase

High frequency range noise and vibration

In the high frequency range, the most dominating amplitude peaks in an averaged, A-weighted sound pressure spectrum were identified at 45 Hz, 55 Hz, 80 Hz, 118 Hz, 130 Hz and 350 Hz range. In Figure 52 is presented the averaged autopower vibration amplitudes versus the averaged sound pressure peaks in frequency domain at 50 – 80 km/h acceleration with fixed sixth gear. As can be concluded from the figure, the vibrations at bus body rear floor measuring points 92 and 102 cause the noise at 40 to 50 Hz range and the measuring points 112 and 122 cause the noise at 80 to 130 Hz range. In addition, ODS analysis was conducted for each of the problem frequencies and the animations of the ODS clearly indicated vertical movement of the bus rear section floor areas.

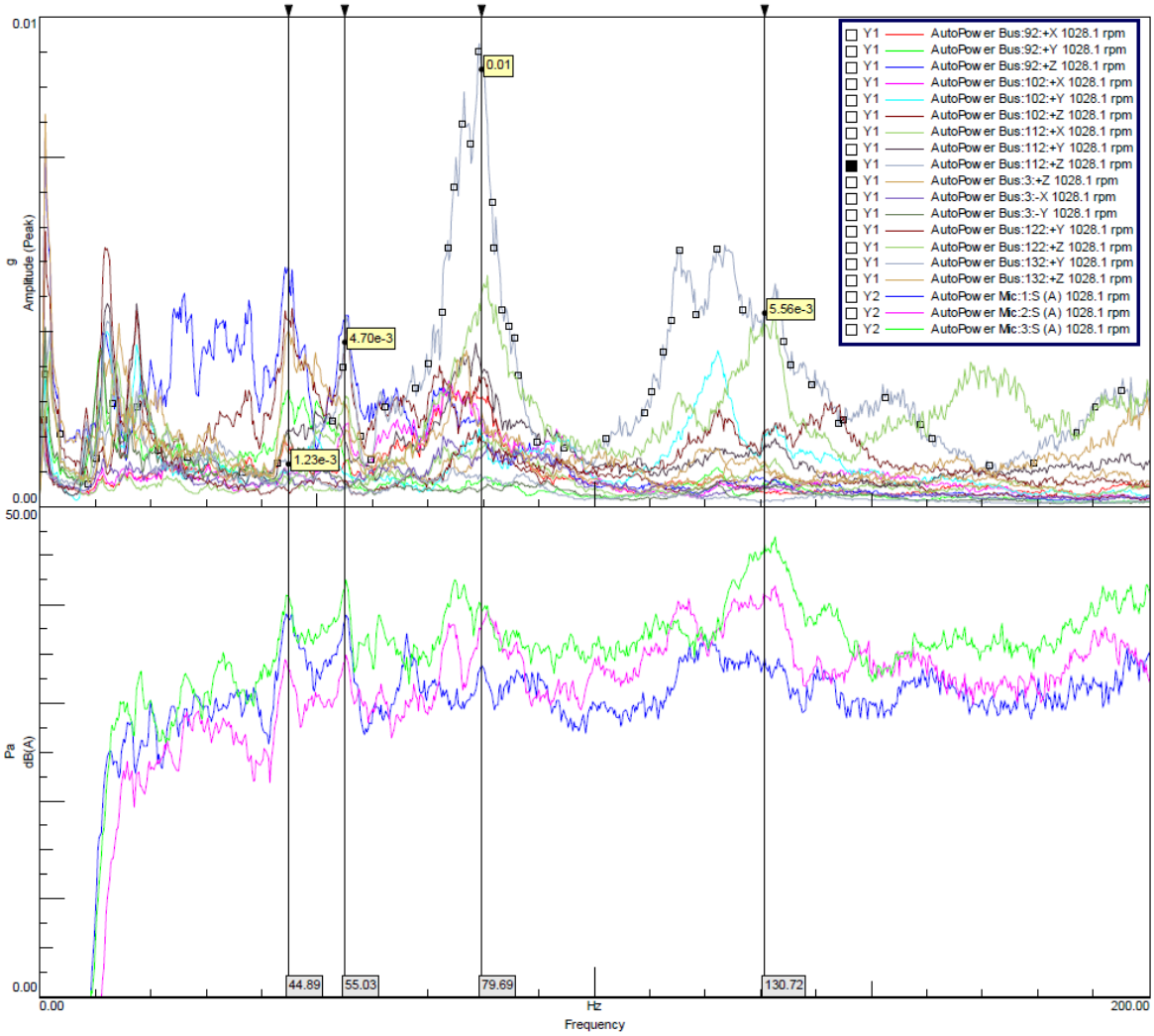

Figure 52. Audible frequency range averaged vibration (upper plot) and sound pressure (lower plot) spectrum at 50 – 80 km/h acceleration showing the dominant frequencies and correlation between vibrations and emitted noise.

Order tracking was utilized to identify the sources of the high frequency range noise and vibration problem. Figure 53 shows the spectral map of the rear seat noise (Mic 3) versus engine speed at 50 - 80 km/h acceleration with fixed sixth gear. The spectral map indicates that the engine orders are exciting the noise at the rear seat area.

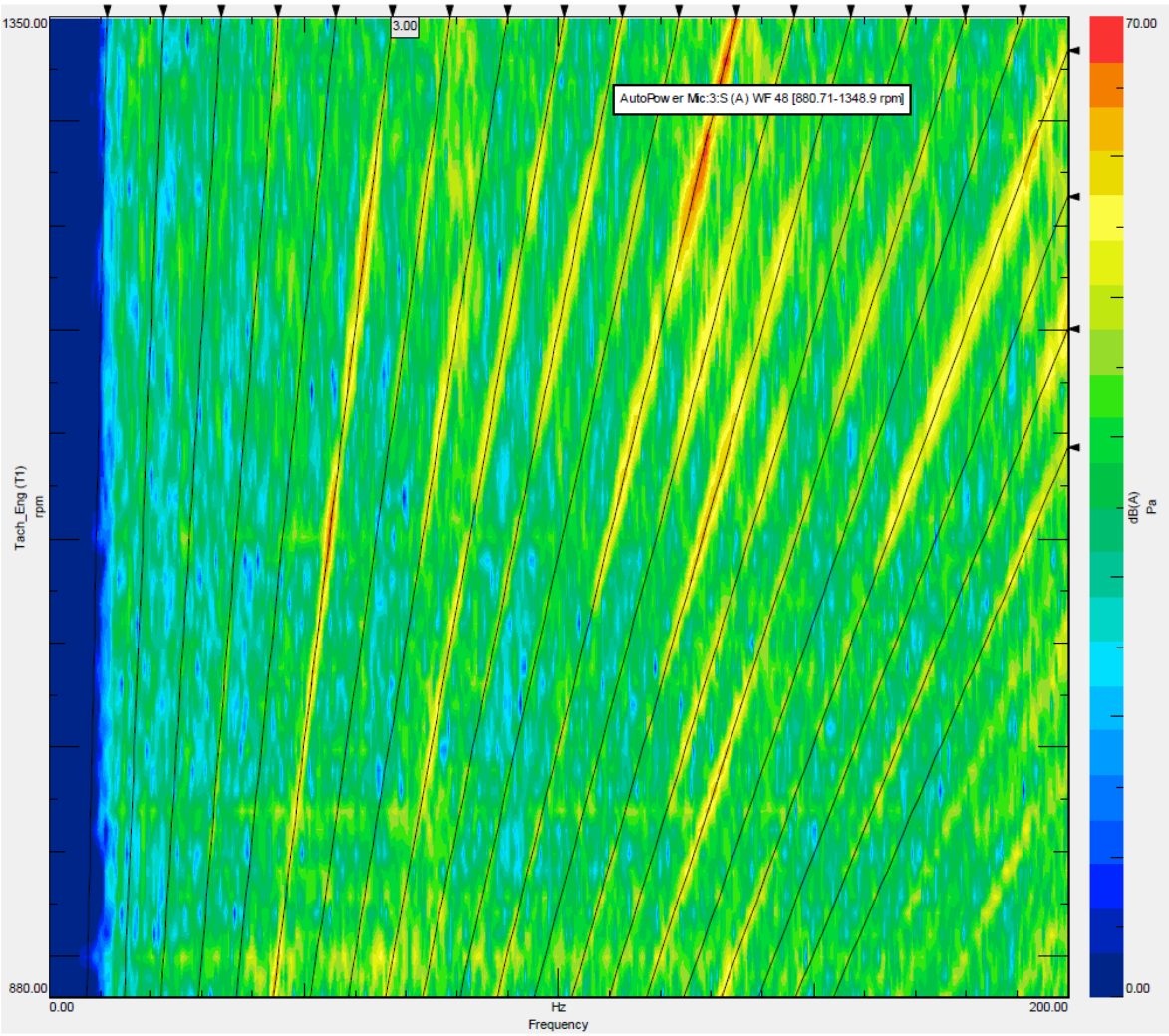

Figure 53. Spectral map of the rear seat area (Mic 3) sound pressure amplitude versus engine rotational speed at 50 - 80 km/h acceleration with fixed sixth gear. Engine orders presented in the figure with 0.5 interval (0.5, 1, 1.5, 2 …).

Similar indication can be seen from the measurement result from the accelerometer near rear axle (MP 112) in vertical direction during 50 – 80 km/h acceleration. The spectral map in Figure 54 shows that the vibrations at 45 Hz and 55 Hz range are excited by the third engine order (firing frequency), vibrations at the 80 Hz range are excited by the fourth and 4,5th engine order and vibrations at 120 – 130 Hz are excited by the sixth engine order, which is double of the engine firing frequency. Thus, it can be concluded also from this vibration measurement that the high frequency noise and vibrations at 45 – 130 Hz frequency range are excited by the engine orders.

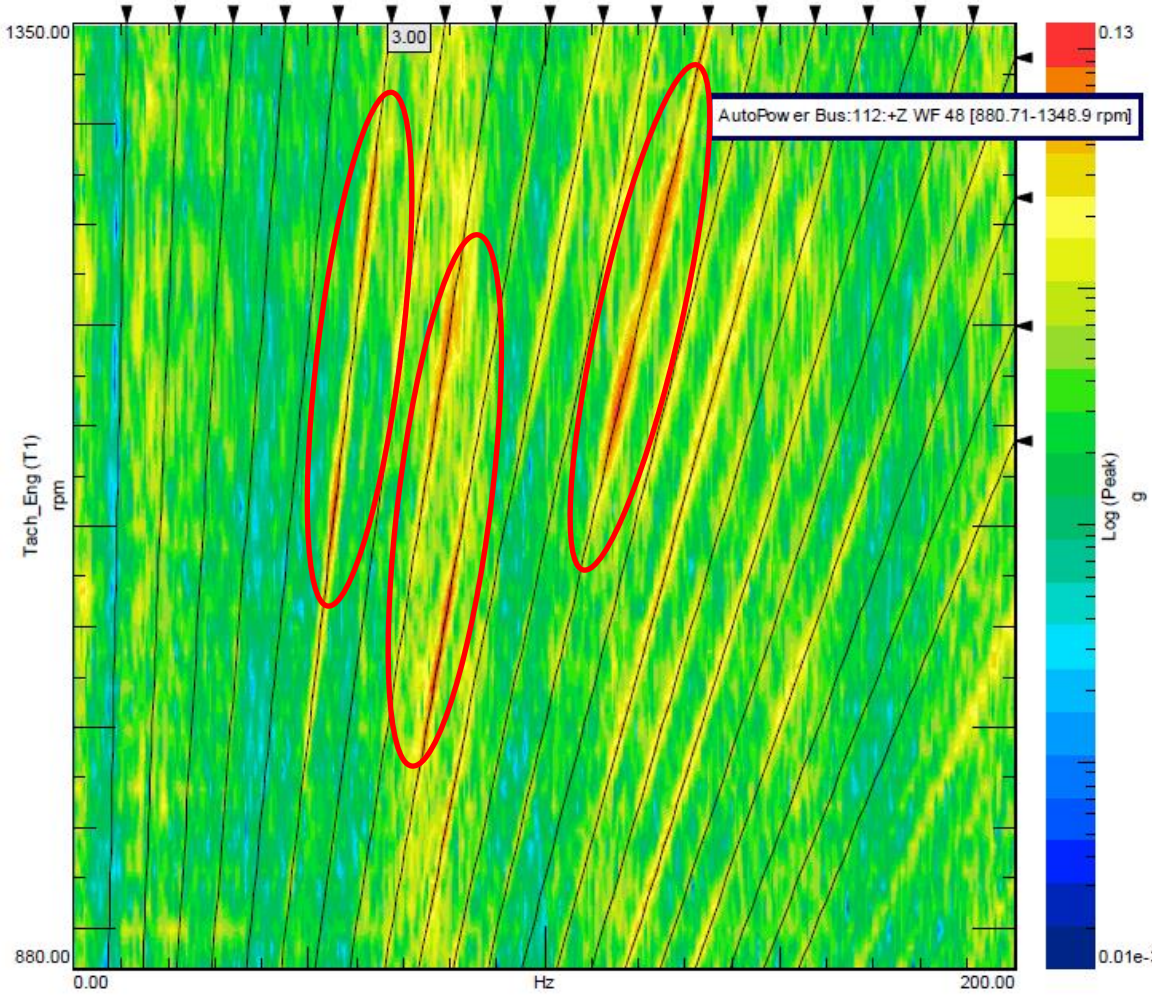

Figure 54. The spectral map from the accelerometer near rear axle (MP 112) in vertical direction versus engine rotational speed. The vibrations at 45 – 55 Hz, 80 Hz and 120 – 130 Hz range are highlighted in the figure

Figure 55 focuses in the overall contribution of noise at the rear seat position microphone (Mic 3) in 1 – 1000 Hz frequency range by utilizing operational transfer path analysis at 0 – 80 km/h acceleration. The TPA instrumentation setup differed from the previously mentioned OMA test setup, but the contributors included in Figure 55 are accelerometers at engine mounting points (MP 31 and 41), transmission mounting points (MP 33 and 43) and rear axle (MP 1 and 51). In addition, microphones near engine (Mic 4) and rear axle (Mic 5) are included in the investigation. From the figure can be concluded that the most significant contribution to rear seat noise comes from the engine mounting points, in particular measuring point 41. In other words, based on the TPA investigations, the most dominant contribution for the rear set noise would be structure borne and caused by the engine.

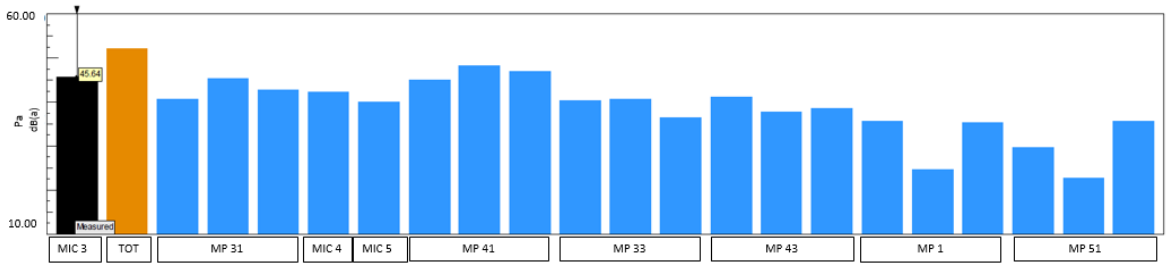

Figure 55. Contribution of rear seat noise (Mic 3) in 1 – 1000 Hz frequency range.

In addition to overall contribution presented in Figure 55, Figure 56 shows an averaged autopower amplitude spectrum from each measuring point and this gives an indication that the rear seat noise (Mic 3) contribution between airborne and structure borne noise is frequency dependent. In 80 Hz range the microphone at the engine compartment (Mic 4) seems to have more significant contribution to the measured sound pressure level at the rear seat region. Thus, the noise at 80 Hz range would seem to be more airborne noise from the engine. Instead, the noise in 130 Hz range seems to be mostly excited by the vertical vibration of the engine mount measurement point (41Z in figure 56). Thus, in this frequency range, the noise would be more dominantly structure borne noise excited by the engine.

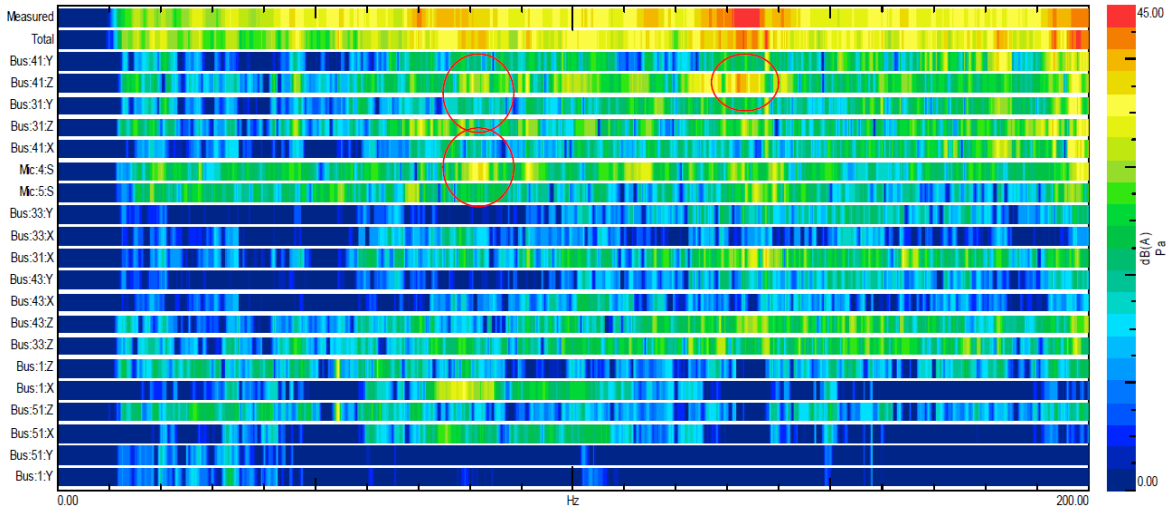

Figure 56. Contribution of rear seat noise in frequency domain.

The last problem frequency, creating audible noise in the bus body, was found at approximately 350 Hz. For the noise and vibrations at this frequency range could be ensured in these measurements to be caused by the 78th order of the drive shaft rotational speed, i.e. the second order of the rear axle crown wheel gear mesh. For example, Figure 57 below

presents the spectral map of the middle floor (Mic 2) noise during 0 – 80 km/h acceleration. At around 50 km/h vehicle speed, which corresponds to approximately 270 rpm drive shaft rotational speed, high noise levels can be seen at approximately 350 Hz, which indicates that the noise at this frequency range is excited by the driving axle gear crown wheel mesh.

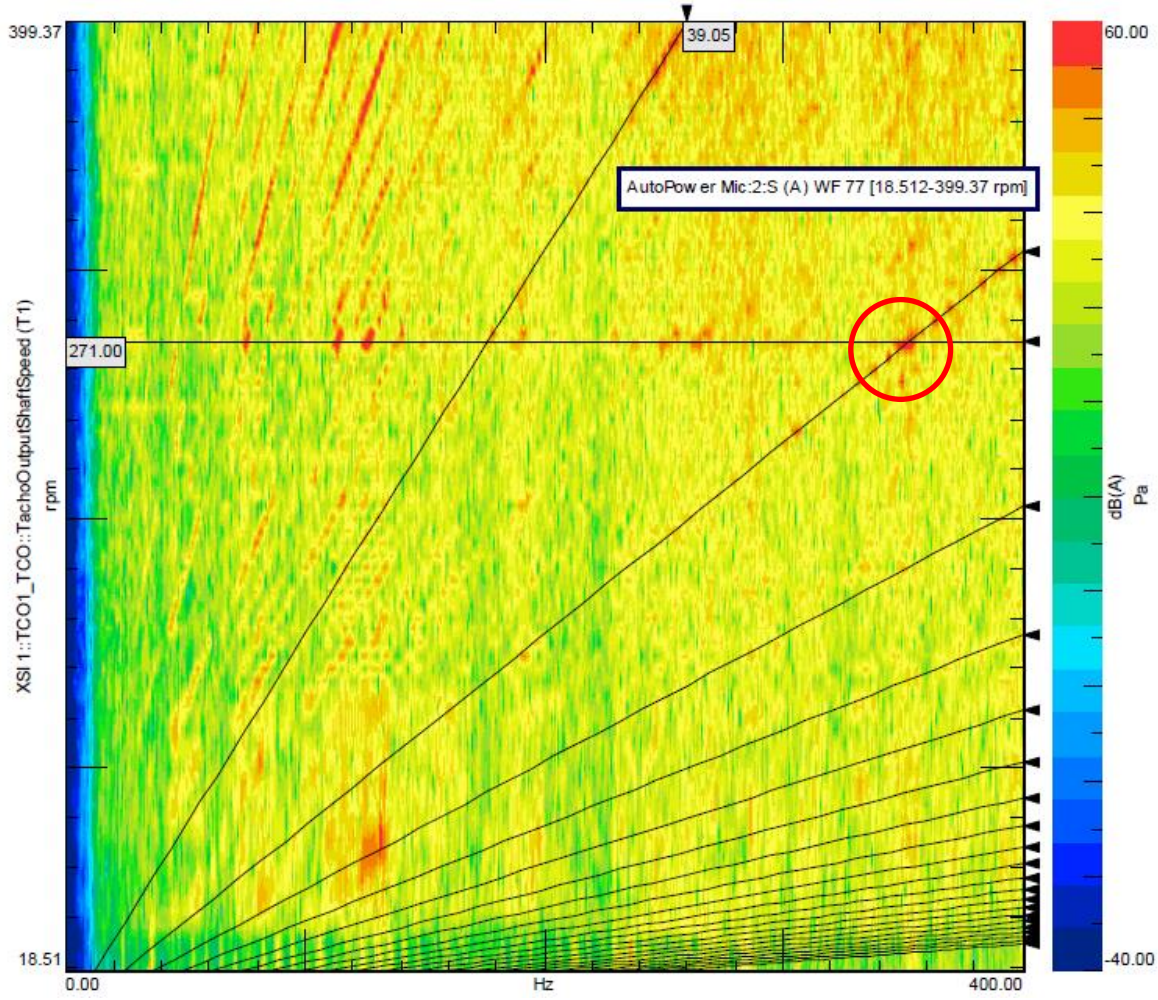

Figure 57. Spectral map versus of middle floor noise (Mic 2) versus drive shaft rotational speed during 0 – 80 km/h acceleration. The 350 Hz noise at approximately 50 km/h (~270 rpm) wheel speed is highlighted in the figure in connection with 78th drive shaft order (Note: the drive shaft rotational speed has been calculated to the spectral map by multiplying the propeller shaft rotational speed collected from CAN bus data (*TachoOutputShaftSpeed*) with rear axle gear ratio 5.57).

5 DISCUSSION AND CONCLUSIONS

This thesis discussed the experimental case study investigations conducted around interior noise and vibrations of a Scania Citywide LE city bus. The investigations aimed at revealing the most significant bus passenger ride comfort related problems in the current bus body structure. The study was motivated by providing information for future bus body development work, considering interior noise and vibration issues. In addition to the case study, also an extensive literature review was conducted around the research topic to provide a theoretical background for the research.

This chapter gives a summary, further analysis and conclusions of the research results presented in the previous chapter. In addition, the objectivity, reliability and validity of the research are reviewed together with a suggestion for further research.

5.1 Reliability of the research

The results of the presented case study are fully based on data collected via measurements which have been explained in chapter 4. Each of the measurements should be possible to reproduce, as e.g. the test phases, transducer positions and type of instrumentation have been specified in the research methods description.

In the data acquisition phase reliability of the results was ensured by e.g. calibration of the transducers and repetition of the test sequences. Before the actual measurements, the noise and vibration transducers were calibrated on site. E.g. the accelerometer readings for each orthogonal direction were calibrated with a predefined vibration input, produced by an accelerometer calibrator (type Brüel & Kjaer 4294). As the calibration was conducted with each transducer connected to the data acquisition system, also the instrumentation cables got inspected simultaneously. In addition, the reliability of the measurements was ensured by repetition of each measurement to accumulate enough data from each individual test sequence and by using reference transducers in same positions during different test setups.

In the analysis phase, the measured spectra from reference sensors were compared between repeated, corresponding measurements to determine the analogy between separate

measurements. In Figure 58 is presented from separate test setups the averaged, autopower acceleration spectrum from accelerometer at driver's seat platform (MP 5) during 0 – 80 km/h acceleration. The figure gives an indication of satisfactory repeatability between different measurements.

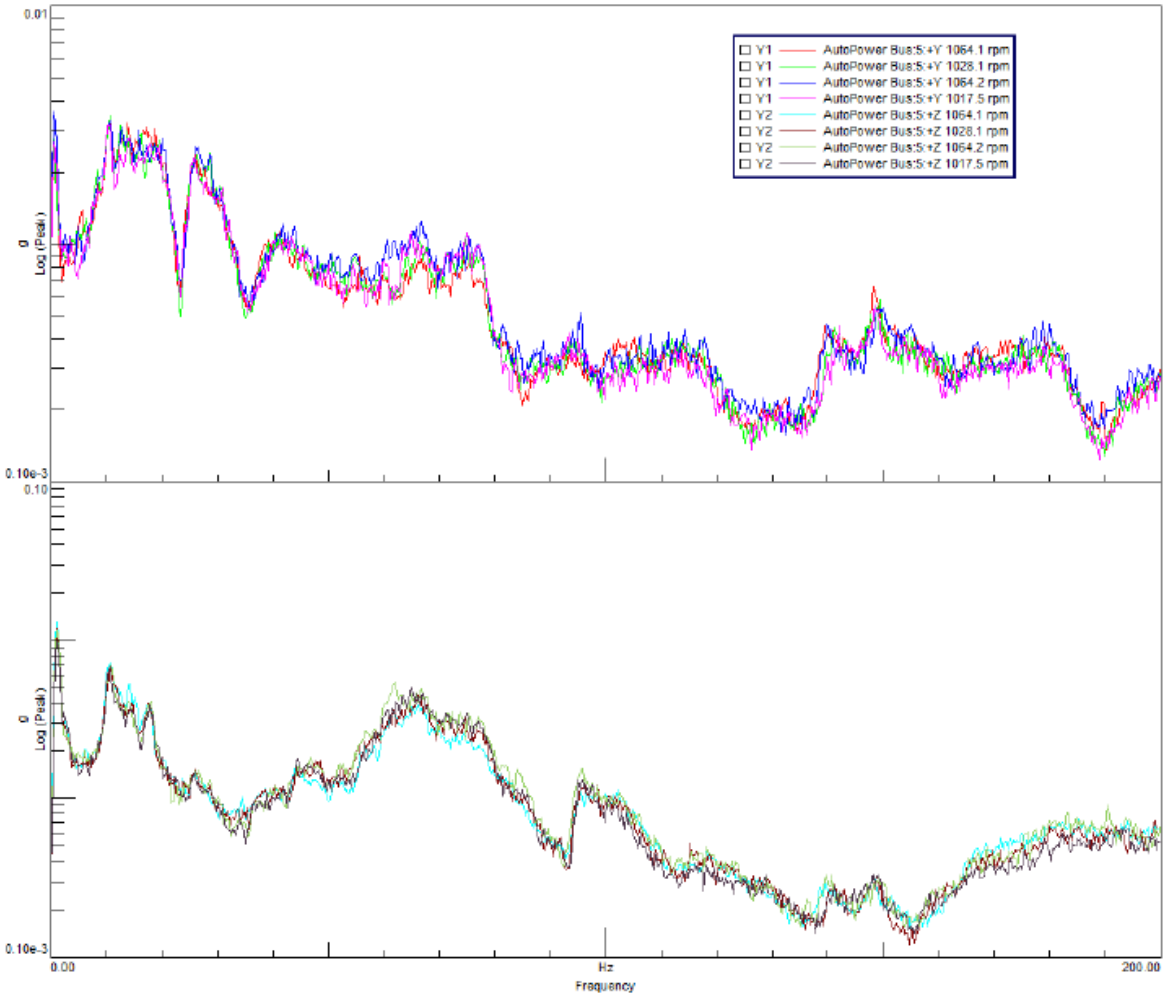

Figure 58. Comparison of autopower spectrum of driver seat platform (MP 5) lateral (upper) and vertical (lower) acceleration between different measurements indicating satisfactory repeatability.

In addition, the modal testing results were subjected to modal assurance criterion (MAC) investigations to determine that the measured modes all have individual mode shapes and thus can be concluded that e.g. enough measurements points have been used in the measurements. In Figure 59 is shown an example of MAC matrix produced from 50 – 80 km/h acceleration OMA measurements with low frequency range modes compared to each

other. The MAC matrix shows that the diagonal elements of the matrix are close to unity and off-diagonal elements have significantly lower similarity. This gives an indication of good quality modal analysis which is important for both validity and reliability of the research.

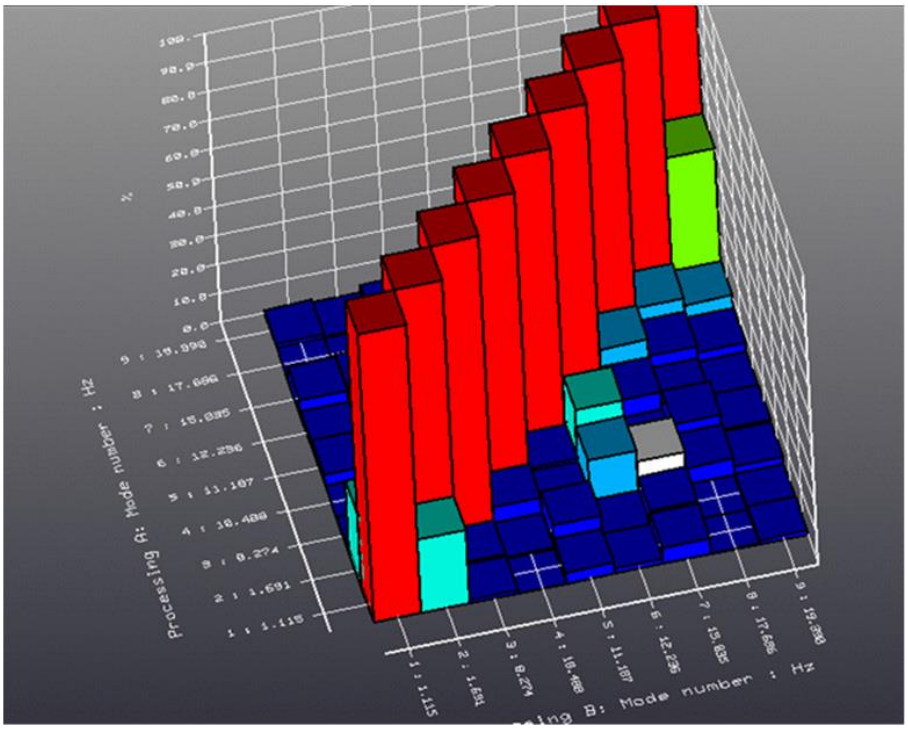

Figure 59. MAC matrix produced from 50 – 80 km/h acceleration OMA measurements. The off-diagonal elements in the matrix are low and diagonal high, indicating good quality of OMA.

5.2 Key findings

The key findings of the research are divided below between the first phase preliminary measurements and the second phase extended measurements. The key findings of the first phase measurements also include the benchmarking measurements, which were conducted with the Mercedes-Benz Citaro city bus.

5.2.1 First phase measurements

The first phase noise and vibration level measurements with the Scania CW LE were conducted simultaneously as a benchmarking measurement with the Mercedes-Benz Citaro. The shared subjective conclusion among the participants was, that the ride comfort of the Scania was poorer when compared to the benchmarking vehicle. The concrete measurements indicated similarly that the Scania had in average 3 dB higher A-weighted noise levels within

the bus interior when compared to the Mercedes-Benz. This conclusion prevailed when the vehicle was in motion i.e. during various driving sequences conducted within the velocity range of 0 – 80 km/h. When the vehicles were stationary, no similar difference in the noise levels was measured. Instead, when the vehicles were stationary, the most significant finding was that the common appliances, i.e. air compressor and the air conditioning system, created approximately 10 dB(A) difference in the body interior noise levels in both vehicles.

For more deeper analysis of the vibration and noise problem with the Scania CW LE, an order tracking analysis was made of acceleration and noise versus the engine and wheel orders. This analysis indicated that there are possible resonances of the bus body structure in 11 Hz, 14 Hz, 80 Hz, 130 Hz and 350 Hz frequency ranges. These vibrations were concluded to be excited by the wheels (11 Hz and 14 Hz), engine (80 Hz and 130 Hz) and driving axle central gear mesh (350 Hz).

The conclusions of the first phase measurements were that there is potential for improvement in the noise and vibration properties of the Scania CW LE when compared to the benchmarking vehicle, Mercedes-Benz Citaro. In addition, the spectral analysis and order tracking analysis indicated several possible resonances of the bus body structure which were excited by the powertrain components in different operating conditions. Thus, more extended investigation of the dynamic behavior and the sources and transfer paths of vibrations and noise was seen relevant for the Scania CW LE.

5.2.2 Extended measurements

The second phase investigations included e.g. operational and experimental modal analysis measurements. Investigations were conducted to determine the dynamic properties of the Scania CW LE's body structure and to find out how the disturbing noise and vibrations, deteriorating the ride comfort, are conducted to the bus passenger compartment in actual operating conditions.

In the low frequency range, the highest response levels were measured at approximately 10 – 12 Hz range. The conclusion from spectral and order tracking analysis were that the vibrations in this frequency range were excited by the second and third wheel orders. Especially dominating was the fourth natural mode at 10.5 Hz, which according to OMA,

appeared as lateral twisting and torsion of the bus body and was excited by the rocking and bouncing of the rigid front axle

Second emphasized problem was the vibrations at engine idling situations with around 700 rpm engine rotational speed. The vibration at 35 Hz range was found to be excited by the third engine order, i.e. the engine firing order. The problem occurred only when engine speed was below 800 rpm and no torque was transmitted to the driving wheels. According to EMA and ODS investigations, the root cause for the idling problem was the lateral flexibility of the rear chassis frame. This caused vibrations throughout the whole bus body but especially vertical vibrations in the rear seat region of the bus passenger compartment.

The third revealed NVH problem was the high frequency range vibrations, i.e. vibrations, which cause audible noise to be emitted within the bus body interior. The spectral analysis on this frequency range indicated noise level peaks at approximately 45 Hz, 55 Hz, 80 Hz, 118 Hz, 130 Hz and 350 Hz. The noise in the 45 – 130 Hz range was proven to be excited by the bus body rear floor section vibrating in vertical direction. As for the source of the vibrations, spectral maps of rear seat region noise and vibration gave clear indication that these vibrations were excited by the engine orders. Instead, for the noise at 350 Hz range, the order tracking analysis indicated that the noise was caused by the second order of the driving axle gear crown wheel mesh, i.e. the 78^{th} order of the drive shaft rotating frequency.

As a conclusion from the extended measurements, four significant problems were found in the NVH performance of the Scania CW LE:

1. 10 – 12 Hz low frequency range vibrations excited by wheel orders
2. 35 Hz engine idling problem promoted by lateral flexibility of the rear chassis frame
3. 45 – 130 Hz noise, excited by the engine and emitted by the vertically vibrating rear floor
4. 350 Hz noise excited by the rear axle gear crown wheel mesh

5.3 Further research

In general, it would be advised to focus on the problems identified in this research and to utilize modelling approach (e.g. finite element method) in further investigations. Modelling

approach would enable testing of different design variables more efficiently. Experimental methods could be used later on in the process for e.g. model verification purposes.

Concerning the idling problem, an investigation should be conducted concerning the lateral flexibility of the rear chassis frame and the engine and transmission vibration isolators' optimization, especially in lateral direction. Of course, one could only rise the idling speed to over 800 rpm, but fixing the lateral flexibility would presumably have positive effects to not only the idling problem, but also other vibration related issues.

In the low frequency range, two possible solutions should be investigated: First, the design of the front axle and front axle suspension should be reconsidered. As the front axle bouncing and rocking causes the vibrations at approximately 10.5 Hz body resonance, the suggestion would be to re-evaluate the suspension parameters of the front axle or consider implementation of independently suspended front axle instead of one with a rigid axle. In addition, one option would be to change the lateral stiffness of the bus body. Thus, the front axle movement would no more coincide with the bus body lateral twisting and torsion mode.

Finally, in the case of the audible, high frequency noise and vibration at 45 – 130 Hz range, the design of the rear floor area should be re-evaluated to increase the stiffness of the rear floor areas in vertical direction. Similarly, for the noise at 350 Hz, the rear axle suspension parameters should be re-evaluated, to block the axle gear noise to be emitted in to the bus body interior cavity.

REFERENCES

Avitable, P. 2001, Experimental modal analysis - A simple non-mathematical presentation. Sound and vibration, vol. 1. [Internet-document]. [Referred to 19.3.2018]. Available at: https://www.researchgate.net/publication/292660833_Experimental_modal_analysis_-_A_simple_non-mathematical_presentation

Aydin, K. & Esenboga, F. 2016. Improvement of the Heat and Sound Insulation of a Bus for Compliance with American Regulations. Advances in Automobile Engineering, vol. 5, no. 1, p. 1 – 11.

Brincker, R. & Ventura, C. 2015. Introduction to Operational Modal Analysis. John Wiley & Sons, Ltd.

Broch, J. T. 1984. Mechanical Vibration and Shock Measurements. Brüel & Kjaer Sound & Vibration Measurement A/S. Denmark.

Brüel & Kjaer Sound & Vibration Measurement A/S. 1994. Primer: Measurement microphones, 2nd edition. [Internet-document]. [Referred to 24.3.2018]. Available at: https://www.bksv.com/media/doc/br0567.pdf

Brüel & Kjaer Sound & Vibration Measurement A/S. 2003. Experimental Modal Analysis. [Internet-document]. [Referred to 19.3.2018]. Available at: http://papai.modal.hu/prezentaciok/Br%C3%BCel%20and%20Kjaer.pdf

Damijan, Z. 2010. Investigation of the Vibroacoustic Climate Inside the Buses MAN SG242 Used in Public Transport Systems. Acoustic and Biomedical Engineering, vol. 118, p. 27 – 30.

Eriksson, P. & Friberg, O. 2000. Ride comfort optimization of a city bus. Struct Multidisc Optim, vol. 20, p. 67 – 75. Springer-Verlag.

Inman, D. J. 2007. Engineering vibration, 3rd edition. Pearson Education Inc. New Jersey.

International Organization for Standardization. 1997. ISO 2631-1 Mechanical vibration and shock – Evaluation of human exposure to whole-body vibration – Part 1: General requirements, 2nd edition.

Jonsson, P., Rynell, P., Hagberg, M., Johnson, P. 2015. Comparison of whole-body vibration exposures in buses: effects and interactions of bus and seat design. Ergonomics, vol. 58, no. 7, p. 1133 – 1142.

Lamula, L., Nieminen, V., Lämsä, V. 2017. Bus Ride Comfort Development; phase 1: Scania LE noise & vibration measurements and MB noise measurement 12.10.2017. Slide presentation of measurement results, VTT.

Möser, M. 2009. Engineering Acoustics – An Introduction to Noise Control, 2nd edition. Springer-Verlag, Berlin.

Nieminen, V. 2018. Extended Experimental Vibration and Noise Analysis of Scania LE-bus. VTT Research Report VTT-R-01830-18. Espoo.

Piersol, A. G. & Paez, T. L. 2010. Harris' shock and vibration handbook, 6th edition. The McGraw-Hill Companies, Inc. New York.

Rainieri, C. & Fabbrocino, G. 2014. Operational Modal Analysis of Civil Engineering Structures. Springer Science+Business Media. New York.

Sekulic, D., Dedovic, V., Rusov, S., Salinic, S., Obradovic, A. 2013. Analysis of vibration effects on the comfort of intercity bus users by oscillatory model with ten degrees of freedom. Applied Mathematical Modelling, vol. 37, p. 8629 – 8644. Elsevier Inc.

Sekulic, D., Dedovic, V., Rusov, S., Salinic, S., Obradovic, A. 2016. Definition and determination of the bus oscillatory comfort zones. International Journal of Industrial Ergonomics, vol. 53, p. 328 – 339. Elsevier B.V.

Siemens AG. 2014a. Modal Analysis. [Internet-document]. [Referred to 19.3.2018]. Available at: https://www.plm.automation.siemens.com/en/products/lms/testing/structural-dynamics/modal-analysis.shtml#lightview%26url=/en_us/Images/Modal_analysis_tcm1023-221413.pdf%26title=Modal Analysis%26description=%26docType=pdf

Siemens AG. 2014b. What is transfer path analysis [Internet-document]. [Referred to 29.3.2018]. Available at: https://www.plm.automation.siemens.com/en_us/Images/What_is_transfer_path_analysis_tcm1023-220904.pdf

Siemens AG. 2016. Modal Assurance Criterion (MAC). [Internet-document]. [Referred to 24.3.2018]. Available at: https://community.plm.automation.siemens.com/t5/Testing-Knowledge-Base/Modal-Assurance-Criterion-MAC/ta-p/368008

Structural Vibration Solutions A/S. Experimental and operational modal analysis. [Internet-document]. [Referred to 24.3.2018]. Available at: http://www.svibs.com/TechnicalReview.

Wang, X., 2010. Vehicle noise and vibration refinement. Woodhead Publishing Limited. Cambridge.

Wikimedia Commons. Mercedes-Benz Citaro. [Internet-document]. [Referred to 03.05.2018]. Available at: https://commons.wikimedia.org/wiki/File: Mercedes_Citaro_C2_TANGO_n%C2%B0372_Romarins.jpg

Yansong, W., Xintian, L., Yan, L. 2010. A Vibro-Acoustic Coupling Analysis of Bus Passenger Compartment Based on the Finite Element Method. International Conference on Intelligent Computation Technology and Automation.